UNIVERSIDADE ESTADUAL DE CAMPINAS
Instituto de Geociências

JOSUÉ SOUZA PASSOS

GEOMORFOPEDOLOGIA DA REGIÃO DE LAVRA VELHA E ATRIBUTOS ESPECTRO-MINERALÓGICOS DO REGOLITO DO DEPÓSITO CUPRO-AURÍFERO HOMÔNIMO (BA)

GEOMORPHOPEDOLOGY OF THE LAVRA VELHA REGION AND SPECTRO-MINERALOGICAL ATTRIBUTES OF THE REGOLITH OF THE LAVRA VELHA CUPRO-AURIFEROUS DEPOSIT (BA)

CAMPINAS

2020

JOSUÉ SOUZA PASSOS

GEOMORFOPEDOLOGIA DA REGIÃO DE LAVRA VELHA E ATRIBUTOS ESPECTRO-MINERALÓGICOS DO REGOLITO DO DEPÓSITO CUPRO-AURÍFERO HOMÔNIMO (BA)

GEOMORPHOPEDOLOGY OF THE LAVRA VELHA REGION AND SPECTRO-MINERALOGICAL ATTRIBUTES OF THE REGOLITH OF THE LAVRA VELHA CUPRO-AURIFERO DEPOSIT (BA)

DISSERTAÇÃO APRESENTADA AO INSTITUTO DE GEOCIÊNCIAS DA UNIVERSIDADE ESTADUAL DE CAMPINAS COMO PARTE DOS REQUISITOS EXIGIDOS PARA OBTENÇÃO DO TÍTULO DE MESTRE EM GEOCIÊNCIAS NA ÁREA DE GEOLOGIA E RECURSOS NATURAIS

DISSERTATION PRESENTED TO THE INSTITUTE OF GEOSCIENCES OF THE UNIVERSITY OF CAMPINAS TO OBTAIN THE DEGREE OF MASTER IN GEOSCIENCES IN SCIENCIAS IN AREA OF GEOLOGY AND NATURAL RESOURCES

ORIENTADOR: PROF. DR. DIEGO FERNANDO DUCART
COORIENTADOR: PROF. DR. ALFREDO BORGES DE CAMPOS

ESTE TRABALHO CORRESPONDE À VERSÃO FINAL DA DISSERTAÇÃO DEFENDIDA PELO ALUNO JOSUÉ SOUZA PASSOS, ORIENTADA PELO PROF. DR. DIEGO FERNANDO DUCART E COORIENTADA PELO PROF. DR. ALFREDO BORGES DE CAMPOS

CAMPINAS
2020

Ficha catalográfica
Universidade Estadual de Campinas
Biblioteca do Instituto de Geociências
Cássia Raquel da Silva - CRB 8/5752

P268g

Passos, Josué Souza, 1991-
Geomorfopedologia da região de Lavra Velha e atributos espectro-mineralógicos do regolito do depósito cupro-aurífero homônimo (BA) / Josué Souza Passos. – Campinas, SP : [s.n.], 2021.

Orientador: Diego Fernando Ducart.
Coorientador: Alfredo Borges de Campos.
Dissertação (mestrado) – Universidade Estadual de Campinas, Instituto de Geociências.

1. Geomorfologia - Ibitiara (BA). 2. Solos - formação. 3. Mineralizações auríferas. 4. Recursos minerais - Ibitiara (BA). I. Ducart, Diego Fernando, 1974-. II. De Campos, Alfredo Borges, 1963-. III. Universidade Estadual de Campinas. Instituto de Geociências. IV. Título.

Informações para Biblioteca Digital

Título em outro idioma: Geomorphopedology of the Lavra Velha region and attributes of the regolith of the Lavra Velha cupro-aurifero deposit (BA).
Palavras-chave em inglês:
Geomorphology - Ibitiara (BA)
Soil formation
Gold Mineralization
Mineral Resources - Ibitiara (BA)
Área de concentração: Geologia e Recursos Naturais
Titulação: Mestre em Geociências
Banca examinadora:
Alfredo Borges de Campos [Coorientador]
Francisco Sergio Bernardes Ladeira
Juliano Alves de Senna
Data de defesa: 30-11-2021
Programa de Pós-Graduação: Geociências

Identificação e informações acadêmicas do(a) aluno(a)
- ORCID do autor: https://orcid.org/0000-0003-1716-8048
- Currículo Lattes do autor: http://lattes.cnpq.br/9509820273723753

UNIVERSIDADE ESTADUAL DE CAMPINAS
INSTITUTO DE GEOCIÊNCIAS

AUTOR: JOSUÉ SOUZA PASSOS

GEOMORFOPEDOLOGIA DA REGIÃO DE LAVRA VELHA E ATRIBUTOS ESPECTRO-MINERALÓGICOS DO REGOLITO DO DEPÓSITO CUPRO-AURÍFERO HOMÔNIMO (BA)

GEOMORPHOPEDOLOGY OF THE LAVRA VELHA REGION AND SPECTRO-MINERALOGICAL ATTRIBUTES OF THE REGOLITH OF THE LAVRA VELHA CUPRO-AURIFEROUS DEPOSIT (BA)

ORIENTADOR: PROF. DR. DIEGO FERNANDO DUCART
COORIENTADOR: PROF. DR. ALFREDO BORGES DE CAMPOS

Aprovado em: 30 / 11 / 2020

EXAMINADORES:

Prof. Dr. Alfredo Borges de Campos - Presidente

Prof. Dr. Francisco Sergio Bernardes Ladeira

Prof. Dr. Juliano Alves de Senna

A Ata de Defesa assinada pelos membros da Comissão Examinadora consta no processo de vida acadêmica do aluno.

Campinas, 30 de novembro de 2020.

JOSUÉ SOUZA PASSOS

Possui graduação em Geologia pela Universidade Federal do Sul e Sudeste do Pará - Unifesspa (2011-2017). Nessa universidade, realizou estudos referentes à caracterização geológica-geomorfológica da planície de inundação do Rio Itacaiúnas, no município de Marabá-PA (2011-2012, PIBIC/FAPESPA). Participou do projeto PROCAV, lançando mão do sensoriamento remoto para o levantamento hidrogeológico de cavidades naturais da Serra Leste, Província Mineral de Carajás - PA (2013-2014, UFPA/FAPESPA/VALE). Em 2013, foi um dos vencedores do Concurso Nacional Cultural Ideia e Energia, lançado pela Petrobras. A proposta premiada referiu-se ao uso das correntes de maré como fonte de energia para o Brasil - cujos detalhes foram publicados na revista Superinteressante na edição de novembro, 2013. Nos anos de 2014 e 2015, foi bolsista pelo programa Ciências sem Fronteiras e ligado ao programa Mining Techniques da instituição Confederation College na cidade de Thunder Bay-Canadá. Nessa configuração, atuou no Resident Geologist Program (RGP) do projeto Ontario Geological Survey (OGS) do Ministry of Northern Development & Mines (MNDM). Além disso, participou como monitor bolsista na Faculdade de Geologia da Unifesspa nas disciplinas Petrologia Ígnea, Petrologia Sedimentar (2016) e Petrologia Metamórfica (2016-2017), bem como monitor voluntário das disciplinas Geomorfologia, Prática de Sedimentologia e Prática Integrada de Petrologia e Geologia Estrutural. Na Faculdade de Engenharia de Minas e Meio Ambiente da Unifesspa, também monitorou as disciplinas Mineralogia Macroscópica e Petrografia.

Em 2018, o autor ingressou no programa de mestrado da Universidade Estadual de Campinas - UNICAMP - no Instituto de Geociências. Sua pesquisa, documentada no presente trabalho, está centrada em estudos geomorfopedológicos e geotecnológicos, lançando mão de tecnologias espectrais para caracterização espectro-mineral dos regolitos desenvolvido sobre o prospecto aurífero Lavra Velha, localizado no centro-oeste do estado da Bahia, Brasil.

Em 2019, desempenhou atividades no Instituto Água e Terra do Estado do Paraná - atuando junto à Diretoria de Geologia (DIGEOL) como residente técnico. Atualmente, é geólogo no Instituto de Meio Ambiente de Santa Catarina, Coordenadoria de Criciúma.

DEDICATÓRIA

Às pessoas que acreditaram neste projeto.

AGRADECIMENTOS

O autor é profundamente agradecido às pessoas que direta e indiretamente contribuíram para a elaboração e conclusão deste trabalho, em especial:

- O presente trabalho foi realizado com apoio da Coordenação de Aperfeiçoamento de Pessoal de Nível Superior – Brasil (CAPES) - Código de Financiamento 001, agradecido!

- Ao professor Diego Fernando Ducart, quem intermediou o acesso à Unicamp, e ao professor Alfredo Borges por se dispor a coorientar o autor. Além desses, aos professores Maria José, Juliano Senna e Francisco Ladeira que contribuíram com suas colocações.

- À empresa *Yamana Gold* pelo auxílio financeiro e logístico, sobretudo, aos geólogos Daniel Camacho e Henrique pela parceria e suporte durante o levantamento de dados de campo, e ao geólogo Leandro pelo apoio sempre. Ademais, aos funcionários que contribuíram com a execução do trabalho, inclusive, subindo e descendo as caixas com amostras, agradecido!

- À minha família (mães Nilda e Valdicélia, pelo amor sempre! Ao pai que acreditou em mim, Cléo, e aos meus irmãos: Débora, Derik, Douglas, Marcos e Artur).

- Às pessoas que me motivaram incondicionalmente. Grande suporte! Por elas, sobretudo, eu pensava em não desistir: Ester, Eriane e Odemir. Amo vocês! Foi por vocês!

- Aos meus amigos sempre presentes: Silvio Rabelo, Meyre James, Marcílio Rocha, Ozeneide Carvalho e Eduardo Pereira e ao grupo Geochapados (Igor, João, Roberto, Gabi, Erik, Hernan, Kleber, Cauê, Laila, Vini, Gabriel, Nara e Paty), esses sempre me tiram boas risadas.

- Aos amigos do Instituto Água e Terra do Paraná, Lucas, Talitha, Mariana, Eduardo, Vinícius e Vitor. Obrigado pela motivação, pela paciência e por me ouvir.

- Aos amigos da Unicamp, Douglas e Mari, Zé e Poli, Felipe e Ana, Igor, Daniel (Dan), Robert, João Motta, Keyla, Hans, Priscila, Elias Prado, Lucho, Eduardo, João Pitombeira, Wellington, Thaizínea, Raphinha, Halina, Raísa, Jussara, Antônio, Kamila, Isabel, Gustavo, Letícia, Lais, João Rafael, Lucas, Larissa, Ian, Endel, João Gabriel, Beatriz, Guilherme, Tom, Najilah, Caio, Paola e Alcione.

- Aos meus coordenadores nos últimos meses, foram grandes motivadores: Luciano Loyola (IAT) e André Dias (IMA), sou grato pela compreensão e motivação!

- Agradecimento mais que especial:

- À minha eterna mentora, professora Ana Valéria dos Reis Pinheiro. Tens meu respeito e meu carinho também. Pessoa que sempre me motiva, ajuda, aconselha...um anjo em carne!

- À minha família de Campinas: André, Bruno, Carlos, Cleberson, Laura, Sanny, Simmon e Thaissa. Nessas pessoas encontrei forças. Encontrei inspirações. Encontrei uma razão para continuar...essas pessoas fizeram meus dias melhores! Sou eternamente grato pela existência de cada um.

- Novamente, ao Simmon Viegas e ao Carlos Medina, sem os quais, certamente, eu não teria concluído este trabalho. Meu eterno agradecimento! (Cartel da Espectroscopia!)

EPÍGRAFE

Eu não enxergo mais o inferno que me atraiu
Dos cegos do castelo me despeço e vou
A pé até encontrar
Um caminho, o lugar
Pro que eu sou
...Eu vou cuidar do meu jardim!

(Cegos do Castelo – Nando Reis)

RESUMO

Lavra Velha está localizada no Domínio Fisiográfico da Chapada Diamantina e tornou-se alvo de pesquisas científicas motivadas pela descoberta de um depósito mineral pertencente à classe iron-oxide-copper-gold (IOCG), situado na cidade de Ibitiara, no estado da Bahia, Brasil. Antes da presente dissertação, as pesquisas desenvolvidas na região focaram, sobretudo, na caracterização petrográfica e geoquímica das rochas encaixantes e hospedeiras do depósito cupro-aurífero. No entanto, tornou-se conveniente entender a relação dos regolitos desenvolvidos sobre o depósito com as zonas mineralizadas em níveis mais profundos. Nessa perspectiva, realizou-se a compartimentação geomorfopedológica da área do depósito e suas cercanias, bem como a caracterização espectro-mineral dos regolitos desenvolvidos sobre os alvos prospectivos dos corpos mineralizados e, assim, identificou-se os melhores indicadores no regolito de ocorrência de minério em níveis mais profundos. Em ampla escala, a região é constituída por cinco compartimentos geomorfopedológicos. Os modelados de relevo plano a suave ondulado, bem como de geoformas onduladas e de cristas alinhadas e escarpadas desenvolveram-se sobre as rochas do embasamento cristalino e as metassedimentares do Supergrupo Espinhaço. Latossolos são sustentados por relevo plano a suave ondulado enquanto Neossolos, Cambissolos e afloramentos rochosos ocorrem vinculados aos modelados ondulados e às escarpas e cristas alinhadas. Luvissolos predominam sobre geoformas onduladas associadas, sobretudo, à presença de rochas máficas. As características funcionais da paisagem configuram um relevo semelhante ao modelo apalachiano, e sugerem um rebaixamento de terreno via erosão geoquímica-mecânica por meio de um forte controle litoestrutural. Em escala de depósito, três setores de estudo baseados em distintos aspectos, tais como espessura do regolito e natureza da rocha fonte, foram utilizados para realização da caracterização espectro-mineral e geoquímica dos perfis de regolito. A mineralogia dominante, identificada a partir da espectroscopia de reflectância com aplicação na região do visível e infravermelho próximo (VNIR) e infravermelho de ondas curtas do (SWIR), é distinta nos setores previamente determinados. Elas são: 1) caulinita pouco cristalina, predominante em regolitos rasos desenvolvidos sobre conglomerados; 2) muscovite cristalina, predominante em regolitos rasos desenvolvidos sobre granitoides e; 3) fengita + nontronita + caulinita bem ordenada, em regolitos profundos desenvolvidos sobre rochas graníticas interceptadas por rochas máficas. Essa última associação mostrou-se um potencial indicador de teores elevados de ouro em níveis profundos do depósito cupro-aurífero Lavra Velha.

Palavras chave: Geomorfopedologia; Regolito; Espectro-Mineralogia; Depósito Lavra Velha

ABSTRACT

Lavra Velha is located in the Physiographic Domain of Chapada Diamantina and became the target of scientific researches motivated by the discovery of a mineral deposit belonging to the iron-oxide-copper-gold (IOCG) class, located in the city of Ibitiara, in Bahia state, Brazil. Before the present dissertation, the investigations developed in the region focused mainly on the petrographic and geochemical characterization of the rocks that host the cupro-auriferous ore. However, turned out to be convenient to understand the relationship between the regoliths developed on the deposit and the mineralized zones at depth. In this respect, a survey of geological, geomorphological and pedological data was carried out aiming at the geomorphopedological compartmentalization of the deposit area and its surroundings. The spectro-mineral characterization of the regoliths developed on the prospective targets of deeper mineralized bodies was also carried out to identify indicators in regolith of ore occurrence at deeper levels. On a large scale, the Lavra Velha region consists of five main geomorphological compartments. In this perspective, Oxisols occur on flat to gently undulating landforms while Entisols, Inceptisols and rock outcrops appear in the aligned crests, cliffs and undulating hills. Alfisols predominate in undulating hills associated with mafic rocks. Features of the landscape show landforms resembling the Appalachian geomorphological model and suggest landform evolution by geochemical and mechanical erosion under a strong litho-structural control. On a deposit scale, three sectors of study based on different aspects, such as the thickness of the regolith and the nature of its substrate, were used to carry out the spectral-mineral and geochemical characterization of the regolith profiles. The dominant mineralogy, identified from reflectance spectroscopy using the visible and near infrared (VNIR), as well as shortwave infrared (SWIR) region, is distinct in the sectors previously mentioned. The dominant mineral or mineral association are: (1) poorly crystalline kaolinite in shallow regolith profiles developed right on metaconglomerate, (2) well-crystalline muscovite in shallow regolith profiles overlying granitic rocks, and (3) phengite + nontronite + well-crystalline or well-ordered kaolinite in deeper regolith profiles overlying granitic rocks intruded by several mafic rocks. The phengite + nontronite + well-ordered kaolinite association is a potential footprint in regolith for zones of higher grades of gold at depth in the Lavra Velha deposit.
Keywords: Geomorphopedology; Regolith; Spectro-Mineralogy; Lavra Velha Deposit

SUMÁRIO

CAPÍTULO - 1

1- ASPECTOS INTRODUTÓRIOS:

GEOMORFOPEDOLOGIA DA REGIÃO DE LAVRA VELHA E ATRIBUTOS ESPECTRO-MINERALÓGICOS DO REGOLITO DO DEPÓSITO CUPRO-AURÍFERO HOMÔNIMO (BA)

1 ASPECTOS INTRODUTÓRIOS

1.1 APRESENTAÇÃO

A área de Lavra Velha, que inclui o depósito de ouro homônimo, ambos objetos deste estudo, faz parte do contexto geológico do Bloco Paramirim e do Domínio Fisiográfico da Chapada Diamantina Ocidental, na porção norte do Cráton São Francisco. Essa área tem sido alvo de pesquisas importantes nos últimos anos (Campos, 2013; Carlin, 2018; Medina, 2020), sobretudo, em virtude da descoberta de rochas mineralizadas, cujo direito de pesquisa e exploração pertencem atualmente à empresa canadense *Yamana Gold*.

O depósito está posicionado no extremo norte do Granitoide Ibitiara que aflora em uma extensa janela estrutural que constitui uma anticlinal também denominada Ibitiara. Campos (2013) enquadrou-o em um modelo IOCG (*Iron-Oxide-Copper-Gold Ore Deposits*) e sugeriu sua origem a partir da fusão de um manto litosférico subcontinental, metassomatizado em ambiente de arco magmático.

As rochas hospedeiras são constituídas por distintas associações minerais com estruturas brechóide, as quais conduziram Campos (2013) a dividi-las nas brechas hidrotermais, a saber: (i) brecha calcio-silicática constituída por calcita-magnetita-calcopirita-(±epidoto-clorita); (ii) brecha sulfetada composta por calcopirita-piritamagnetita-hematita-(±turmalina-clorita); (iii) brecha hematítica formada pela associação hematita-magnetita-turmalina-(±sericita); e (iv) brecha sericítica constituída por sericita-hematita-turmalina-(±martita). De modo geral, essas rochas encontram-se fortemente alteradas e interceptadas por um sistema de veios e vênulas constituídos pela associação hidrotermal - hematita, turmalina, muscovita, quartzo e clorita. Além disso, pesquisas conduzidas por Medina (2020) mostram que, no depósito Lavra Velha, os níveis cupríferos ocorrem associados a, pelo menos, duas diferentes associações minerais, as quais são (ouro±pirita±tennantite±bismuthinite±magnetite) e (ouro±hematita).

Embora se tratando de uma região com evidente potencial metalogenético, a pesquisa e exploração mineral, na área em apreço, dificulta-se em virtude das coberturas regolíticas sobrepostas aos afloramentos e, consequentemente, às rochas mineralizadas. Essa problemática – corpos mineralizados capeados por pacotes de regolito de espessuras variadas - ocorre em vários depósitos a nível global. Dessa forma, pesquisadores vêm desenvolvendo estudos orientados ao aprimoramento de técnicas para o diagnóstico de footprints contidos no próprio regolito e, assim, utilizá-los como ferramenta auxiliar na identificação de rochas

mineralizadas em níveis mais profundos (Laukamp et al. 2016; Lampinen et al., 2019). O sucesso nos resultados desses modelos de investigação pode contribuir significativamente para a prospecção de depósitos minerais não aflorantes.

Antes da presente dissertação, grande parte dos trabalhos com vistas ao estudo e compreensão da área de Lavra Velha visava apenas à caracterização petrográfica e geoquímica das rochas da região. Desse modo, não havia uma discussão e integração dos aspectos do meio físico (relevo-rocha), bem como do regolito desenvolvido sobre o prospecto aurífero em apreço, apontando seu respectivo papel como um indicador de alvos para investigação detalhada e sua relação com níveis mineralizados mais profundos.

Neste contexto, a meta central desta dissertação é investigar a relação entre o regolito desenvolvido sobre o depósito de ouro Lavra Velha e áreas mineralizadas em níveis mais profundos. Estendendo-se à meta central, pretende-se apontar fatores relevantes para a formação e espacialização de regolito na região de Lavra Velha a partir da compartimentação geomorfopedológica em um pequeno quadrante, cuja porção central compreende os alvos auríferos e suas cercanias. Para alcançar o propósito mencionado, foram obtidos dados geomorfológicos, pedológicos, espectrais e geoquímicos a partir de procedimentos técnicos e operacionais de campo e escritório.

A apresentação deste documento foi arquitetada segundo o modelo de dissertação integrada de artigos e, assim, contempla 3 capítulos. O corpo central está composto pelos capítulos 2 e 3, referentes a dois artigos científicos, os quais são precedidos por textos integrantes que correspondem ao capítulo 1 - capítulo introdutório, com objetivo da pesquisa e a síntese dos materiais e métodos. Os artigos serão apresentados na ordem a seguir:

Capítulo 2: Artigo 1 **-** ***Rock-Landform-Soil Relationship for Geomorphopedological Characterization in the Region of the Lavra Velha, Occidental Chapada Diamantina, Bahia, Brazil:***

Esse manuscrito, publicado na Revista Brasileira de Geomorfologia, (Qualis/CAPES A1, 2019; DOI: http://dx.doi.org/10.20502/rbg.v21i2.1751), apresenta dados sobre o contexto geológico, geomorfológico e pedológico da região de Lavra Velha, que associados à influência estrutural, permitiram entender a configuração do relevo e sua influência nos processos pedogenéticos, contribuindo, ainda, para o entendimento da distribuição de ordens de solo. Para tanto, foram sobrepostas informações obtidas em fontes diversas da literatura (artigos, teses, dissertações e relatórios), bem como em expedições de

campo realizadas ao longo da área em apreço. Os resultados obtidos permitiram definir as principais unidades geomorfopedológicas de um pequeno quadrante representativo da região de Lavra Velha visando, assim, à orientação para levantamentos e pesquisa em escala de detalhe.

Capítulo 3: Artigo 2 **-** ***Spectral-Mineral Characterization Of The Regolith Developed In The Lavra Velha Prospect And Its Significance For Mineral Exploration, Chapada Diamantina, Brazil***

Esse manuscrito informa e discute os principais componentes mineralógicos dos regolitos desenvolvidos sobre os alvos de investigação na área do depósito Lavra Velha em diferentes cenários geomorfopedológicos. As assembléias minerais foram identificadas a partir do uso da espectroscopia de reflectância, utilizando-se a região do infravermelho de ondas curtas (SWIR) do espectro eletromagnético como ferramenta principal. Além disso, utilizaram-se dados prévios de geoquímica total resultantes de análises realizadas no laboratório ALS Chemex, no Peru, para compreensão das principais associações geoquímicas ao longo dos perfis. Os resultados obtidos levaram ao entendimento da distribuição mineral e associações geoquímicas afins ao longo dos horizontes dos regolitos distribuídos sobre o depósito. Desse modo, definiram-se as principais características espectro-mineralógicas e geoquímicas, em níveis superficiais, que indicam a ocorrência de zonas mineralizadas em níveis mais profundos.

1.2 LOCALIZAÇÃO E ACESSO À ÀREA DE ESTUDO

A região de Lavra Velha e o prospecto de ouro homônimo estão localizados na cidade de Ibitiara, centro-oeste do estado da Bahia, Brasil. Partindo de Salvador, capital do estado, o acesso pode ser feito via terrestre até o município de Seabra, seguindo, então, em direção à cidade de Ibitiara. O trajeto é realizado pelas vias pavimentadas BR- 324, BR-116 e BR-242. A partir de Ibitiara, o acesso ao prospecto, localizado ao norte da cidade, é feito pela via pavimentada BA-152 que está conectada a uma rede de estradas e caminhos não pavimentados.

1.3 CONTEXTO GEOLÓGICO

Lavra Velha está posicionada no domínio Fisiográfico da Chapada Diamantina, a norte do Cráton São Francisco, no domínio morfotectônico do Aulacógeno ou Corredor Paramirim (Cruz e Alkimin 2006; Carlin 2018). Esse domínio representa uma estrutura de

direção NNW, desenvolvida a partir de rifts paleo–neoproterozoicos, superpostos e parcialmente invertidos (Pedrosa-Soares et al. 2001). O desenvolvimento da estrutura está vinculado ao imbricamento de cunhas do embasamento sob as rochas supracrustais ao longo do eixo do rift, alcançando, ainda, rochas do Supergrupo Espinhaço e do Supergrupo São Francisco (Alkmim et al. 1993).

Em escala regional, a geologia da região de Lavra Velha é representada por sequência de rochas arqueanas, assim como associações plutono-vulcanossedimentares de idade paleo a mesoproterozoica e intrusões de rochas máficas. As unidades são representadas da seguinte maneira: i) Complexo Paramirim, constituído por ortognaisses granodioríticos e migmatíticos com tonalitos, granodioritos, monzogranitos, sienogranitos e sienitos subordinados; ii) Granito Ibitiara, unidade representada por dioritos, tonalitos e granitos cálcio-alcalinos, sódicos e peraluminosos, datado, pelo método UPb em zircões, por Teixeira (2005), em 2091±6,6 Ma (Guimarães et al., 2005); iii) Granito Matinos, representado por granodioritos e granitos, predominantemente monzogranitos, porfiríticos, foliados a gnáissicos, com termos tonalíticos subordinados (Guimarães et al., 2005); iv) Formação Serra da Gameleira, composta por quartzo metarenito bimodal, metagrauvaca e metarcóseos, associados a metaconglomerado polimítico, metaconglomerado oligomítico, metarenitos e metabrechas; v) Formação Novo Horizonte, formada por dacitos, riolitos, quartzo pórfiro e feno andesitos (Guimarães et al., 2005); vi) Formação Ouricuri do Ouro, composta por metaconglomerados, metarenitos líticos e conglomeráticos, metarcóeos e metagrauvacas que sobrepostas em contato abrupto e erosivo sobre as rochas vulcânicas da Formação Novo Horizonte; vii) Formação Lagoa de Dentro, com os sedimentos rítmicos e lacustres, composta por metassiltitos e metargilitos com restritas lentes de sedimentos psamíticos (Guimarães et al, 2005); e viii) rochas máficas, gabróicas, que segundo Guimarães et al. (2005), ocorrem intrudidas no conjunto metavulcanossedimentar do Supergrupo Espinhaço na forma de diques e sills com orientação preferencial N-S e NW-SE.

1.4 OBJETIVOS

A meta desta dissertação consiste em estabelecer a relação do regolito desenvolvido sobre o depósito Lavra Velha com zonas mineralizadas em níveis mais profundos. Estendendo-se à meta central, pretende-se apontar importantes fatores para a formação e distribuição do regolito na área do depósito e suas cercanias.

Para que a meta central fosse atingida, traçaram-se os seguintes objetivos específicos:

i) Estabelecer as principais unidades geomorfopedológicas da região de Lavra Velha;

ii) Definir mudanças mineralógicas de regolito desenvolvido sobre o depósito cupro-aurífero de Lavra Velha;

iii) Diagnosticar variações geoquímicas no regolito do depósito Lavra Velha e associá-las ao contexto geológico da área de estudo e;

iv) Avaliar o uso da espectrometria de reflectância como ferramenta para análise dos componentes de regolito em áreas mineralizadas.

1.5 MATERIAIS E MÉTODOS

A fim de se alcançar os objetivos traçados, utilizou-se diversas técnicas de investigação referentes ao tema e compatíveis com a proposta abordada.

1.5.1 Materiais

I) Mapas de geologia, geomorfologia e pedologia inéditos e compilados de projetos anteriores, tais quais trabalhos de conclusão de curso, dissertações, artigos e reports tanto sobre a base cartográfica quanto sobre a evolução geológica/metalogenética da área e depósito em apreço;

II) 17 Furos de sondagem, fornecidos pela empresa Yamana Gold, contendo amostras do regolito presente sobre os corpos mineralizados e suas cercanias;

III) Dados de geoquímica de rocha total e regolito, fornecidos pela empresa Yamana Gold;

V) Espectrorradiômetro ASD TerraSpec®-4 Hi-Resolution (Empresa Yamana Gold);

VII) Software específico: i) para análise de dados de espectroscopia de reflectância: TSG-8™ e ii) para elaboração dos produtos cartográficos: ArcMap™, disponíveis no Laboratório de Processamento de Informações Georreferenciadas (LAPIG) da Unicamp.

1.5.2 Métodos

1.5.2.1 Pesquisa Bibliográfica

A pesquisa bibliográfica consistiu, em primeiro plano, no levantamento de dados referentes aos aspectos geológicos, geomorfológicos, pedológicos e metalogenéticos da região de Lavra Velha. A partir disso, realizou-se um novo levantamento bibliográfico dividido em duas vertentes (I e II) distintas, mas complementares para a elaboração do produto final. Segue uma breve explanação dos levantamentos bibliográficos e respectivas vertentes de conhecimento.

1.5.2.1.1 Levantamento Bibliográfico (estudo geomorfopedológico)

Esse levantamento referiu-se à busca de informações sobre associação rocha-relevo-solo e, assim, compartimentação geomorfopedológica. Esse conhecimento fez-se necessário para melhor compreender os fatores que influenciam no desenvolvimento e distribuição de regolito ao longo da paisagem de modo geral. Desse modo, utilizaram-se conceitos abordados nos trabalhos conduzidos por, entre outros autores, Tricart e Killian (1979), Castro e Salomão (2000), Lacerda et al. (2008) e Villela et al. (2013, 2015), ainda que não tenham sido seguidos todos os passos roteirizados por esses autores.

1.5.2.1.2 Levantamento Bibliográfico (estudo espectro-mineralógico)

Essa bibliografia consistiu, principalmente, na ótica da caracterização de regolitos sobrejacentes a depósitos minerais por meio da aplicação das técnicas espectrais. Contou-se com artigos que versam sobre o assunto em diferentes regiões do mundo.

1.4.2.2 Procedimento de Campo e Escritório

Realizou-se uma campanha de campo, em setembro de 2018, durante 15 dias, visando o levantamento *in situ* de dados de geologia, geomorfologia e pedologia, a fim de se complementar, corroborar e aprimorar o levantamento de dados previamente disponíveis nos trabalhos conduzidos por Ribeiro (1974), Guimarães et al. (2005), Campos (2013) e Carlin (2018), assim como de relatórios internos disponibilizados pela empresa *Yamana Gold*.

O levantamento geológico consistiu no reconhecimento, descrição e coleta de rochas e estruturas ao longo de um quadrante de 150 Km² contendo o prospecto Lavra Velha em sua porção central.

O levantamento geomorfológico levou em conta a observação e registro dos elementos da paisagem, bem como as técnicas utilizadas por Nascimento et al. (2018). Assim,

o conjunto cartográfico de escritório (hipsometria, declividade e forma de vertentes) foi sobreposto para elaboração do produto final, o mapa geomorfológico.

O levantamento e caracterização de solos foram realizados por meio da descrição em campo e, assim, permitiu a análise de aspectos morfológicos para a classificação de ordens até o segundo nível.

1.4.2.3 Aquisição e Processamento de Dados Espectrais

Os 17 furos de sondagem utilizados na elaboração deste trabalho foram escolhidos de modo a formarem três secções (ENE-WSW) que compreendessem tanto zonas mineralizadas quanto não mineralizadas do depósito de ouro Lavra Velha. A amostragem consistiu na aquisição sistemática de medidas espectrais em intervalos de 25 cm de cada furo. Cada medida salva representa em média 70 medições da mesma área de aquisição.

O espectrorradiômetro utilizado, *ASD TerraSpec®-4 Hi-Resolution*, coletou dados na faixa de comprimento de onda de 350-2500 nm, com uma resolução espectral de 6 nm e intervalo de amostragem de 1 nm na região do comprimento de onda SWIR. Essas medições foram realizadas utilizando a sonda de contato acoplada ao equipamento que contém uma lâmpada de halogênio como fonte de luz fornecendo, assim, a iluminação adequada aos procedimentos. Adicionalmente, os espectros adquiridos foram convertidos de radiância para reflectância utilizando o sinal do *Spectralom*^{TM}, via uma calibração deste instrumento, realizada a cada 15 minutos no processo de aquisição espectral.

Após a aquisição das assinaturas espectrais, os dados foram processados, analisados e interpretados a fim de se extrair informações mineralógicas essenciais, sobretudo, abundância, cristalinidade e composição química. Essa identificação e extração de respectivos dados semiquantitativos foram feitas com base nas características de geometria e absorção diagnóstica de cada espectro, incluindo, assim, a posição do comprimento de onda, a largura e a profundidade das feições. Para tanto, utilizou-se o software *The Spectral Geologist* (TSG-8^{TM}) e contou-se com as bibliotecas espectrais de referência da USGS (Kokaly et al., 2017) e dos guias GMEX (Pontual et al., 2008a, 2008b). Adicionalmente, utilizaram-se as concepções apresentadas nos trabalhos conduzidos por Cudahy et al. (2008), Haest et al. (2012) e Prado et al. (2015) para elaboração dos parâmetros espectrais e interpretação.

1.4.2.4 Geoquímica

As amostras para análise geoquímica foram obtidas em intervalos máximos de um metro nos 17 furos de sondagem e, então, analisadas por ICP-MS para leitura dos seguintes

elementos: Al, Ca, Fe, Mg, Na, P, K, S, Ti (em %), As, B, Ba, Be, Bi, Cd, Ce, Co, Cr, Cu, Ga, La, Li, Mn, Mo, Ni, Pb, Sb, Sc, Se, Sn, Sr, Th, Tl, U, V, W, Y, Zn e Zr (em ppm) e Au (em g/t). O procedimento técnico contou com abertura ácida em 4 ácidos ou em água régia 1:3 (HNO_3 e HCl) e foi operado no laboratório ALS Chemex, Peru.

REFERÊNCIAS BIBLIOGRÁFICAS

ALKMIM, F.F.; NEVES, B.B.B.; ALVES, J.A.C. Arcabouço Tectônico do Cráton do São Francisco: uma revisão. In: MISI, A; DOMINGUEZ, J.M.L. O Cráton do São Francisco. Salvador: SBG, 1993, p. 45-62.

CASTRO, S. S.; SALOMÃO, F. X. T. Compartimentação morfopedológica e sua aplicação: considerações metodológicas. GEOUSP, São Paulo, n. 7, p. 27-37, 2000.

CAMPOS, L. D. O Depósito de Au-Cu Lavra Velha, Chapada Diamantina Ocidental: Um exemplo de depósito da classe IOCG associado aos terrenos paleoproterozoicos do Bloco Gavião. Dissertação (Mestrado), Instituto de Geociências, Universidade Federal de Brasília. 2013. 104p.

CARLIN, A. C.; ZANARDO, A.; NAVARRO, G. R. B. Caracterização petrográfica das rochas encaixantes da mineralização aurífera do Depósito Lavra Velha– região de Ibitiara, borda oeste da Chapada Diamantina, Bahia. Geociências, v. 37, n. 2, p. 253-265, 2018.

CRUZ, S.C.P. & ALKIMIM F.F. The tectonic interaction between the Paramirim Aulacogen and the Araçuai Belt, São Francisco Craton region, Eastern Brazil. Anais da Academia Brasileira de Ciências, v. 78, n. 1, p.151-173, 2006.

CUDAHY, T.J., JONES, M., THOMAS, M., LAUKAMP, C., CACCETTA, M., HEWSON, R., RODGER, A., VERRALL, M., 2008. Next Generation Mineral Mapping: Queensland Airborne HyMap and Satellite ASTER Surveys. CSIRO Exploration & Mining ReportP2007/364152.

GUIMARÃES, J.T.; MARTINS, A.A.M.; ANDRADE FILHO, E.L.; LOUREIRO, H.S.C.; ARCANJO, J.B.A.; NEVES J.P.; ABRAM, M.B.; SILVA, M.G.; BENTO, R.V. Projeto Ibitiara-Rio de Contas: Estado da Bahia, Programa Recursos Minerais do Brasil, Escala 1:200.000. Publicação CPRM. Convênio CBPM/CPRM. Salvador, 2005. 193p.

HAEST M., CUDAHY T., LAUKAMP C., GREGORY S. 2012. Quantitative mineralogy from visible toshortwave infrared spectroscopic data: II. 3D mineralogical

characterization of the Rocklea Dome channel iron deposit, Western Australia. Economic Geology, 107:229–249.

KOKALY, R.F., CLARK, R.N., SWAYZE, G.A., LIVO, K.E., HOEFEN, T.M., PEARSON, N.C., WISE, R.A., BENZEL, W.M., LOWERS, H.A., DRISCOLL, R.L., AND KLEIN, A.J., 2017, USGS Spectral Library Version 7: U.S. Geological Survey Data Series 1035, 61 p.

LAMPINEN, H. M., LAUKAMP, C., OCCHIPINTI, S. A., & HARDY, L. 2019. Mineral footprints of the Paleoproterozoic sediment-hosted Abra Pb-Zn-Cu-Au deposit Capricorn Orogen, Western Australia. Ore Geology Reviews, 104, 436-461.

LAUKAMP, C.; SALAMA, W.; GONZÁLEZ-ÁLVAREZ, I. Proximal and remote spectroscopic characterisation of regolith in the Albany–Fraser Orogen (Western Australia). Ore Geology Reviews, v. 73, p. 540-554, 2016.

LACERDA, M. P. C.; QUEMÉNÉUR, J. J. G., ANDRADE, H.; ALVES, H. M. R.; VIEIRA, T. G. C. Study of the relationship pedo-geomorphological in the soil distribution with argillic horizons in the landscape of Lavras (MG), Brazi. Revista Brasileira de Ciência do Solo, v. 32, n. 1, p. 274-284, 2008. DOI: http://dx.doi.org/10.1590/S0100-06832008000100026.

NASCIMENTO, S. T., CASTRO, P. D. T. A., AZEVEDO, Ú. R. D. Geodiversidade dos compartimentos geomorfológicos do Anticlinal de Mariana, Minas Gerais. Geociências, v. 37, n. 3, p. 497-504, 2018.

PEDROSA-SOARES, A.C.; NOCE, C. M.; WIEDMANN, C.; PINTO, C.P. The Araçuaí-West-Congo orogen in Brazil: an overview of a confined orogen formed during Gondwana assembly. Precambrian Research, n. 110, p. 307-323, 2001.

PONTUAL S., MERRY N.J., GAMSON P. 2008a. GMEX - Spectral analysis guides for mineral exploration: spectral interpretation field manual. Ausspec International Ltd, 1, 188 p.

PONTUAL S., MERRY N.J., GAMSON P. 2008b. GMEX - Spectral analysis guides for mineral exploration: practical applications handbook. Ausspec International Ltd, 2, 86 p.

PRADO, E. M. G., SILVA, A. M., DUCART, D. F., TOLEDO, C. L. B., & DE ASSIS, L. M. (2016). Reflectance spectroradiometry applied to a semi-quantitative analysis of the mineralogy of the N4ws deposit, Carajás Mineral Province, Pará, Brazil. *Ore Geology Reviews*, *78*, 101-119.

TEIXEIRA, L.R. Projeto Ibitiara - Rio de Contas: relatório temático de litogeoquímica. Salvador: CPRM, 2005. 33p. Programa Levantamentos Geológicos Básicos do Brasil - PLGB. Relatório interno.

TRICART, J.; KILIAN, J. La eco-geografia y la ordenación del medio natural. Barcelona: Anagrama, 1979. 288 p.

VILLELA, F. N. J.; ROSS, J. L. S.; MANFREDINI, S. Análise geomorfopedológica na borda leste da Bacia Sedimentar do Paraná, sudeste do Brasil. Revista Brasileira de Geomorfologia, v. 16, n. 4, p. 669-682, 2015. DOI: http://dx.doi.org/10.20502/rbg.v16i4.608.

VILLELA, F. N. J.; ROSS, J. L. S.; MANFREDINI, S. Relief-Rock-Soil relationship in the transition of Atlantic Plateau to Peripheral Depression, Sao Paulo, Brazil. Journal of Maps, v. 9, n. 3, p. 343-352, 2013. DOI: 10.1080/17445647.2013.805170.

CAPÍTULO - 2

1. ROCK-LANDFORM-SOIL RELATIONSHIP FOR GEOMORPHOPEDOLOGICAL CHARACTERIZATION IN THE REGION OF LAVRA VELHA, OCCIDENTAL CHAPADA DIAMANTINA, BAHIA

Josué Souza Passos

Diego Fernando Ducart

Carlos Martin Medina

Alfredo Borges de Campos

www.ugb.org.br
ISSN 2236-5664

Revista Brasileira de Geomorfologia

v. 21, nº 2 (2020)

http://dx.doi.org/10.20502/rbg.v21i2.1751

ROCK-LANDFORM-SOIL RELATIONSHIP FOR GEOMORPHOPEDOLOGICAL CHARACTERIZATION IN THE REGION OF LAVRA VELHA, OCCIDENTAL CHAPADA DIAMANTINA, BAHIA

RELAÇÃO ROCHA-RELEVO-SOLO PARA CARACTERIZAÇÃO GEOMORFOPEDOLÓGICA NA REGIÃO DE LAVRA VELHA, CHAPADA DIAMANTINA OCIDENTAL, BAHIA

Josué Souza Passos
Institute of Geosciences, State University of Campinas
R. Carlos Gomes, 250, Campinas, São Paulo. Zip Code: 13083-855. Brazil
ORCID: https://orcid.org/0000-0003-1716-8048
E-mail: j211345@dac.unicamp.br

Diego Fernando Ducart
Institute of Geosciences, State University of Campinas
R. Carlos Gomes, 250, Campinas, São Paulo. Zip Code: 13083-855. Brazil
ORCID: https://orcid.org/0000-0003-2085-9691
E-mail: dducart@unicamp.br

Carlos Martin Medina
Institute of Geosciences, State University of Campinas
R. Carlos Gomes, 250, Campinas, São Paulo. Zip Code: 13083-855. Brazil
ORCID: https://orcid.org/0000-0001-9097-464X
E-mail: carlosmmedina14@gmail.com

Alfredo Borges De-Campos
Institute of Geosciences, State University of Campinas
R. Carlos Gomes, 250, Campinas, São Paulo. Zip Code: 13083-855. Brazil
ORCID: https://orcid.org/0000-0002-7507-1482
E-mail: acampos@ige.unicamp.br

Informações sobre o Artigo

Recebido (Received):
17/08/2019
Aceito (Accepted):
14/01/2020

ROCK-LANDFORM-SOIL RELATIONSHIP FOR GEOMORPHOPEDOLOGICAL CHARACTERIZATION IN THE REGION OF LAVRA VELHA, OCCIDENTAL CHAPADA DIAMANTINA, BAHIA

Josué Souza Passos[1], Diego Fernando Ducart[1], Carlos Martin Medina[1], Alfredo Borges de Campos[1]

[1]Institute of Geosciences, University of Campinas (UNICAMP)

ABSTRACT

The Lavra Velha region is situated on the western edge of the Chapada Diamantina and comprised of a crystalline basement and a metasedimentary cover that corresponds to the Ibitiara Granitoid and the Espinhaço Supergroup, respectively. The Chapada Diamantina is internationally recognized for mineral production and tourism, and because of that it has become a constant target for novel research that aims at characterizing its main geological and physiographic aspects. The present work aims at pointing out geomorphopedological associations of the Lavra Velha region by analyzing the interdependence between rock, landform and soil. To this end, geology, geomorphology and pedology data were obtained from literature, remote sensing data and field expeditions. In the studied area, we recognized metasedimentary and crystalline rocks, on which flat to gently undulating landforms beside crests and cliffs developed. Oxisols occur on flat to gently undulating landforms while Entisols, Inceptisols and rock outcrops appear in the aligned crests, cliffs and undulating hills. Alfisols predominate in undulating hills associated with mafic rocks. Features of the landscape show landforms resembling the Appalachian geomorphological model as first described by William Morris Davis, and they suggest landform evolution by geochemical and mechanical erosion under a strong litho-structural control. The geomorphopedological associations allowed the understanding of the relationship between the major elements of the physical environment from Lavra Velha region and, consequently, a predictive model of the rock-landform-soil distribution that can be useful for geomorphopedological mapping of the western edge of the Chapada Diamantina.

Keywords: Rock-Landform-Soil Relationship, Lavra Velha Region, Occidental Chapada Diamantina.

1 INTRODUCTION

The analysis of the rock-landform-soil association is essential for the study of landscape evolution. According to Torrado *et al*. (2005), the pedogenetic processes are controlled by the dynamics of several factors, among which stand out are climate, geomorphology, and geology. The climate influences soil development, both through the availability of water that acts as a weathering agent and a chemical leaching of minerals, as well as by temperature which works as a catalyst for chemical reactions leading to degradation of rocks. The landform directly influences the pedogenetic evolution, since it controls the amount of water infiltrated through the terrain, and consequently, the speed of the chemical reactions that promote rock weathering (CURI & FRANZMEIER, 1984). Typically, soils that come from quartz-rich rocks tend to present medium to coarse texture and acidic pH (MEDEIROS *et al.*, 2013). In contrast, soils resulting from the decomposition of basic/ultrabasic rocks tend to be clayey and alkaline (TORRADO *et al*., 2006).

Research focused on the understanding of the rock-landform-soil relationship and its influence on several types of natural phenomena have been developed throughout the world since the 1960s (e.g. TROEH, 1964; LEPSCH *et al*., 1977; TRICART & KILLIAN, 1979; THOMAS *et al*., 1999; CASTRO & SALOMÃO, 2000; LACERDA *et al*., 2008). However, surveys involving these three landscape components simultaneously in association with litho-structural variables are still limited. Despite this, the geomorphopedological characterization, in which there is a soil-landform-rock analysis associated with litho-structural elements, has been approached as an important mechanism to understand the landscape evolution and soil distribution, as shown in the works conducted by Villela *et al*. (2013) and Villela *et al.* (2015).

In the Brazilian regions where research is focused on the integrated analysis of landscape components, generally, present economic, touristic, socio-environmental and scientific value; thus, the efforts to develop research centered on geological, geomorphological and pedological characterization are strategic. Thereby, the Physiographic Domain of the Chapada Diamantina, historically recognized as a significant producer of gold and national tourism heritage, has become the target of several studies aimed at characterizing its main physiographic aspects (BATTILLANE *et al*., 1996; NÓBREGA *et al*., 2006; SEVERO & MELO, 2018). However, few works directly approach the geomorphopedological relationship in that region, which would be a useful study for producing models capable of understanding soil distribution according to its geological, geomorphological and structural settings.

Furthermore, the outcomes could be used for socio-environmental, socio-economic and land-use planning.

Therefore, this study is focused mainly on the recognizing of rock-landform-soil association and its correlation with litho-structural factors for the geomorphopedological characterization of the Lavra Velha region, which is a target of increasing mineral prospecting, mostly of gold-copper bearing rocks (e.g Lavra Velha Deposit, Campos 2013; Carlin et al. 2018) and tourism activities as well. The region is located on the occidental portion of the Chapada Diamantina in Brazil, and the result is a precursor model archetype for integrated modeling of the geomorphopedological setting in this physiographic domain.

2 STUDY AREA

The study area is situated north of Ibitiara, in the midwest of the state of Bahia, Brazil (Figure 1). It corresponds to a quadrant of 150 km^2, between latitudes 12° 29‘ 20“ and 12° 37’ 05” S, and 42° 18’ 59” and longitudes 42° 10’ 22” W. Starting from Salvador, the state capital, access to the area can be achieved by land via highways BR- 324, BR-116 and BR-242. The landform of the region is represented by the Sertanejo Pediplain made up of elongated, parallel ridges running in a north-south direction, belonging to the Espinhaço Supergroup of Pre-Cambrian age (RIBEIRO, 1974). The predominant vegetation is the open arboreal caatinga, without palms. The climate is semi-arid, hot and dry, corresponding to the BSh climate in the Koppen (1936) classification. The annual average temperature is 26.5 °C and the average annual rainfall is only 746 mm, with higher rainfall volumes from October to April.

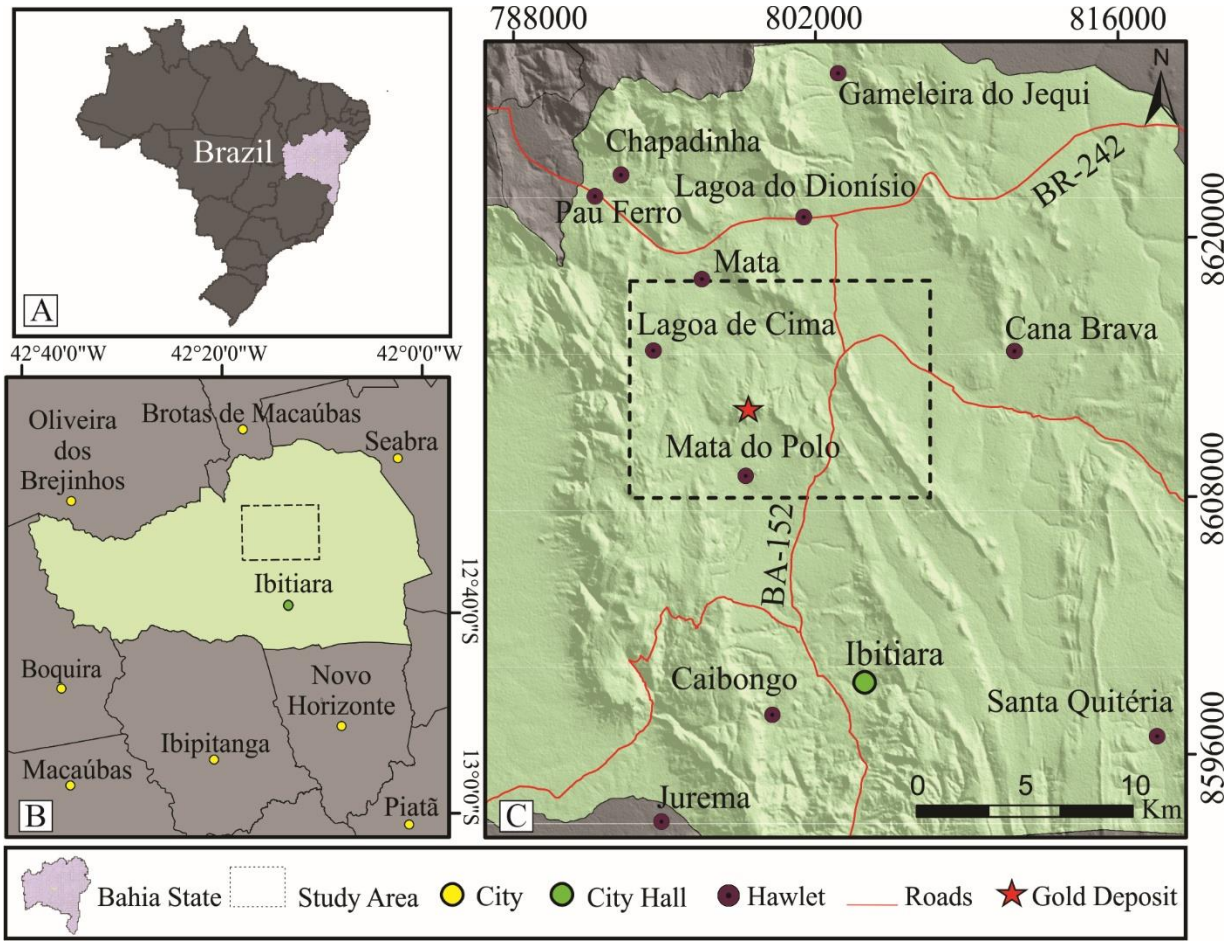

Figure 1: Map indicating the study area location. (A) Location of Bahia state in Brazil; (B) Main cities located around the city of Ibitiara where the study area is (box outlines area shown in B and C). C) Focus on the study area (the green background is part of the city of Ibitiara).

3 MATERIALS AND METHODS

Aiming at delineating the geomorphopedological units, we gathered information such as geology, geomorphology, pedology, drainage, hypsometry, slope, and topography from the specialized literature, along with office and field data. Studies conducted by Tricart & Killian (1979), Castro & Salomão (2000), Lacerda et al. (2008), and Villela et al. (2013, 2015) were considered in order to approach the morphopedological setting and, consequently, to make the final geomorphopedological map. Steps and different sources of data will be presented as follows.

Geological data was obtained from the research developed by the Geological Survey of Brazil for the Ibitiara-Rio das Contas Project (2005), as well as the geological mapping conducted by Campos (2013) and Carlin et al. (2018). In addition, a field expedition was undertaken to describe outcrops and collect rock samples from the region.

The techniques used by Nascimento et al. (2018) were followed for the geomorphological mapping due to the satisfactory outcome achieved by their approach in an area with a similar geomorphological setting of the study site. The cartographic base included topographic maps from the SEI on the scale of 1:100,000, and Digital Elevation Models (DEM) from the PALSAR sensor aboard the ALOS satellite, with the spatial resolution of 12.5 meters. This data was adjusted to assist in the elaboration of hypsometry, slope declivity, slope aspect, geology, pedology and geomorphology maps. These maps were overlapped and used for understanding rock-landform-soil relationships. The digitization and elaboration of the cartographic base, as well as the models presented in this work, were done in the Georeferenced Information Processing Laboratory (LAPIG) of the University of Campinas (IG/UNICAMP).

The survey, characterization, and spatialization of soils relied on the research developed by Ribeiro (1974) in the city of Ibitiara, as well as data from the Brazilian Agricultural Research Corporation (EMBRAPA, 2001), and the Bahia Environment and Water Resources Institute (INEMA, 2014). Moreover, a field expedition was carried out to recognize and describe morphological attributes of soil profiles. In the present study, laboratory analyses were not performed to get physical and chemical attributes of the soil. In the field the soil was classified up to the second level and additional attributes can be found in the sources mentioned previously.

Geomorphopedological units were determined based on the maps previously mentioned, mainly on the geological, geomorphological and pedological maps, which were integrated by overlaying their records. Therefore, the units were differed from each other through the rock-landscape-soil combination.

4 RESULTS

4.1 GEOLOGY

The study area consists of rocks corresponding to Granitoid Ibitiara, Espinhaço Supergroup and intrusive mafic rocks as shown in the geological map (Figure 2).

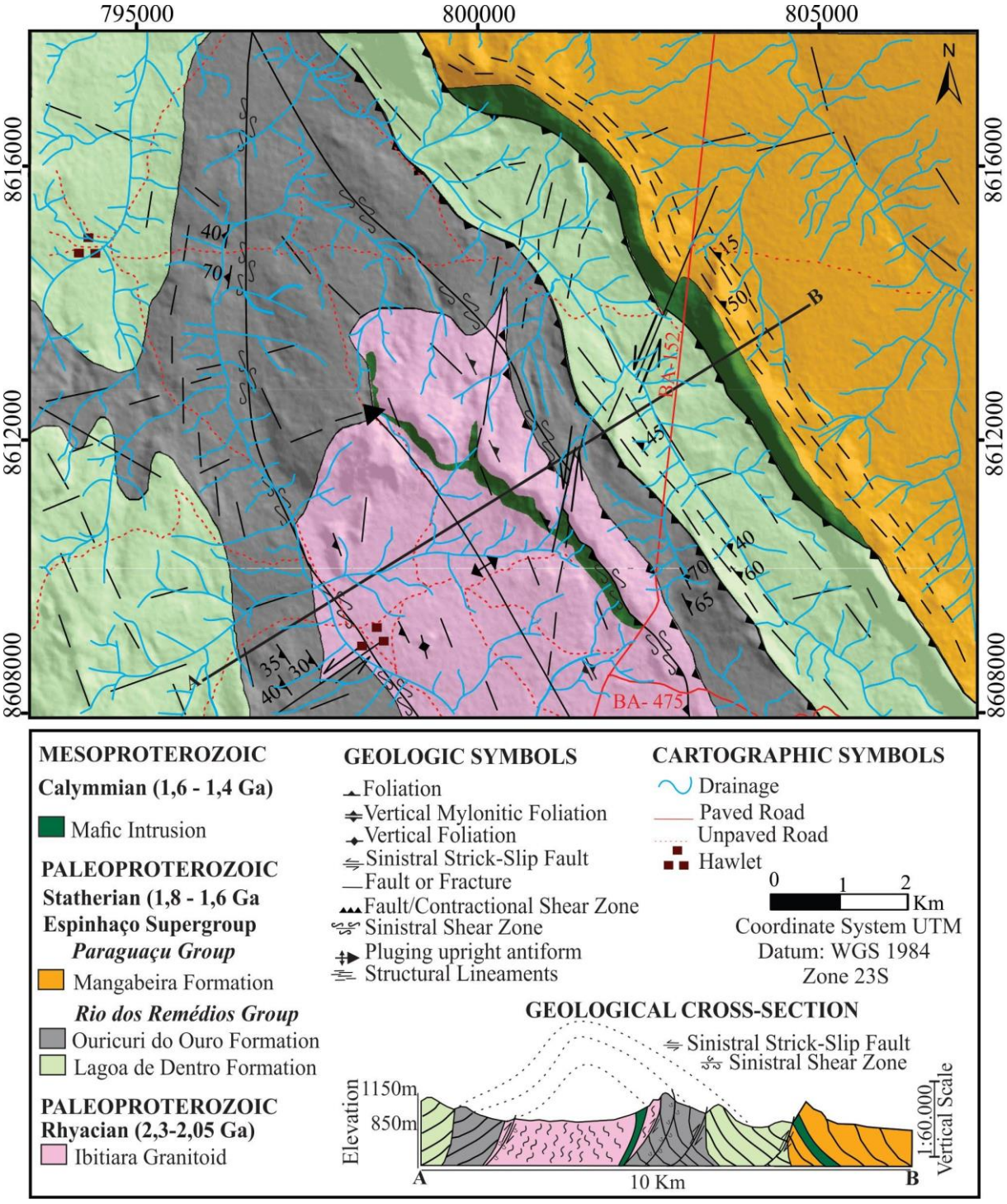

Figure 2: Simplified geological map of the study area along with geological cross-section. Map modified from Guimarães et al. (2005); Campos (2013); and Carlin (2018).

The Ibitiara Granitoid includes rocks of 2.091 ± 6.6 Ma, dated by U-Pb method in zircons (Guimarães *et al*., 2005), which were affected by epidotization, potassification, sericitization and hematization (CAMPOS, 2013; CARLIN, 2018). It prevails in a structural window, in the nucleus of an antiformal structure of direction NNW-SSE, surrounded by rocks of the Espinhaço Supergroup (CAMPOS, 2013).

In the study area, the main rocky outcrops occur as blocks (Figure 3A), along structural aligned hills, mainly in the northern end of the Ibitiara anticline. The granitoid is fine to medium grained, hololeucocratic, and vary from granitic to granodioritic composition. The most mineral constituents are quartz, altered plagioclase, altered K-feldspar (orthoclase), as well as muscovite, tourmaline, chlorite, hematite, magnetite and epidote. In general, these rocks are foliated, following the NNW-SSE regional trend, with inflections to NNE-SSW and high angle of dip.

The Espinhaço Supergroup encompasses rocks of the Rio dos Remédios Group, represented by Lagoa de Dentro and Ouricuri do Ouro tectosequences and by metasedimentary rocks of the Paraguaçu Group. According to Guimarães *et al*. (2005), the formations Lagoa de Dentro and Ouricuri do Ouro correspond to tectosequences of metasediments with interdigitated lateral contact. In the surveyed region, the best rocky expositions of the Lagoa de Dentro/Ouricuri do Ouro tectosequences are located at the top of undulating hills, as well as at the top of Mangabeira ridge and some roadcuts. Outcrops are mainly in blocks or flagstone and comprise mostly metasandstones and polimitic metaconglomerate with rounded pebbles and boulders related to basement rocks, as well as lithic metasandstones, metarkoses and metagraywackes (Figura 3B).

The Paraguaçu Group is represented by rocks of low metamorphism and deformation degree from the Mangabeira Formation, composed of metasandstones, impure metachert, and metasiltstone, and from the Araçuaí Formation, composed mainly of metagraywacke (GUIMARÃES *et al*., 2005). In the investigation area, those rocks are exposed mainly in the top of hills and escarpments of the Boqueirão de Fogo ridge. The outcrops occur as both, blocks, and flagstones, and comprise mainly metasandstones (Figure 3C).

Mafic rocks are intrusive into the rocks mentioned above, mostly in the form of dykes and sills. In general, they consist of gray to green and isotropic gabbros with thick plagioclase crystals (Figure 3D).

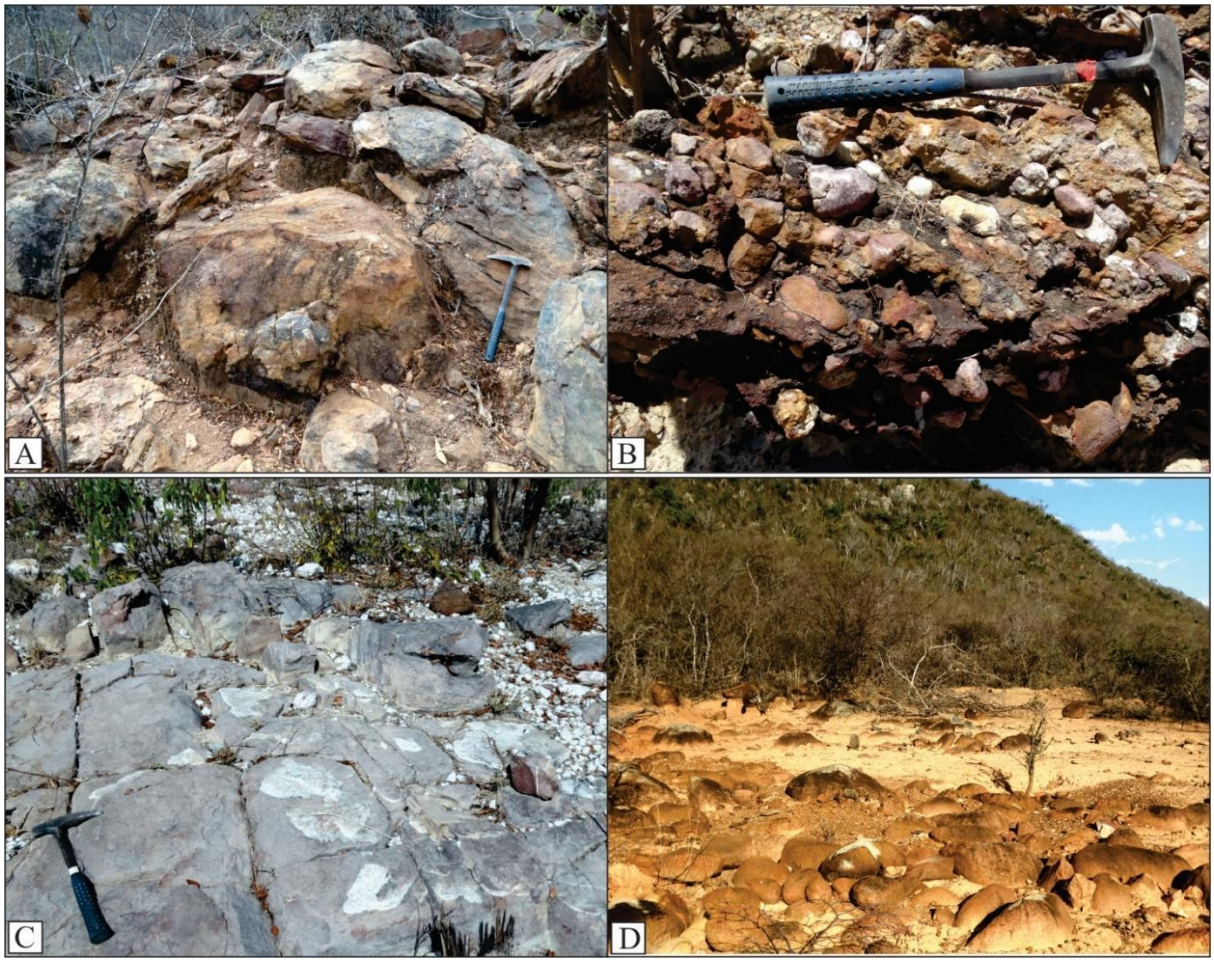

Figure 3: Outcrop photographs of main lithologies distributed in the study area. (A) Ibitiara Granitoid; (B) metaconglomerate of the Ouricuri do Ouro Formation; (C) Fractured Metasandstone of the Paraguaçu Group; (D) Blocks of isotropic metagabbro.

4.2 GEOMORPHOLOGY

In the study area, the elevation ranges from 850 meters to 1,150 meters. Most area is represented by flat landform and gently undulating hills surrounded by elongated, narrow and steep slope ridges. The drainage patterns consist mainly of trellis and rectangular, varying according to the litho-structural control. The geomorphological compartmentalization of the area encompasses three large units (Figure 4).

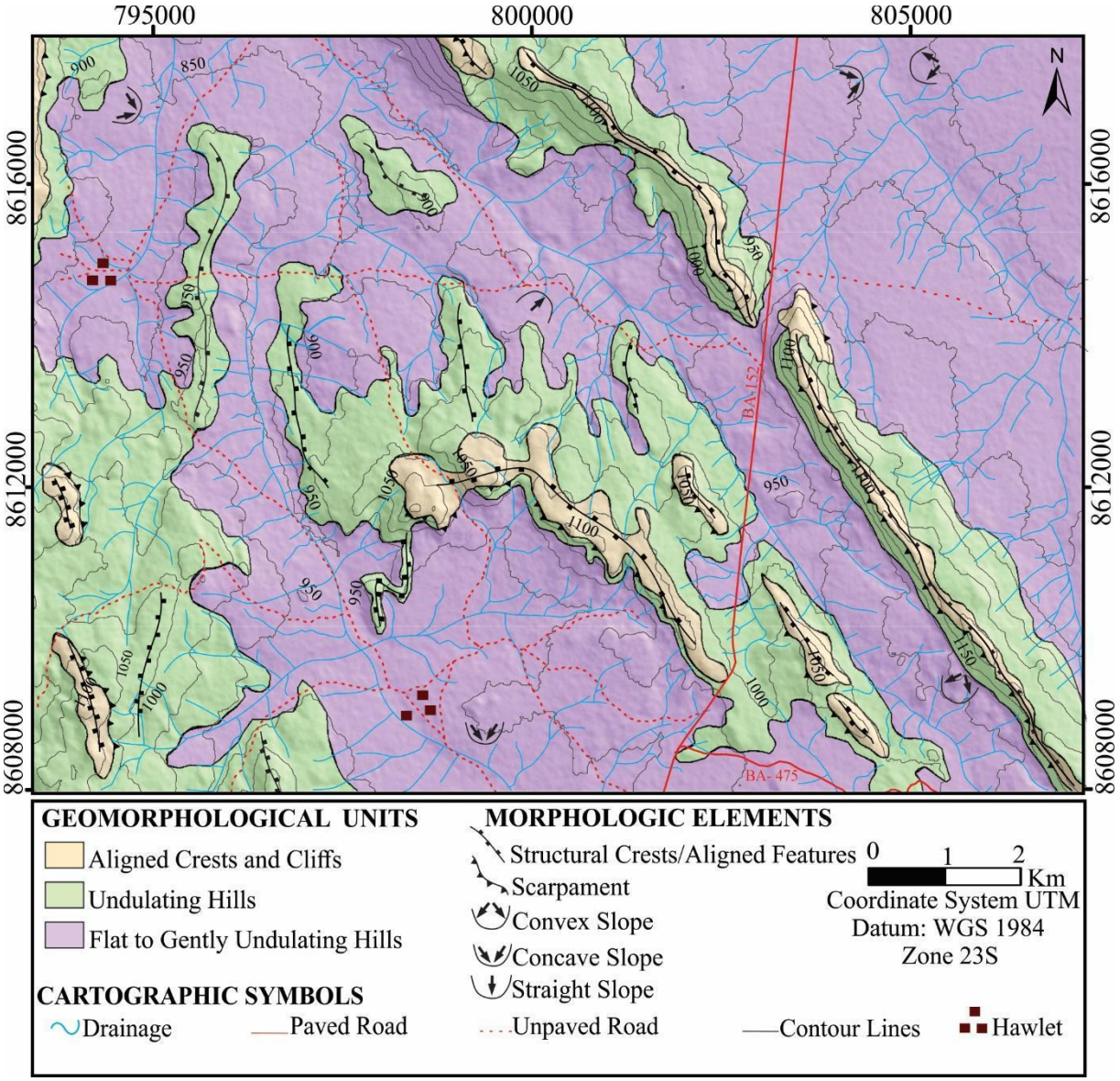

Figure 4: Simplified geomorphological map showing the major geomorphic compartments in the study area.

Unit I is comprised of parallel and aligned ridges and escarpments with steep slopes (> 45%) and low drainage density (Figure 5A). Unit II consists of undulating hills with slope top-bottom roughness less steep than Unit I (8%< slope < 45%). In general, the geomorphic features show convex or rounded top hills and medium to high drainage density (Figure 5B). Unit III encompasses a flat landform to gently undulating hills with predominantly rounded tops and medium to high drainage density (Figure 5C). In this unit, locally, rocky outcrops and relict features of rounded to flat hills top at higher altitudes arise (Figure 5D).

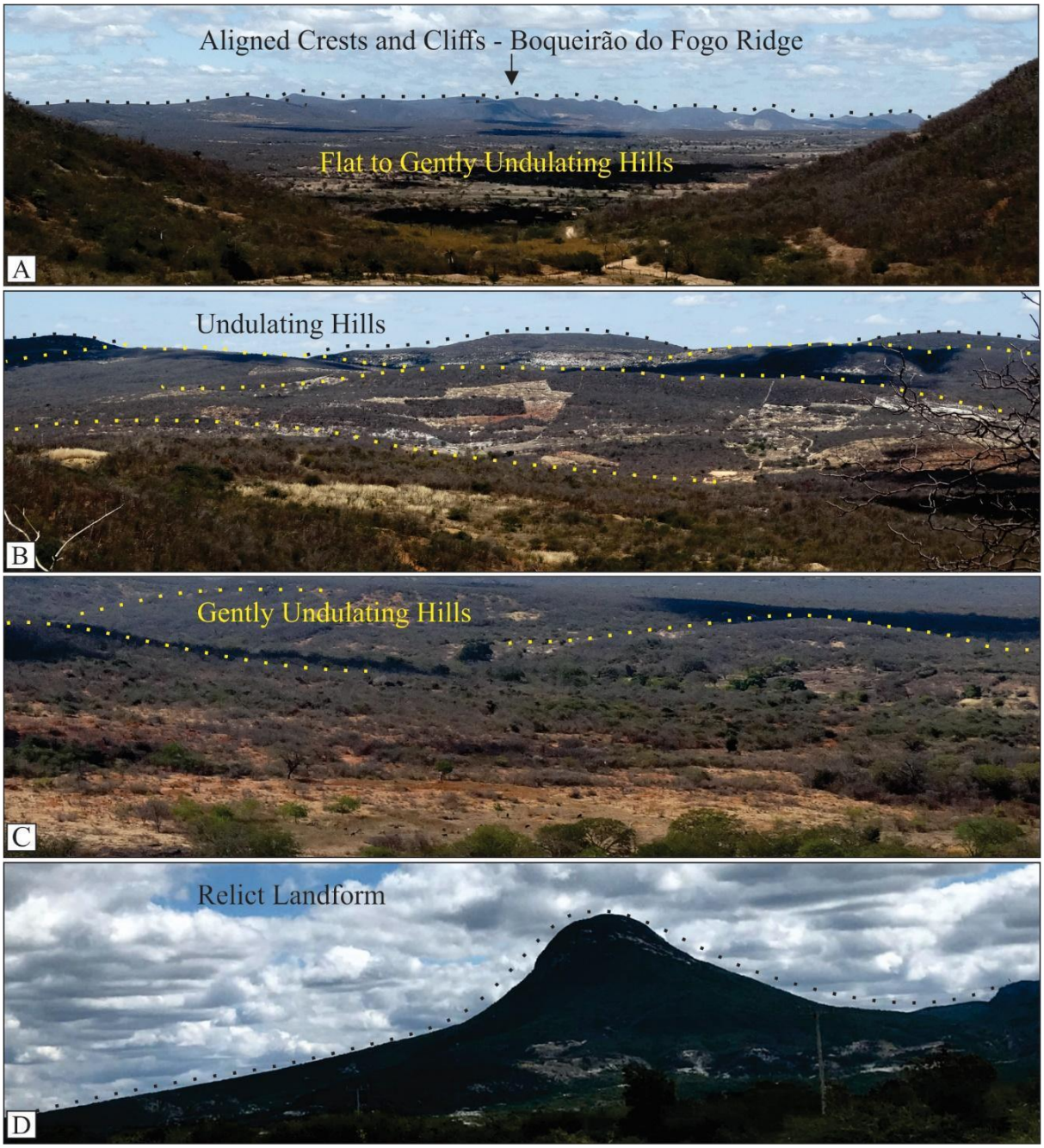

Figure 5: Field photographs of the landforms within the study area. (A) Undulating hills and flat to gently undulating terrain in front of aligned and parallel crests and cliffs of the Boqueirão do Fogo Ridge (Background); (B) Set of undulating hills; (C) Gently undulating hills to flat topography; (D) Relict landform made of metasedimentary rock.

4.3 PEDOLOGY

Soils in the Lavra Velha region consist predominantly of Oxisols, Alfisols, Entisols and Inceptisols as shown in the soil orders map (Figure 6).

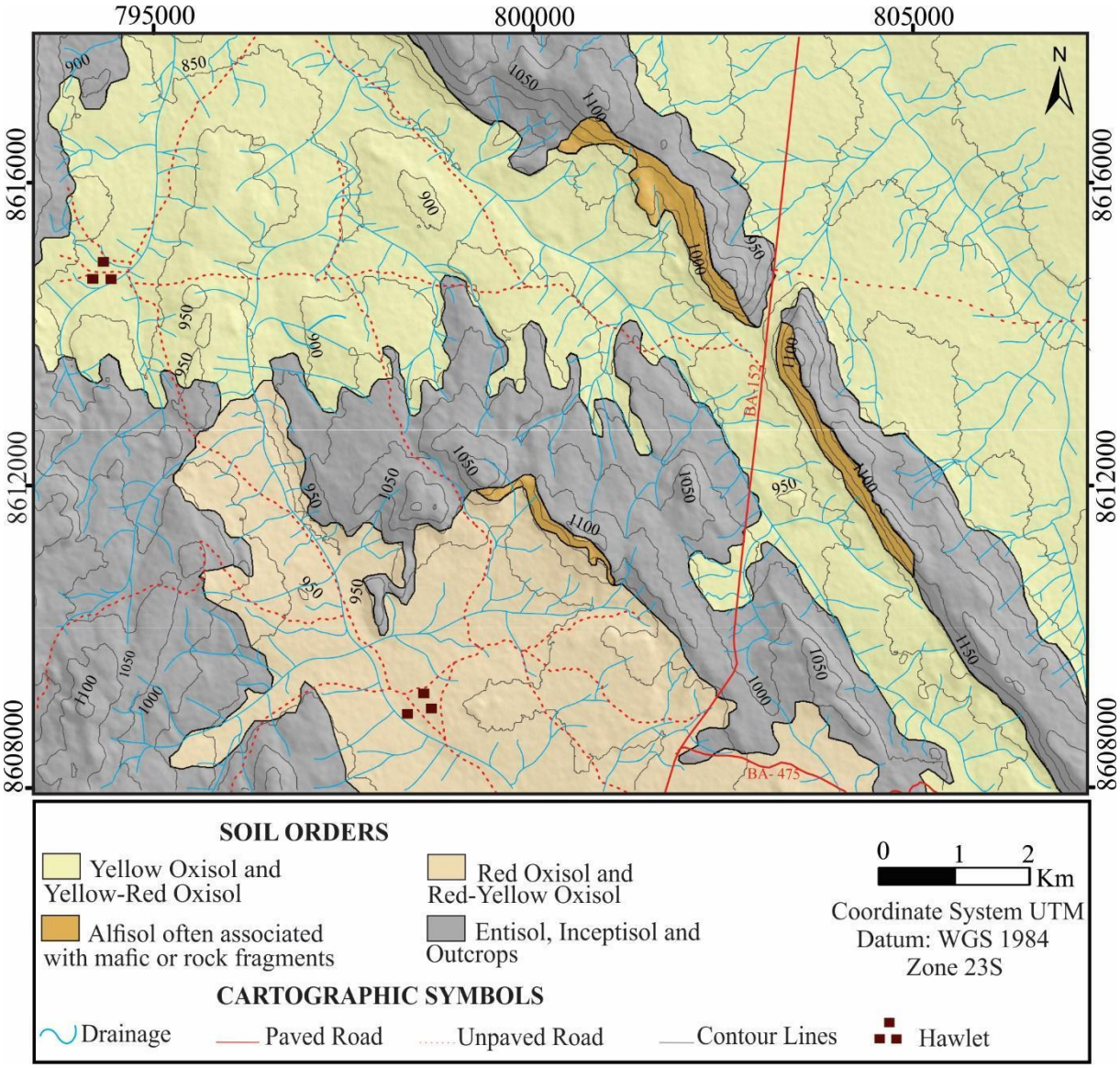

Figure 6: Soil orders map of the study area.

The Oxisols (Figure 7A, B, C) are deeper than 200 cm and shows little differentiation into horizons. They occupy 50% of the study area and consist generally of moderate A horizon with yellow-brown colors, and porous B horizon with sandy clay to clayey sand textures and colors ranging from yellow, red-yellow and red (variations 10R; 10YR; 7.5YR; 5YR and 2.5 YR in the Munsell color chart).

Concerning the Alfisols (Figure 7D), they are shallow and occupy only 1% of the study area. In general, they present an A horizon often marked by a cover with rock fragments of different sizes that characterize desert paving or surface stoniness. The B horizon is textural type with reddish colors (5YR and 2.5 YR in the Munsell color chart). Also, cracks can be observed in this horizon in function of the presence of 2:1 clay mineral.

Entisols is dominantly litholic and occurs constantly associated with Inceptisols and rock outcrops (Figure 7E and F). Because of this characteristic, we have chosen to group spatially these two soil orders. The Entisols is shallow, with moderate A horizon developed directly on C horizon. The texture is mainly sandy-loam and, occasionally, stony. It differs from the Inceptisols because of the absence of B horizon. Thus, the set (entisols and Inceptisols) occupies 49% of the study area, in which the main profile exposures occur in the Boqueirão do Fogo, Mangabeira and Lavra Velha ridges.

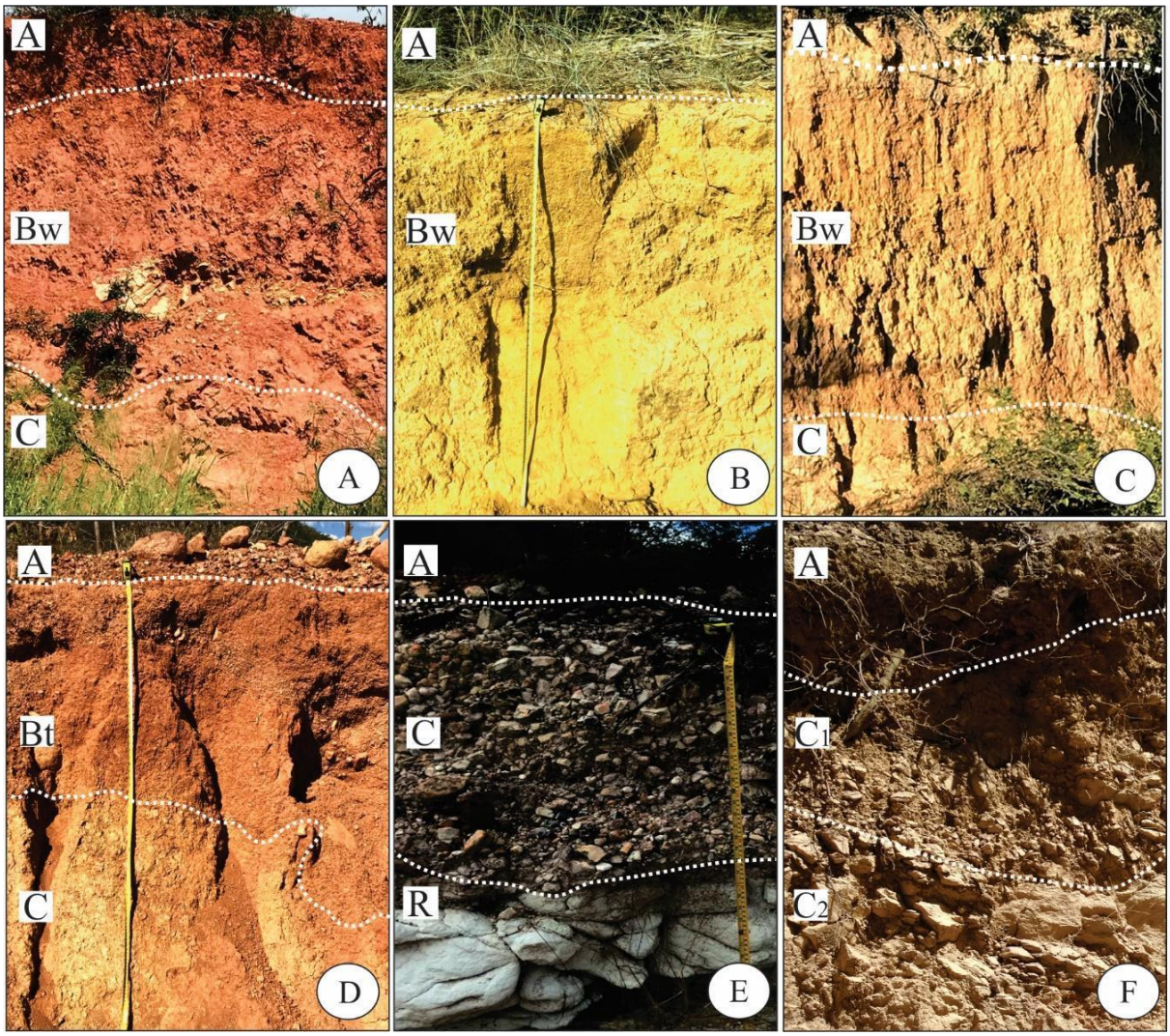

Figure 7: Soil profiles of the study area. (A), (B) and (C) red, yellow and red yellow Oxisols respectively; (D) Alfisol showing a surface stoniness; (E) and (F) Entisols formed on metasandstones and granite respectively. Abbreviations are from the Brazilian Soil Classification System: A= A Horizon, Bw=Weathered B horizon, Bt= Textural B horizon, C = C Horizon/saprolite, R= Bedrock.

4.4 GEOMORPHOPEDOLOGY

The geomorphopedological model established for the region of interest is consequence of the integrated analysis of geological, geomorphological and pedological data along with structural meanings obtained from laboratory and field works. Therefore, these units are not only a function of combined and overlapped rock-landform-soil data (morphopedological elements), but also of litho-structural factors in accordance with the work conducted by Villela et al. (2015). From this analysis, five main geomorphopedological units were defined (Figure 8).

Units I and II consist of Oxisols, which are associated mostly with gently undulating hills and flat landform present in open valleys. Locally, undulating hills may occur. While the Unit I is supported by crystalline rocks corresponding to the Ibitiara Granitoid, the Unit II is composed of metasedimentary rocks of the Ouricuri do Ouro and Lagoa de Dentro formations besides metasedimentary rocks of the Paraguaçu Group.

Unit III is composed of Alfisols associated to undulating hills. It mainly occurs at the bottom of slopes developed on the Ibitiara Granitoid and the Paragaçu Group, in which mafic intrusion occur. On this unit, there is often pebbles and boulders from gabbroic rocks in different stages of decomposition.

Units IV and V correspond to Entisols and Inceptisols associated with rock outcrops, which occur at parallel and aligned crests, and cliffs. The Unit IV is maintained by crystalline rocks related to the Ibitiara Granitoid, whilst the Unit V is supported by metasandstones and metaconglomerates of the Ouricuri do Ouro and Lagoa de Dentro formations, as well as by metasandstones of the Paraguaçu Group.

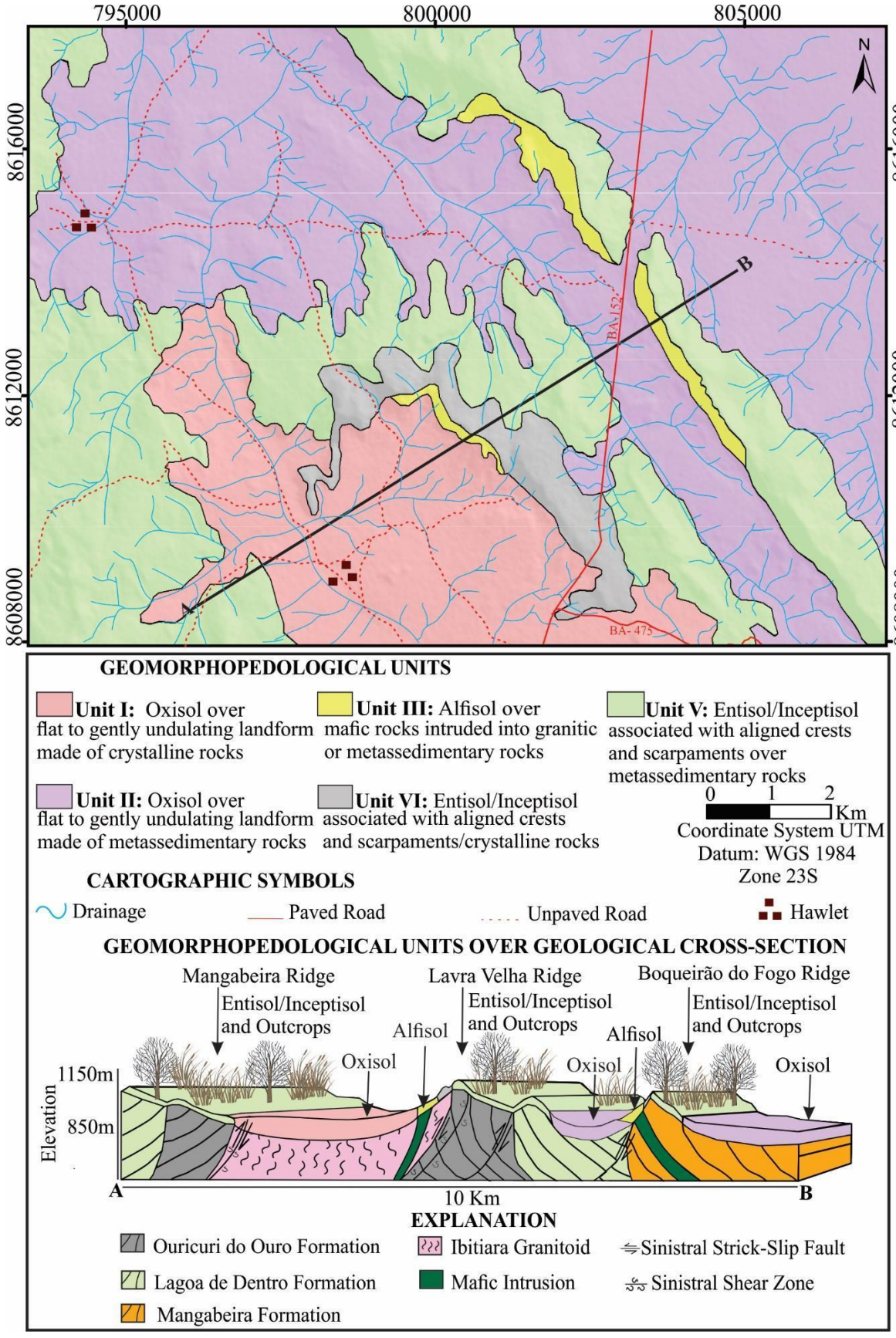

Figure 8: Geomorphopedological map of the study area along with a combination of relief-rock-soil cross-section.

5 DISCUSSION

5.1 ROCK-LANDFORM RELATIONSHIP AND PEDOGENETIC IMPLICATION

The Entisols and Inceptisols, developed on more pronounced landforms (slope> 45%), are located at the highest topographic levels (950m< altimetry> 1150m). Hence, the topography seems to have strong influence in the pedogenetic evolution of those soil types at Lavra Velha region by controlling weathering agents and development of weathered materials. This is due to the fact that areas with steep slope influence water infiltration, thus the soils are predisposed to less intense leaching and to become shallow. Therefore, by this mechanism, those soil types were possibly developed toward the top of the Lavra Velha, Boqueirão and Mantiqueira ridges. This perspective is agreed with the work carried out by Benites et al. (2007). These authors also reported Entisols and Inceptisols associated with rock outcrops toward the top of the Espinhaço mountain range, whose the development is a function mainly of topography and lithology.

Regarding bedrock influences on Entisols and Inceptisols formation, the presence of muscovite/sericite on soil profiles developed on granitoid, and quartz and clay minerals on soil profiles developed on rocks from Espinhaço Group, along with rock fragments from the lithology right under the soil profile, indicate incipient pedogenic processes which depend largely on primary minerals composition and their transformation into secondary minerals.

The Alfisols are associated with undulated landforms (8% < slope < 45%) in the sectors of altitudes which ranges from 900m to 1000m mostly. The occurrence of this soil order and litholic Entisols are quite common in these landforms in the northeast of Brazil (AGBENIN & TIESSEN, 1995). In the study area, the main occurrences of Alfisols are associated with mafic rocks intruded into the Ibitiara Granitoid and metasandstones of Paraguaçu Group. The development of these soils seems to be influenced not only by the strong rock-landform relationship, but also by the composition of the parent material. The landform controls surface weathering agents while mafic rocks are the main sources of raw material for soils' development. The mineralogy of those rocks, composed by calcium feldspar and ferromagnesian silicates, once transformed in secondary minerals generated soils with 5YR and 2.5YR shades and high activity clay. This result is consistent with the work conducted by Ribeiro (1974) in the Ibitiara city which describes similar soils developed on mafic rocks.

The yellow, red-yellow, and red Oxisols are formed in the flat and gently undulating landforms, at topographic levels that rarely exceed 950m and slopes often less than

20% steep. These landforms favor the infiltration of water and make the action of weathering agents more effective with more intense weathering down in the soil profile and close to bedrocks, including the formation of deeper soil. The development of these soils occurs on both metasedimentary and crystalline substrates. In the crystalline substrate, the Oxisols tend to be predominantly red-yellow or red, perhaps, due to the abundant presence of hematite, resulting from the hydrothermal alteration that affects the Granitoid Ibitiara, which were reported by Campos (2013) and Carlin (2018). On the other hand, when these soils are developed on rocks of the Espinhaço Supergroup, they are predominantly yellowish Oxisols, indicating the presence of goethite and smaller proportions or absence of hematite. This interpretation is based on Fontes (1991) and Resend (1976), who reported that goethite and hematite are not only the main Fe forms present in Brazilian Oxisols, but also the reason for their yellow and red colors.

5.2 STRUCTURAL SETTING OF LANDSCAPE AND SOIL DISTRIBUTION

The configuration of the landscape and the distribution of the soils of the Lavra Velha region seem to be strongly conditioned by litho-structural factors. The drainage and the landform patterns developed in old folded and exhumed geological setting, when associated with local and regional sections, along with litho-structural components, reveal the controls exerted by the compressive tectonic that affected the area. It was reported by Guimarães et al. (2005) and is in line with Campos (2013). The landscape shows a parallel and aligned ridge-and-valley landform displayed as a well typical Appalachian-style folded relief as mentioned in De Barros et al. (2019). Figure 9 (A, B and C) shows schematic and simplified block diagrams, adapted from Suertegaray (2003), in which are illustrated a generic evolution of a folded landform from the Appalachian landscape.

The geological setting, which the Lavra Velha region is included, was affected in varying degrees by NNW-SSE-trending shear zones and by dissimilar folding developed during the Brasiliano orogeny (GUIMARÃES et al., 2005; CRUZ & ALCKMIN, 2006). As a result, in the late proterozoic, the landscape was marked by a setting of anticline and syncline folds. De Vries & Benthem (2013), and Cawood & Bond (2019) report that during compressive structural events, the development of a serie of fracture families (longitudinal and transverse joints) is common in the closeness of the anticline hinge. Hence, those joints fractures would facilitate the ingress of weathering agents, such as water and plant roots and, consequently, effect landform evolution, as stated in the works conducted by Graham et al. (1994) and Oilier & Pain (1996). From this perspective, at the end of the Brasiliano orogeny,

the Lavra Velha region would be affected by weathering more intensively near to the anticline hinges because of the deformational structures that would increase the permo-porosity of the rocks in these areas. The weathering and geochemical erosion could be also heightened due to paleoclimate oscillation over geological time, which would contribute to the deeper soils formation (Ribeiro, 1974), as well as the collapse of anticlinal hinge areas. In this respect, the configuration of the Lavra Velha landscape region would be pronounced by ridges, represented mostly by limb portions or, perhaps, synclines, and valleys, represented mainly by anticlines, along NNW-SSE direction as indicators of the litho-structural control.

From the perspective of analyzing the landscape configuration, it becomes easier to understand patterns of soil distribution in the Lavra Velha region. The more developed soils are in the lower area of the terrain, which among others include the fold hinge zone of the Ibitiara Granitoid anticline. These areas, as mentioned previously, were probably more susceptible to the geochemical erosion that leaded to the collapse of the mineral structures present in the original rocks and, as a result, the lowering of the land-surface together with the development of deeper soils. This perception is in accordance with works conducted by Hill (1995), Oilier & Pain, (1996), and Frazier & Graham (2000). Those previous studies showed the differential weathering of fractured rocks, and, consequently, the influence of fractures on pedogenic processes in addition to their role in the transformation of bedrocks into soils.

Relative to the less developed soils, these are distributed in areas with sharp landform that reflect the structural crests aligned to the axis of the anticlinal fold, besides the shear zones. Beyond that, these soils also occur at the top of residual geological bodies that were shaped by old planation surfaces and thus recording differential erosion processes. These landforms are often found in the Brazilian semi-arid, and they represent portions of the substrate resistant to the processes of pediplanation and pedogenesis in the northeastern region (DOS SANTOS *et al.*, 2010).

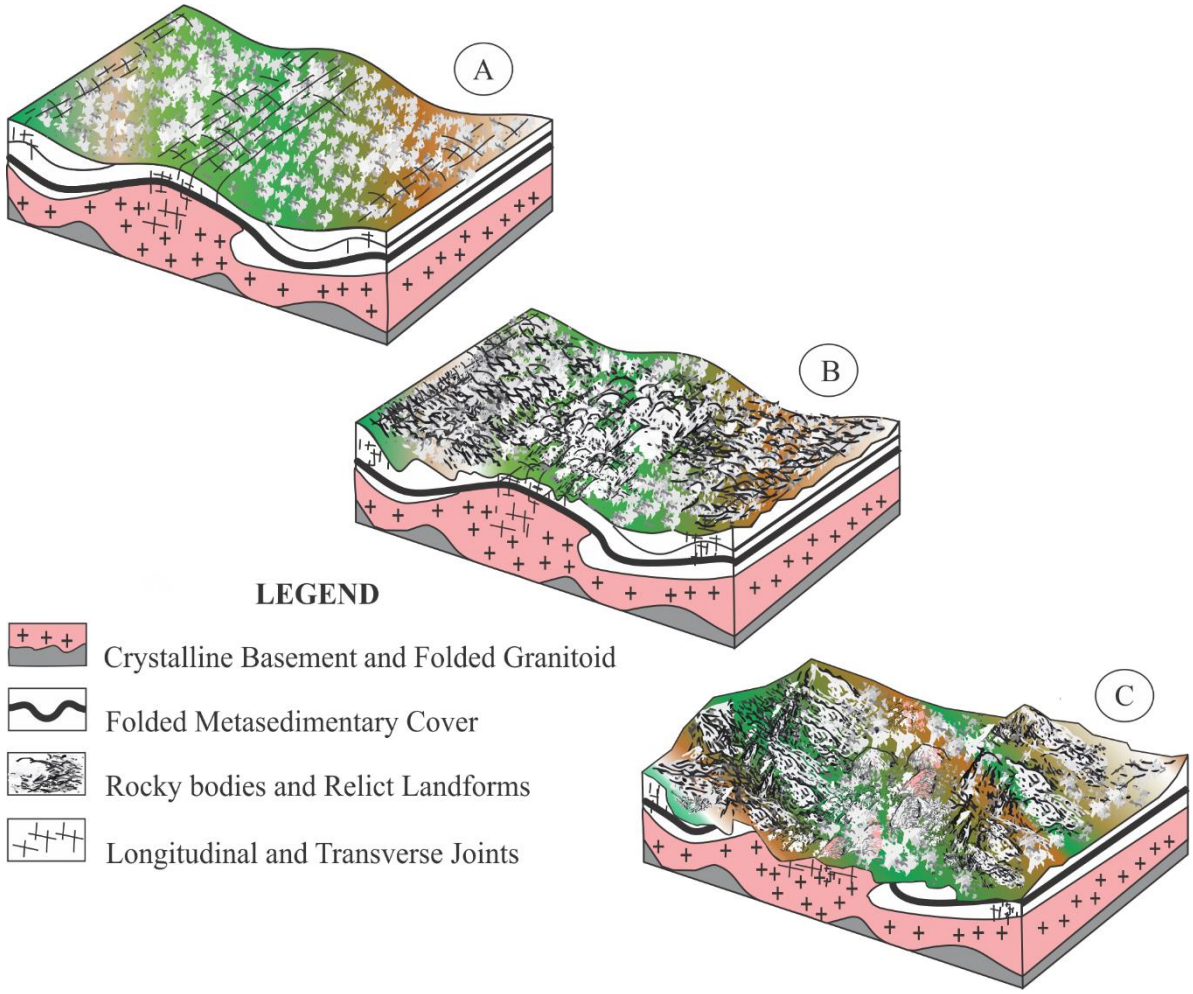

Figure 9: Schematic block diagrams illustrating a general landscape setting evolved from folded landform. The current landscape setting of the Lavra Velha region could be attributed to the general stages of this geomorphological evolution model. (A) Folded landforms with longitudinal and transversal joints associated to the anticline hinge. This area is most favorable for weathering since it has its permo-porosity increased by the set of fractures; (B) Lowering of the land-surface, mainly around the fold hinge. Rocky bodies may outcrop and remain as relict landforms; (C) Ridge and valley topography formed as result of the dissected landforms. Stages A, B and C are based on the Appalachian-style folded landform as described by Suertegaray (2003).

7 CONCLUSIONS

The rock-landform-soil relationship associated with litho-structural attributes allowed the definition of the main geomorphopedological units in the Lavra Velha region. The five mapped units are composed of Entisols, Inceptisols, Alfisols and Oxisols maintained by landforms and rocks associated with the Ibitiara Granitoid, the Espinhaço Supergroup and the mafic intrusions.

The structural landscape framework resembles the Appalachian-style folded landform as initially proposed by William Morris Davis and illustrated later by Suertegaray (2003). Landscape setting control the development and distribution of soils, in which deep soils (Oxisols) are associated with flat and gently undulating landforms, which denotes sectors intensively affected by deformational structures. On the other hand, shallow soils (Entisols and Inceptisols) are associated with higher altitude terrain that correspond mostly to parallel and aligned ridges. The distribution of Alfisols is mainly associated with lithology. These soils are developed from intrusive mafic rocks.

Other sectors in the western region of the Chapada Diamantina does not present mapping of the rock-landform-soil association. Thereby, the geomorphopedological model proposed in this work can be used for the prediction and individualization of similar units in other portions of this physiographic domain, in order to assist in technical and scientific studies. Higher altitude areas are favorable to the identification and mapping of lithologies and deformational structures, while areas associated to the lower landforms present the best exposures of soil profiles that could be useful to pedological and pedogeochemical surveys.

8 ACKNOWLEDGMENTS

The authors are thanked to the Coordination for the Improvement of Higher Education Personnel (CAPES) - Finance Code 001; to the Postgraduate Program in Geosciences of the Institute of Earth Science at the University of Campinas - UNICAMP, and to the members of Yamana Gold for their financial and logistical support for field work. We are also thanked to the geologist and master's student Simmon Viegas de Souza for assistance and useful discussions.

REFERENCES

AGBENIN, J. O.; TIESSEN, H. Soil properties and their variations on two contiguous hillslopes in Northeast Brazil. **Catena**, v. 24, n. 2, p. 147-161, 1995. DOI: https://doi.org/10.1016/0341-8162(94)00033-B

BATTILANI, G. A.; GOMES, N. S.; GUERRA, W. J. Evolução diagenética dos arenitos da Formação Morro do Chapéu, Grupo Chapada Diamantina, na região de Morro do Chapéu, Bahia. **Revista Geonomos**. v. 4, n. 2, p. 81-89, 1996. DOI: 10.18285/geonomos.v4i2.203.

BENITES, V. M.; SCHAEFER, C. E. G.; SIMAS, F. N.; & SANTOS, H. G. Soils associated with rock outcrops in the Brazilian mountain ranges Mantiqueira and Espinhaço. **Brazilian Journal of Botany**, v. 30, n. 4, p. 569-577, 2007. DOI: http://dx.doi.org/10.1590/S0100-84042007000400003

CASTRO, S. S.; SALOMÃO, F. X. T. Compartimentação morfopedológica e sua aplicação: considerações metodológicas. GEOUSP, São Paulo, n. 7, p. 27-37, 2000.

CAMPOS, L. D. **O Depósito de Au-Cu Lavra Velha, Chapada Diamantina Ocidental: Um exemplo de depósito da classe IOCG associado aos terrenos paleoproterozoicos do Bloco Gavião.** Dissertação (Mestrado), Instituto de Geociências, Universidade Federal de Brasília. 2013. 104p.

CARLIN, A. C.; ZANARDO, A.; NAVARRO, G. R. B. Caracterização petrográfica das rochas encaixantes da mineralização aurífera do Depósito Lavra Velha– região de Ibitiara, borda oeste da Chapada Diamantina, Bahia. **Geociências**, v. 37, n. 2, p. 253-265, 2018.

CAWOOD, A. J.; BOND, C. E. Broadhaven revisited: A New Look at Models of fault–Fold Interaction. **Geological Society of London, Special Publications**, v. 487. 2019. DOI: https://doi.org/10.1144/SP487.11

CRUZ, S.C.P. & ALKIMIM F.F. The tectonic interaction between the Paramirim Aulacogen and the Araçuai Belt, São Francisco Craton region, Eastern Brazil. Anais da Academia Brasileira de Ciências, v. 78, n. 1, p.151-173, 2006

CURI, N.; FRANZMEIER, D. P. Toposequence of Oxisols from the Central Plateau of Brazil 1. **Soil Science Society of America Journal**, v. 48, n. 2, p. 341-346, 1984. DOI:10.2136/sssaj1984.03615995004800020024x

DE BARROS, A.C.; AZEVEDO, C. T. B.; LIRA, D. R.; SILVA M. D.; SOUZA C. L.C. The semi-arid Domain of the northeast of Brazil. In Salgado, A.; Santos, L.; Paisani, J. (Org) **The Physical Geography of Brazil. Geography of the Physical Environment**. 2019. 119-150p. DOI: https://doi.org/10.1007/978-3-030-04333-9

DE VRIES, H. C.; BENTHEM, M. Analysis of fracture network geometries and orientations within a fold-and-thrust structure in the Northern Apennines, Italy. **Semantic Scholar**. 2013. 21p.

DOS SANTOS, J. M.; SALGADO, A. A. R. Gênese da superfície erosiva em ambiente semi-árido-Milagres/Ba: Considerações Preliminares. **Revista de Geografia** (Recife), v. 27, n. 1, p. 236-247, 2010.

FRAZIER, C. S.; GRAHAM, R. C. Pedogenic transformation of fractured granitic bedrock, southern California. **Soil Science Society of America Journal**, v. 64, n. 6, p. 2057-2069, 2000. DOI: 10.2136/sssaj2000.6462057x

FONTES, M. P. F.; WEED, S. B. Iron oxides in selected Brazilian Oxisols: I. Mineralogy. **Soil Science Society of America Journal**, v. 55, n. 4, p. 1143-1149, 1991. DOI: 10.2136/sssaj1991.03615995005500040040x

GUIMARÃES, J.T.; MARTINS, A.A.M.; ANDRADE FILHO, E.L.; LOUREIRO, H.S.C.; ARCANJO, J.B.A.; NEVES J.P.; ABRAM, M.B.; SILVA, M.G.; BENTO, R.V. **Projeto Ibitiara-Rio de Contas: Estado da Bahia, Programa Recursos Minerais do Brasil, Escala 1:200.000.** Publicação CPRM. Convênio CBPM/CPRM. Salvador, 2005. 193p.

INEMA (2014). **Instituto de Meio Ambiente e Recursos Hídricos.** Solos da Bahia.
http://www.inema.ba.gov.br/wp-content/files/MTematico_solos.pdf
[accessed: January 20, 2019]

HILL, S. M. The differential weathering of granitic rocks in Victoria, Australia. **AGSO Journal of Australian Geology and Geophysics**, v. 16, p. 271-276, 1995.

KÖPPEN, W. Das geographische System der Klimate. In: KÖPPEN, W.; GEIGER, R. **Handbuch der Klimatologie**. Berlin: Gebrüder Borntträger. 1936. 1- 44p.

LACERDA, M. P. C.; QUEMÉNÉUR, J. J. G., ANDRADE, H.; ALVES, H. M. R.; VIEIRA, T. G. C. Study of the relationship pedo-geomorphological in the soil distribution with argillic horizons in the landscape of Lavras (MG), Brazi. **Revista Brasileira de Ciência do Solo**, v. 32, n. 1, p. 274-284, 2008. DOI: http://dx.doi.org/10.1590/S0100-06832008000100026

LEPSCH, I. F.; BUOL, S. W.; DANIELS, R. B. Soil-landscape Relationships in the Occidental Plateau of São Paulo State, Brazil: II. Soil Morphology, Genesis, and Classification 1. **Soil Science Society of America Journal**, v. 41, n. 1, p. 109-115, 1977. DOI:10.2136/sssaj1977.03615995004100010031x

SEI. Superintendent of Economic and Social Studies of Bahia. Mapa Topográfico.

http://www.sei.ba.gov.br/site/geoambientais/mapas/pdf/municipal/mapa_descritivo_2913002.pdf . [January 20, 2019]

EMBRAPA (2001). **Superintendência de Estudos Econômicos e Sociais da Bahia**. Mapa de Solos.

https://www.sei.ba.gov.br/images/inf_geoambientais/cartogramas/pdf/carto_solos.pdf

[accessed: January 20, 2019]

SEVERO, G. D.; Melo, R. Geologia e Geoturismo na Chapada Diamantina. **Gestión Turística,** n.14, p. 69-81, 2018.

MEDEIROS, P. S. C. D.; NASCIMENTO, P. C. D.; INDA, A. V.; SILVA, D. S. D. Soil characterization and classification of granitic soils in toposequence in Southern Brazil. **Ciência Rural**, v. 43, n. 7, p. 1210-1217, 2013. DOI: 10.1590/S0103-84782013000700011

Nascimento, S. T., Castro, P. D. T. A., Azevedo, Ú. R. D. Geodiversidade dos compartimentos geomorfológicos do Anticlinal de Mariana, Minas Gerais. **Geociências**, v. 37, n. 3, p. 497-504, 2018.

OLLIER, C.; PAIN, C. Regolith, Soils and Landforms. **Geological Magazine**. v. 134, n. 1, p. 121-142, 1997. DOI:10.1017/S0016756897386130

RIBEIRO, L. P. **Caracterização dos solos de Ibitiara- BA**. Dissertação (Mestrado em Geociências). Instituto de Geociências, Universidade Federal da Bahia, Salvador. 1974. 113p.

SCHOBBENHAUS, C.; HOPPE, A.; BAUMANN, A.; LORCK, A. Idade U/Pb do vulcanismo Rio dos Remédios, Chapada Diamantina, Bahia**.** Congresso Brasileiro de Geologia. Balneário Camboriú. **Anais**... Balneário Camboriú: SBG. 1994. v. 2. 397-399p.

SUERTEGARAY, M.A. **Terra: feições ilustradas.** Editora da UFRGS, 2003. 264p.

THOMAS, A. L., DAMBRINE, E., KING, D., PARTY, J. P., & PROBST, A. A spatial study of the relationships between streamwater acidity and geology, soils and relief (Vosges, northeastern France). **Journal of hydrology**, v. 217, n. 1-2, p. 35-45, 1999.

DOI: https://doi.org/10.1016/S0022-1694(99)00014-1

TORRADO, P. V.; LEPSH, I.F.; CASTRO, S. S. Conceitos e aplicações das relações pedologia-geomorfologia em regiões tropicais úmidas. **Tópicos Ciências do Solo**, v. 4, p.145-192, 2005.

TORRADO, P. V.; MACIAS, F., CALVO, R., CARVALHO, S. G. D., & SILVA, A. C. Gênese de solos derivados de rochas ultramáficas serpentinizadas no sudoeste de Minas Gerais. **Revista Brasileira de Ciência do Solo**, v. 30, n. 3, p. 523-541, 2006. DOI: http://dx.doi.org/10.1590/S0100-06832006000300013

TRICART, J.; KILIAN, J. La eco-geografia y la ordenación del medio natural. Barcelona: Anagrama, 1979. 288 p.

TROEH, F. R. Landform Parameters Correlated to Soil Drainage 1. **Soil Science Society of America Journal**, v. 28, n. 6, p. 808-812, 1964.
DOI:10.2136/sssaj1964.03615995002800060035x

VILLELA, F. N. J.; ROSS, J. L. S.; MANFREDINI, S. Análise geomorfopedológica na borda leste da Bacia Sedimentar do Paraná, sudeste do Brasil. **Revista Brasileira de Geomorfologia**, v. 16, n. 4, p. 669-682, 2015. DOI: http://dx.doi.org/10.20502/rbg.v16i4.608

VILLELA, F. N. J.; ROSS, J. L. S.; MANFREDINI, S. Relief-Rock-Soil relationship in the transition of Atlantic Plateau to Peripheral Depression, Sao Paulo, Brazil. **Journal of Maps,** v. 9, n. 3, p. 343-352, 2013. DOI: 10.1080/17445647.2013.805170

CAPÍTULO - 3

3- SPECTRAL-MINERAL CHARACTERIZATION OF THE REGOLITH DEVELOPED IN THE LAVRA VELHA PROSPECT AND ITS SIGNIFICANCE FOR MINERAL EXPLORATION, CHAPADA DIAMANTINA, BRAZIL

Josué Souza Passos

Diego Fernando Ducart

Carlos Martin Medina

Alfredo Borges de Campos

SPECTRAL-MINERAL CHARACTERIZATION OF THE REGOLITH DEVELOPED IN THE LAVRA VELHA DEPOSIT AND ITS SIGNIFICANCE FOR MINERAL EXPLORATION, CHAPADA DIAMANTINA, BRAZIL

Josué Souza Passos[1], Diego Fernando Ducart[1], Carlos Martin Medina[1], Alfredo Borges de Campos[1]

[1]Institute of Geosciences, State University of Campinas (UNICAMP)

ABSTRACT

Hydrothermal deposits are commonly characterized by mineral and geochemical signatures that prolong beyond the orebody. These footprints are vastly used in exploration programs but often obscured by regolith profiles developed on the surface. Visible near infrared (VNIR) and shortwave infrared (SWIR) were used to perform spectral-mineral characterization of the regolith developed on the Lavra Velha iron oxide-copper-gold deposit, located in the Chapada Diamantina region, northeastern Brazil. The deposit contains gold mineralized bodies developed at different depths and hosted by rocks that show sericitization, iron oxide formation, saussuritization, and albitization. Three sectors of regolith profiles representing different evolution scenarios over the deposit were selected for mineral and geochemical characterization based on bedrock, geoforms and regolith thickness. The mineral assemblages determined from regolith VNIR and SWIR data along with prior geochemical information allowed to separate distinct mineral associations that dominate each sector. They are (1) poorly crystalline kaolinite found in shallow regolith profiles developed on metaconglomerates (sector I), (2) phengite + nontronite + well-crystalline or well-ordered kaolinite found in deeper regolith profiles that overly granitic rocks intruded by several mafic rocks (sector II), and (3) well-crystalline muscovite found in shallow regolith profiles that cover granitic rocks (sector III).The phengite + nontronite + well-ordered kaolinite association is the potential footprint for zones of higher grades of gold found in the studied regoliths. The combined use of spectral-mineral and geochemical data of weathered materials showed to be a useful exploration technique to recognize regolith footprints potentially associated with deeper mineralized zones in the study region.

Keywords: Lavra Velha, Spectral Analysis, Regolith Footprint, Mineral Exploration

1 INTRODUCTION

Regolith has been a significant challenge for mineral prospecting and exploration as it often hides several footprints associated with ore deposits, such as mineralogical and geochemical signatures (Laukamp et al., 2016; Anand, 2016). Because of this, researchers and prospectors have attempted to create and improve methodologies and techniques that allow to recognize footprints in regolith profiles aiming at finding deeper mineral deposits (Laukamp et al., 2016; Lampinen et al., 2017).

The Lavra Velha area is located in northeastern Brazil (Campos 2013; Carlin et al., 2017) and is covered by regoliths with different depths. In this area, there is an iron-oxide-copper-gold (IOCG) deposit also named Lavra Velha that is part of the Western Chapada Diamantina Gold Province reported recently by Texeira et al. (2019). Most geological studies carried out on that deposit were focused on petrography, geochemistry, and hydrothermal alteration of bedrocks and host rocks (Campos 2013; Carlin et al., 2017; Medina, 2020). However, outcrops and mineralized zones are often covered by regoliths, which potentially can be used for prospecting ore deposits. Therefore, there is a need to investigate correlations between regolith profiles and target-prospecting in order to better guide exploration programs and to support professionals to focus their work on areas with higher probabilities of successful exploration.

In general, X-ray diffraction (XRD), optical spectroscopy, electron microprobe, and petrography are techniques applied to identify and describe regolith components however, they are expensive and time-consuming. The use of reflectance spectroscopy (e.g. Laukamp et al., 2016; Lampinen et al., 2017; Burley et al., 2017), integrated with fieldwork and geochemistry, have become an advantage procedure to carry out similar work (Lampinen et al., 2019). This is because this technique is inexpensive, non-destructive, and a fast tool to characterize hydrothermal and weathered materials, thus improving mineral exploration.

Reflectance spectroscopy is based on absorption. While iron oxides (e.g. hematite) produce typical absorption patterns in the visible near infrared (VNIR) spectral region, hydroxyl-bearing minerals (e.g. kaolinite, mica, and smectite) have diagnostic absorption patterns in the short-wave infrared (SWIR) (Meurier, 2005). The absorption patterns of Fe oxides are mainly caused by electronic processes involving bonded Fe^{+3}, for instance, to an octahedral site by oxygen ligands (hematite) or oxygen and hydroxyl ligands (goethite), while in clay minerals they are results of a combination of Al-OH, Fe-OH and Mg-

OH bending, and OH stretching vibrations (Clark et al., 1990). Based on absorption data and patterns, mineralogical information such as relative abundance, composition, and crystallinity of several minerals can be acquired (Clark et al., 1990; Van der Meer, 2004; Cudahy et al., 2008; Haest et al., 2012; Prado et al., 2015).

The aim of this work was to characterize the regoliths developed over the Lavra Velha deposit for improving mineral prospecting in this auriferous district. To achieve this we look at trends in VNIR-SWIR absorption data as indicators of mineral occurrence in the regoliths and relate the trends to corresponding geological and geochemical data collected from drill cores samples of the targeting areas. The spectral-mineral data were also examined to detect changes in mineral relative abundance, crystallinity, and composition throughout the deposit.

2 GEOLOGICAL SETTING

2.1 Regional Geology

The geological framework outlined here relies on studies conducted by Almeida et al., (1981), Guimarães et al. (2005), Cruz and Alkmin (2006), Campos (2013), Carlin et al. (2018), and Teixeira et al. (2019).

In a regional geological context, Lavra Velha is in the Paramirim Aulacogen, in northern of the São Francisco Craton (SFC), northeastern Brazil **(Figure 1A)**. The SFC is bounded by the Neoproterozoic Brasília, Araçuaí, Rio Preto, Riacho do Pontal, and Sergipano fold-thrust belts **(Figure 1B)**, and it is broadly covered by Precambrian and Phanerozoic successions, among which includes the Paramirim Aulacogen and the São Francisco Basin (Cruz & Alkmim, 2006).

The Paramirim Aulacogen corresponds to a NNW direction structure, which evolved from superposed and partially inverted paleo-Neoproterozoic rifts **(Figure 1B)**. The basement is inserted in the Gavião Block domain, which represents the segment of the oldest rocks of the São Francisco Craton (Cruz & Alkmim, 2006). The Paramirim Aulacogen evolution started in the Paleoproterozoic with the formation of aborted intracratonic rifts, along with N-S and NW-SE direction faults, on which the Espinhaço Supergroup was deposited (Schobbenhaus, 1996). During the Brasiliano orogeny, the collision between the Amazon and São Francisco cratons, and the interaction of the Araçuaí Belt with the Paramirim

Aulacogen resulted in its partial inversion because of the WSW-ENE shortening. Thus, the distensional structures were progressively inverted towards the south of the Aulacogen (Cruz & Alkmim, 2006). A zone of maximum inversion cut the aulacogen in the NNW-SSE direction, and it corresponds to the Paramirim Corridor (Alkmim et al., 1993). The origin of this Corridor is associated with the imbrication of basement rocks under the supracrustal rocks, along the rift axis. This structure encompasses rocks of the Espinhaço and São Francisco supergroups (Alkmim et al., 1993).

2.2 Local Geology

The local geology of the study area and the cooper-auriferous deposit (Au>Cu) of Lavra Velha, the main target of this work, comprise rocks of the Granitoid Ibitiara, the Espinhaço Supergroup, besides intrusive mafic rocks **(Figure 1C)**. The Ibitiara Granitoid includes rocks of 2.091 ± 6.6 Ma, dated by the U-Pb method in zircons (Guimarães *et al*., 2005), which were affected by epidotization, potassification, sericitization, and hematization (Campos, 2013; Carlin, 2018). The main rock outcrops occur as blocks, along structurally aligned hills, mainly in the northern end of the Ibitiara anticline. The granitoid is fine to medium-grained, hololeucocratic, and varies from granitic to granodioritic composition (Carlin, 2018). The mineralogy is made of quartz, altered plagioclase, altered K-feldspar (orthoclase), as well as muscovite, tourmaline, chlorite, hematite, magnetite, and epidote.

The Espinhaço Supergroup encompasses the Rio dos Remédios Group, represented by Lagoa de Dentro and Ouricuri do Ouro tecto-sequences, and the Paraguaçu Group. The Lagoa de Dentro and Ouricuri do Ouro formations (Guimarães et al., 2005) correspond to metasediments with interdigitated lateral contact. Outcrops are found mainly as blocks or flagstone and comprise mostly metasandstones and polymictic metaconglomerates with rounded pebbles and boulders related to basement rocks, as well as lithic metasandstones, metarkoses, and metagreywacke. Souza (2017) reports that the Ouricuri do Ouro Formation corresponds to alluvial fan systems made up of distinct facies associations involving proximal deposits of non-cohesive debris-flow, proximal and intermediate sheet-floods, and distal sandy flood plains.

The Paraguaçu Group is represented in the study area by rocks of low metamorphism and deformation degree from the Mangabeira Formation. It indicates the expiry of the alluvial systems controlled by mechanical subsidence and the onset of a passive

sedimentation stage in arid conditions (Guimarães et al., 2005), and comprises meta-sandstone, impure metachert, and metasiltstone.

Mafic rocks are intrusive into the rocks mentioned above. In general, they consist of gray to green and isotropic gabbros with thick plagioclase crystals. Teixeira (2005) reports that these rocks belong to the tholeiitic magmas series, and Guimarães et al. (2005) obtained the age of 1.49 ± 0.3 Ga by U-Pb method in zircons.

The structural design encompasses folds, sinistral strike-slip faults, narrow shear zones, foliations and structural lineaments. The rocks follow a NNW-SSE orientation with inflections to NNE-SSW, which are reflections of larger regional structures (Alkmim et al., 1993), and correspond to the presence of the structural features found in the area. The Ibitiara Granitoid prevails in the nucleus of an antiformal fold with NNW-SSE direction, surrounded by rocks of the Espinhaço Supergroup, which is characterized by a foliation of the same direction and dip of several angles to SW and NE.

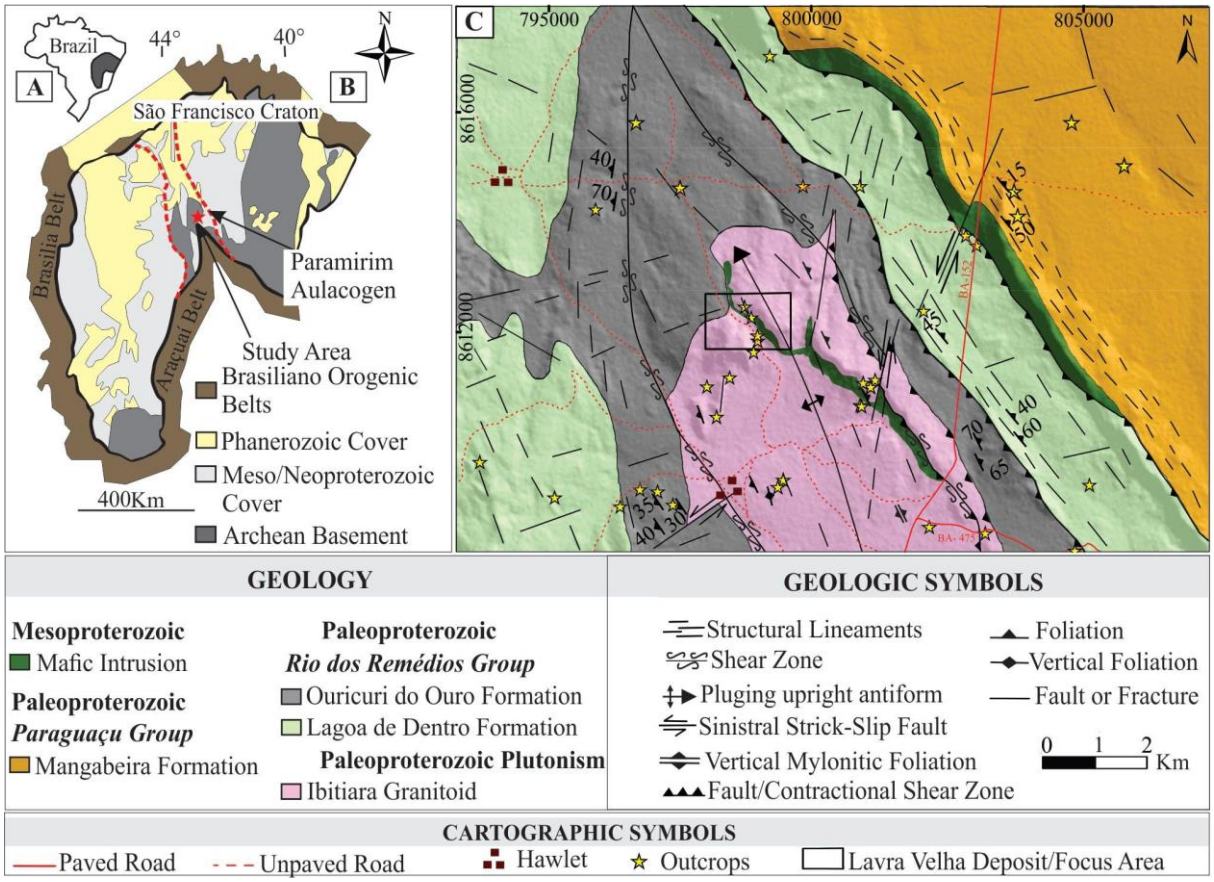

Figure 1. *Simplified geologic framework of the Lavra Velha region. (A) Location of the São Francisco Craton in Brazil. (B) Location of the Paramirim Corridor, where the study area is inserted (red star), in São Francisco Craton (Cruz and Alkmim, 2006). (C) General geology of the Lavra Velha area and location of the Lavra Velha Deposit (Black Square). Geology Map modified from Guimarães et al. (2005), Campos (2013), Carlin (2018), and Yamana Gold intern reports.*

3 LANDSCAPE FEATURES

Considerations about the landscape features of the Lavra Velha region have been described regionally by Oliveira (1968), Guimarães et al. (2005), and more locally by Ribeiro (1974), and Passos et al. (2020).

Regionally, the landform is represented by the Sertanejo Pediplain and by elongated and parallel ridges, with north-south direction, belonging mostly to the Espinhaço Supergroup Oliveira (1968). Locally, three large units have been defined for the geomorphological compartmentalization (Passos et al., 2020) with elevation ranging from 850 meters to 1,150 meters. These are: (i) parallel and aligned ridges and escarpments with steep slopes (> 45%) and low drainage density; (ii) undulating hills with slope top-bottom roughness less steep (8% < slope < 45%); and (iii) flat landform to gently undulating hills with predominantly rounded tops and medium to high drainage density.

The association of regional and local sections shows that the landform directly reflects underlying structures and lithologies, thus revealing the controls exerted by the compressive tectonic that affected the area as studied by Guimarães et al. (2005). The landscape exhibits a parallel and aligned ridge-and-valley landform displayed as a well typical Appalachian-style folded relief (Passos et al., 2020).

Deep valleys were formed from the metasedimentary rocks of the Espinhaço Supergroup and the Ibitiara Granitoid. These areas coincide mostly with hinge areas, including the Ibitiara Granitoid hinge zone. The hinge areas were more susceptible to the geochemical erosion that led to the collapse of the mineral structures present in the original rocks and, as a result, the lowering of the land-surface (Passos et al., 2020). The Granitoid Ibitiara and Espinhaço Supergroup are also exposed as steep-sided ridges that represent portions that record differential erosion processes.

The climate of the Lavra Velha region is typically semi-arid, hot, and dry, corresponding to the BSh climate in the Koppen (1936) classification. The annual average temperature is 26.5 °C and the average annual rainfall is 746 mm, with higher rainfall volumes from October to April. The predominant vegetation is the open arboreal caatinga, without palms. Soil orders consist predominantly of Oxisols, Alfisols, Entisols, and Inceptisols (Ribeiro, 1974; Passos et al., 2020).

4 MATERIAL AND METHODS

4.1 Drill Holes and Fieldwork

A quantity of 170 meters of regolith from 17 vertical to inclined drill holes was selected to represent the lateral and vertical stratigraphic, mineralogical, and geochemical variations of the regolith developed on the prospect. The drill holes were distributed in three sections with ENE-WSW direction of the Lavra Velha Prospect area. To better understand the relationship among different regolith units and ore at depth, the drill holes were chosen from both mineralized and unmineralized locations.

Additionally, those data were complemented and associated with geology, geomorphology, and pedology information from the specialized literature and from a fieldwork campaign previously performed at the Lavra Velha area to recognize and correlate the landscape features of its surroundings. Detailed information can be found in the work conducted by Passos et al, (2020).

4.2 Reflectance Spectroscopy and Mineralogy

A total of 680 reflectance spectra were measured on the regolith profiles from all 17 drill cores of the Lavra Velha targets. The measurements were carried out every 25 centimeters of the drill cores using an Analytical Spectral Device - Inc. TerraSpec™ 4 Hi-Res spectroradiometer. The spectra were converted from radiation to reflectance using the Spectralon^{TM} signal, which was calibrated every 15 minutes during data collection.

The device enables the simultaneous collection of reflectance spectra in the visible and near-infrared (VNIR; 350–1000 nm), and short-wave infrared (SWIR; 1000–2500 nm) wavelength ranges. The two wavelength ranges, collected by the spectroradiometer, allow rapid mapping of major regolith forming minerals, through the identification of specific absorption patterns related to specific ions or molecular bonds. The VNIR can be used to characterize, for example, iron oxides and REE, whereas the SWIR, the spectral region applied in this study, enables the characterization of hydroxyl-bearing minerals including white micas, kaolin and smectites.

The slope of the spectral curves from 600 to 740 nm was used to diagnosticate iron hydroxides. The absorption feature around 860 nm allowed identifying hematite, whilst

the absorption feature at 920 was used to recognize goethite, which has been done in previous works (Hunt and Ashley, 1979; Townsend, 1987).

Spectral data were analyzed using the commercial software SCIRO/The Spectral Geologist (TSG-8). The automatic classification of the TSG software was tested as the first approach for mineral identification. After that, the spectral data were processed, and their parameters determined. In this respect, the classification of each mineral was carried out based on its spectral features as has been done in previous studies (Clark et al., 1990; Cudahy et al., 2008; Haest et al., 2012; Naleto et al., 2019). This mineral recognition was conducted to avoid doubts about the TSG mineral automatic recognition and, therefore, to better characterize each mineral specimen. The relative abundance, composition and crystallinity, referred to as mineral structural order in this work, of white mica, kaolinite, and smectites were obtained based on their hydroxyl-related absorption features following works conducted by the authors previously mentioned.

The kaolinite relative abundance was acquired from the calculation of the depth of the Al-OH absorption pattern at 2208 ± 3 nm. The kaolinite structural order was obtained from the reflectance ratio at 2,160 and 2,180 nm plus the depth of the absorption at 2208nm, according to Senna et al., (2008).

The white mica relative abundance was calculated from measuring the depth of the ~2200 Al-OH absorption (Clark, 1999; van Ruitenbeek et al., 2006). The white mica crystallinity index was defined by the division of the depth of Al-OH absorption at ~2200 nm by the absorption at ~1900 nm (e.g., Sonntag et al., 201). The shifts in the wavelength of the feature around 2200 nm were used to separate Al-poor white mica (muscovite) from Al-rich white mica (phengite) (Duke, 1994).

The absorption pattern around 2,290 nm was used to assess the nontronite relative abundance. To do so, it was measured the differences in depth of the 2290 nm feature, and then, it was compared to Al-OH clay absorption around 2200 nm as carried out by Naleto et al. (2019).

4.3 Geochemical Analysis

Regolith samples for geochemical analysis were taken at intervals of 1-meter maximum from vertical profiles provided by Yamana Gold Company. The elemental analyses were carried out using the 4 acids or aqua regia dissolution (1:3 of HNO_3 and HCl) methods

for extraction of Al, Ca, Fe, Mg, Na, P, K, S, Ti (in %), As, B, Ba, Be, Bi, Cd, Ce, Co, Cr, Cu, Ga, La, Li, Mn, Mo, Ni, Pb, Sb, Sc, Se, Sn, Sr, Th, Tl, U, V, W, Y, Zn e Zr (in ppm) e Au (in g/t). The Au was analyzed via lead collection fire assay on 50g samples. Trace elements were determined by inductively coupled plasma mass spectrometry (ICP-MS) and major elements by inductively coupled plasma optical emission spectroscopy (ICP-OES). All geochemical analyses were carried out at the ALS Chemex laboratories, in Peru.

5 RESULTS

5.1 REGOLITH SECTORS AND STRATIGRAPHY

Five main geomorphopedological units were determined in the Lavra Velha region from the rock-landscape-soil association (Passos et al., 2020) for an area of 150 Km^2 at a scale of 1:100,000. Three local sectors were chosen in the Lavra Velha prospects based on regolith profiles and underline rock type (**Figure 2)**. Each sector represents a portion of the main ore targets in the deposit: West, East and Central Lavra Velha. Figure 2 also provides three cross-sections that were chosen to investigate the mineral distribution and variation along the deposit area. The main stratigraphic characteristics observed in the regolith profiles encompassed by each sector can be seen in **Figure 3**. The major aspects of the sectors are also available as follow:

The western portion of the Lavra Velha deposit is occupied by sector I. It consists of a structured hill, better seen in Figure 1, that is part of a geomorphological unit of parallel and aligned ridges at the regional scale (Passos et al., 2020). The regolith profiles were developed immediately on the polymictic metaconglomerate of the Ouricuri do Ouro Formation varying from one to four meters in depth. Saprolites are clayey-sand, yellowish, and with some rocky fragments in the transition to bedrock. The soil surface is porous, with brown-reddish to yellow-brownish colours, and few remnants of organic matter.

The sector II consists of a carved central portion, delimited by a strike-slip fault and an inferred fault. In this sector, regolith profiles comprise deeper distinct horizons (reaching up to 30 meters depth) evolved on the Ibitiara Granitoid. The bedrock is often intercepted by mafic rocks, controlled by faults, and identified along the drill holes. From the bedrock/saprorock, colours vary in greenish and pinkish in the saprolite with sandy-clayey contents and mafic rock fragments. Upper mottled horizons are sandy-clayey, with whitish-

pink and reddish-white portions. The surface soil layers are deep, with pale-brown to yellowish-brown colours, porous and friable textures, and vestige of organic matter.

The sector III is characterized by aligned and structured hills with steep slopes located in the southwestern and eastern portions of the area (Figs. 1 and 2). The regolith profiles are poorly developed compared to the profiles of sector II. They consist of shallow horizons formed from the Ibitiara Granitoid. Overall, the bedrock gradually changes upward to a mottled sandy-clayey saprolite with preserved granitic fragments and muscovite crystals. Soil layers are thin, with pale-brown to dark-brown colours, porous and friable textures, and organic matter traces.

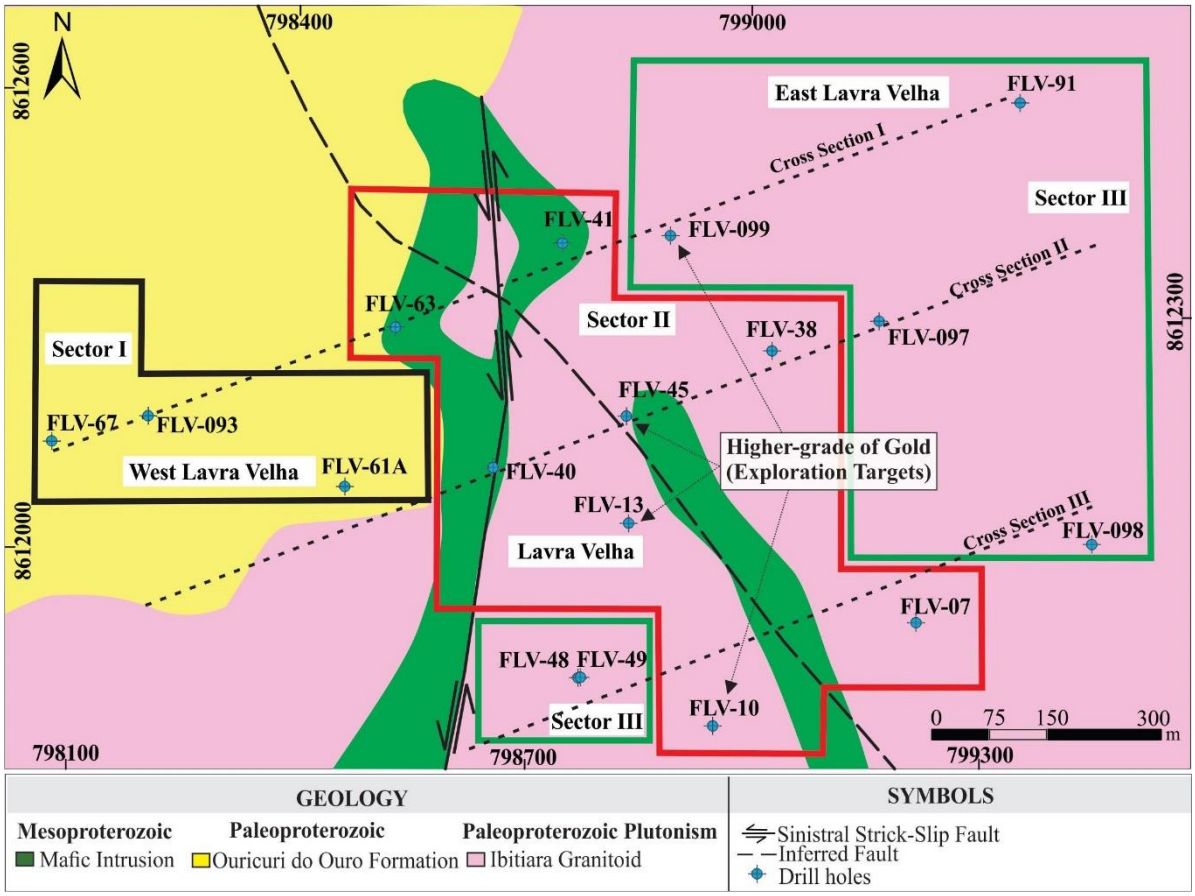

Figure 2. *Geology and Regolith sectors at the Lavra Velha gold deposit site. Sectors are based on regolith depth and bedrock type. The map is based on works conducted by Guimarães et al. (2005), Campos (2013), Carlin (2018), and Yamana Gold intern reports.*

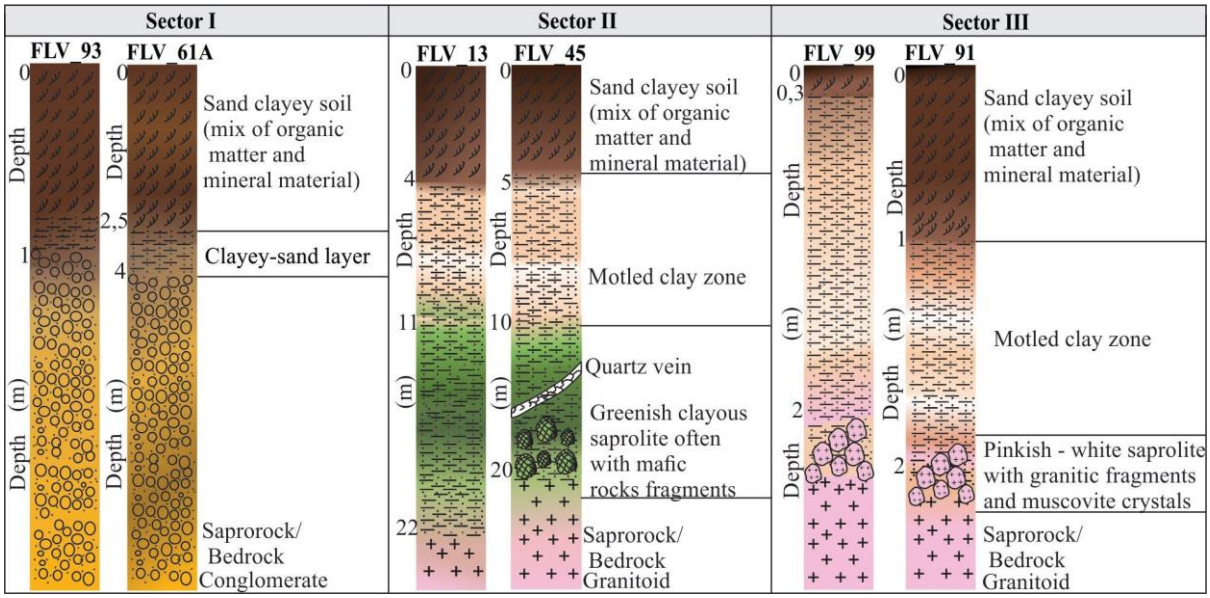

Figure 3. *Stratigraphy of the main regolith profiles at the Lavra Velha gold deposit site. Each sector is illustrated by two representative drill holes.*

5.2 REFLECTANCE SPECTRA: MINERAL IDENTIFICATION

In the spectral interpretation, pure samples mean that no other clay minerals are mixed in, and impure samples mean that at least two Al-OH clay mineral associations were identified. The main recognized clay minerals were white mica, kaolinite, smectite and (nontronite). Tourmaline and chlorite were sporadically found. Fe oxides such as hematite and goethite were also detected. **Figure 4** shows the most significant spectral features of samples distributed in the regolith of the deposit area.

The slope of the spectral curves from 600 to 740 nm is typically used to identify iron oxides, and the absorption feature from 850 to 1000nm allows the separation of iron hydroxides in function of their composition (Hunt and Ashley, 1979). While the absorption feature to identify hematite is around 860 nm, to goethite is around 920 nm (Townsend, 1987). Absorption positions between them are related to mixtures of hematite and goethite.

Kaolinite was identified in spectra by the concisely positioned OH and Al-OH doublet SWIR absorptions at around 1400 nm plus 1415 nm and 2208 nm plus 2160 nm. Although in spectral mixtures with white micas there is an overlap of spectral features, mainly in the 2208 nm wavelength region, kaolinite could be recognized by a consistent inflexion at 2160 nm.

White micas were recognized by the absorption feature at around 2200 nm in addition to the secondary features around at 2350 nm and 2440 nm. These absorption patterns occur due to the presence of Al-OH bound in the octahedral layer and are the result of OH stretch combined to the Al-OH bending mode (Clark et al., 1990). The absence of the absorption feature between 2160 nm and 2180 nm allows to separate this mineral group from kaolinite. The absorption features around 1400 nm, because of OH and H_2O vibration, and around 1900 nm caused by H_2O, were used to determine the white mica crystallinity and, therefore, to separate well-crystalline white mica (muscovite) from poor-crystalline white mica (illite). The variation of the wavelength around 2200 nm also allowed for separating Al-poor white mica, such as phengite, from Al-rich white mica, like muscovite.

Montmorillonite was identified by the typical absorption features related to OH, H_2O and Al-OH bounds, at around 1,410 nm, 1910 nm and ~2200 nm, respectively. Nontronite has similar OH and H_2O absorptions, but it also has a diagnostic absorption feature at around 2290 nm as result of the stretching and bending vibrational modes of the Fe-OH bonds.

Absorptions related to tourmaline were identified in spectra in which kaolinite or white mica are the dominant active minerals. Tourmaline generates an absorption feature at around 2,250 nm assigned to the Fe-OH and Mg-OH molecule bounds or, perhaps, to the B-OH bonds (Clark et al., 1990). Tourmaline also yields a faint absorption at around 2300 nm that may be used to indicate its presence in mixture spectra.

Chlorite was investigated by the following absorptions features: absorption between 2240 - 2270 nm, associated with Fe-OH bounds, and between 2310 - 2370 nm associated with Mg-OH bounds. However, it was not found any spectra of a pure mineral. Since it also gives rise to an additional absorption on mixture spectra at around 2250 nm, we used the tourmaline weak absorption at around 2300 nm to distinguish these two minerals.

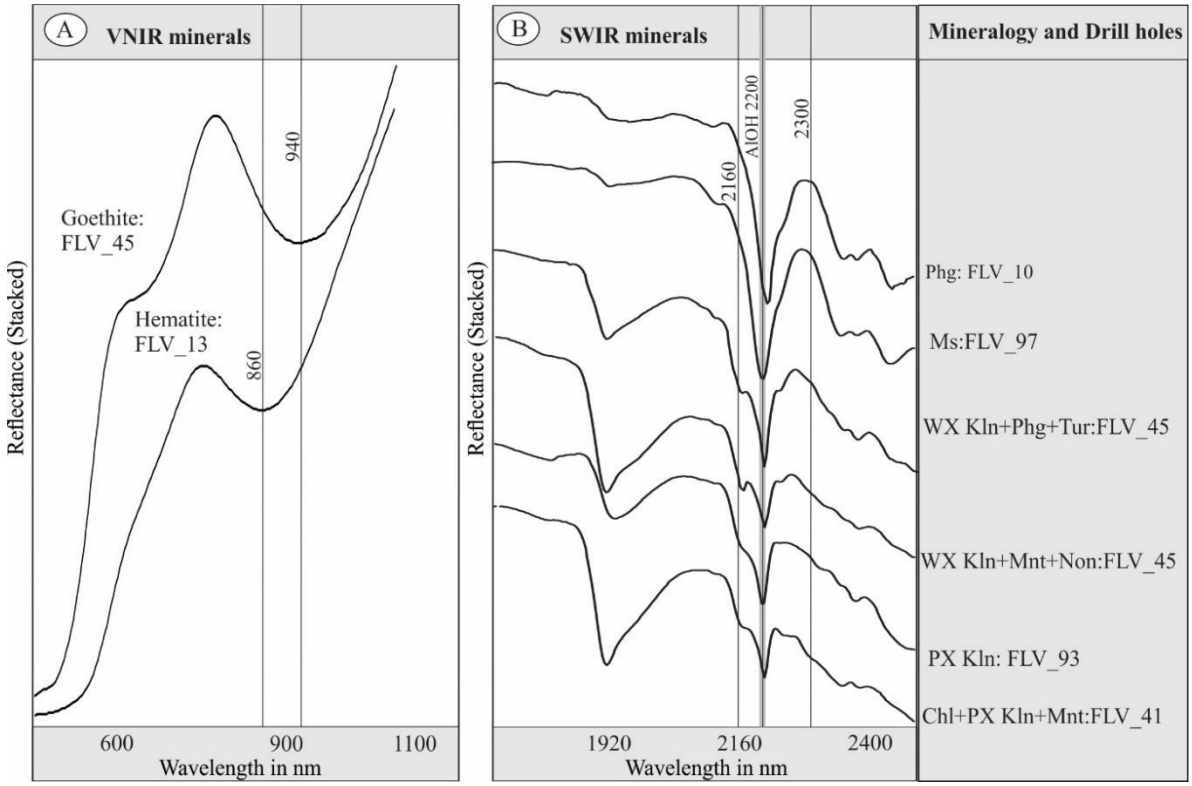

Figure 4) *Representative spectra of the mineral assemblages found in the regolith developed on the Lavra Velha deposit. Abbreviations: poorly Crystalline (PX), well- crystalline (WX), muscovite (Ms), kaolinite (Kln), montmorillonite (Mnt), nontronite (Non), tourmaline (Tur), and Chlorite (Chl).*

5.3 MINERALOGICAL DISTRIBUTION

The most common clay minerals recognized from the Lavra Velha regolith indicate a spatial distribution that coincides with the sectors previously defined in this work (**Fig. 2**). Each sector presents a dominant group of clay minerals. The results obtained using the "The Spectral Geologist" software (TSG - V.8) for the main mineral assemblage groups are presented in **Figure 5.** Overall, there is a significant positive correlation among mineral distribution, regolith profiles and bedrocks. As expected, a larger variety of mineral specimens is present in well-developed regolith developed on the Ibitiara Granitoid associated with mafic rocks. On the other hand, a few mineral specimens dominate poorly developed regoliths. Al-OH absorption feature in Sector I is mainly associated with kaolinite, whilst in Sector III, white mica is the dominant active mineral with kaolinite and tourmaline as subordinates. Regarding the Sector II, white mica, kaolinite, montmorillonite and nontronite occur often as main minerals, while tourmaline and chlorite as mineral traces.

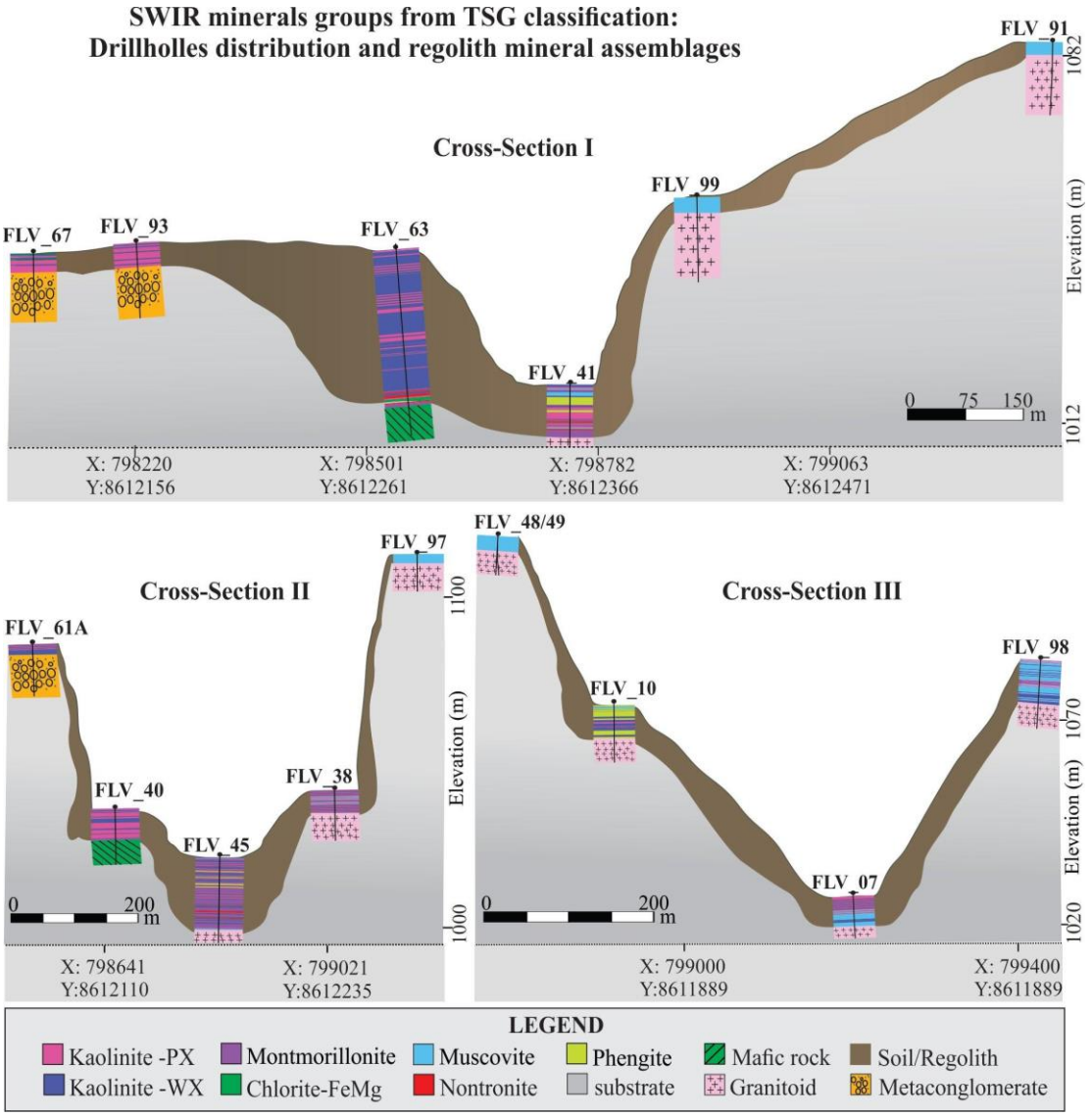

Figure 5) *Mineral distribution and variation along several drill holes of the Lavra Velha deposit. The classification was carried out by using the TSG software. PX and WX stand for poorly crystalline and well-crystalline, respectively.*

5.3.1 Iron (hydro-) oxides distribution

The frequency and distribution of iron hydroxides across the area of the Lavra Velha deposit can be seen from the histogram in **Figure 6**. Since there is a larger number of samples in sector II, because of the thickness of the regolith, the iron hydroxides are significantly present in this area. Hematite and goethite are clearly well distributed in the regolith obtained from all drill holes. However, while hematite tends to be predominant in most parts of the deposit, goethite appears often in sectors II and III.

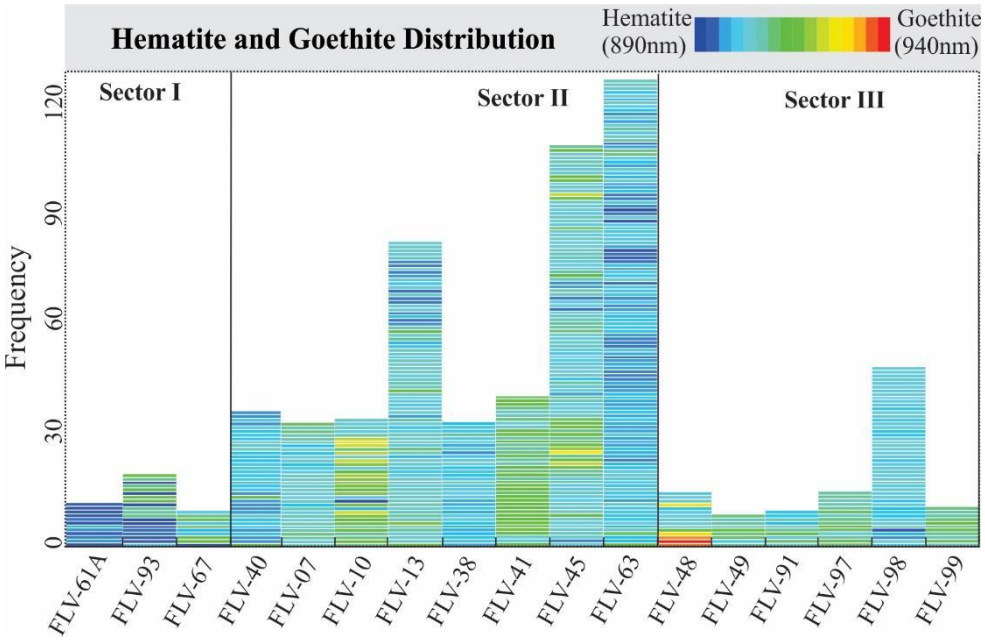

Figure 6) *Distribution of iron hydroxides spectra in regolith profiles of the Lavra Velha deposit.*

Kaolinite: distribution, abundance, and crystallinity

Figure 7 shows the frequency and distribution of the purest spectra of kaolinite, as well as information of kaolinite abundance and crystallinity along each drill hole. For the analysis, only pure spectra of kaolinite were used in order to have no influence of another Al-OH clay mineral that had diagnostic absorption feature between 2185 and 2210 nm, such as white mica and smectite (Clark et al., 1990). A noticeable increase in kaolinite abundance in samples from drill holes of the sector I toward the sector II was detected. Otherwise, in sector III, kaolinite was not identified or only as trace amounts, which precluded investigating its abundance and crystallinity in the regolith profiles of that sector. In most samples of the sector I, where regolith is right over the polymictic metaconglomerate, the kaolinite presented lower crystallinity, which is in clear contrast to kaolinite spectra of the sector II (e.g. FLV_45, FLV_67, FLV_38, FLV_07). In this last, kaolinite showed well-crystalline and, therefore, has a well-ordered structure.

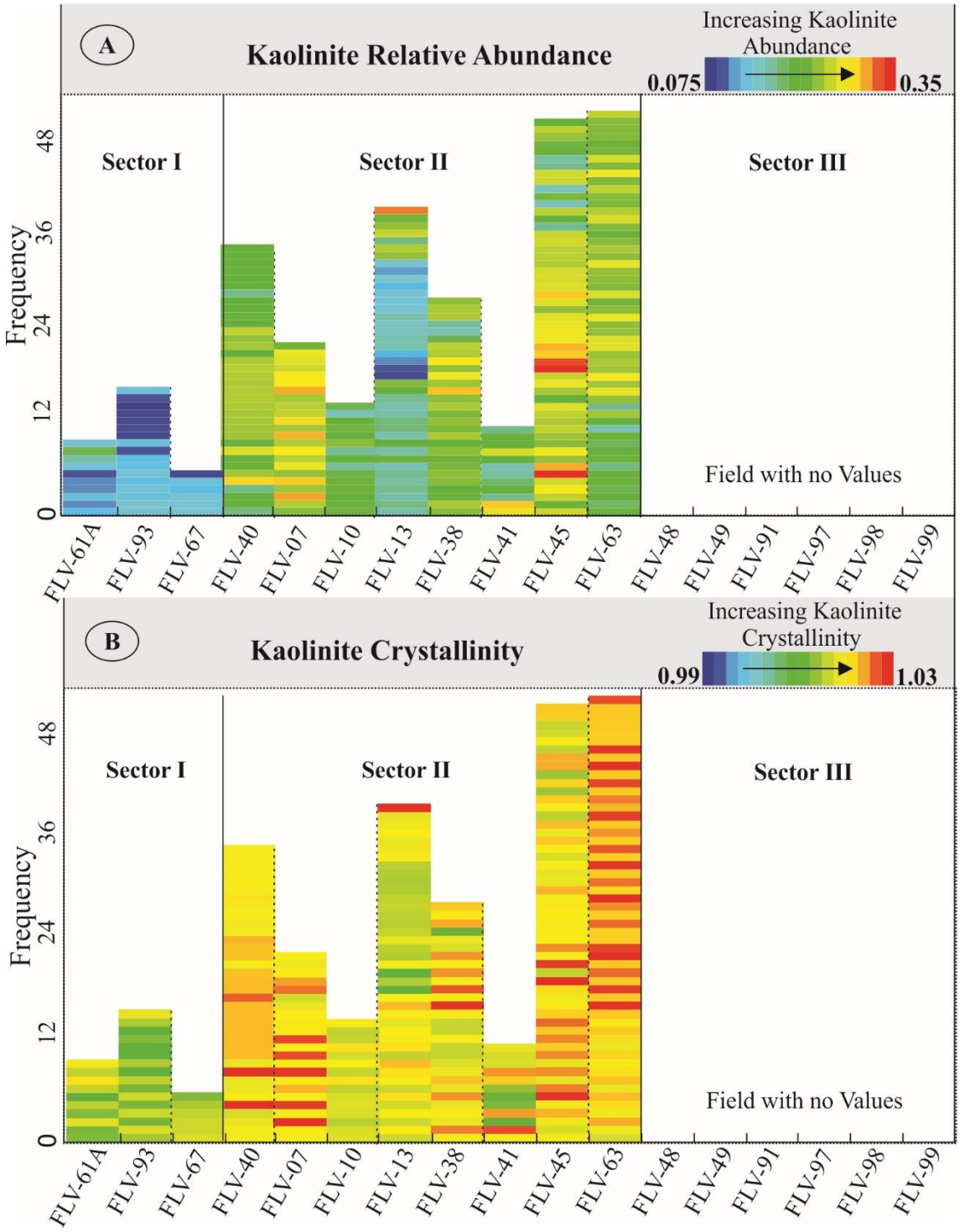

Figure 7) *Kaolinite in regolith profiles of the Lavra Velha deposit. (A) Relative abundance is higher in profiles from sector II. (B) Well-ordered kaolinite occurs mainly along drill holes from sector II, while lower ordered kaolinite in sector I. Field with no values represents drill holes in which kaolinite was not found or was spectrally impure.*

5.3.2 Nontronite abundance

Figure 8 provides nontronite frequency and distribution**.** There is an evident concentration of this clay mineral in the regolith of sector II, mainly in samples from FLV_13,

FLV_45 and FLV_63. In contrast, nontronite was not identified in the drill holes related to the I and III sectors.

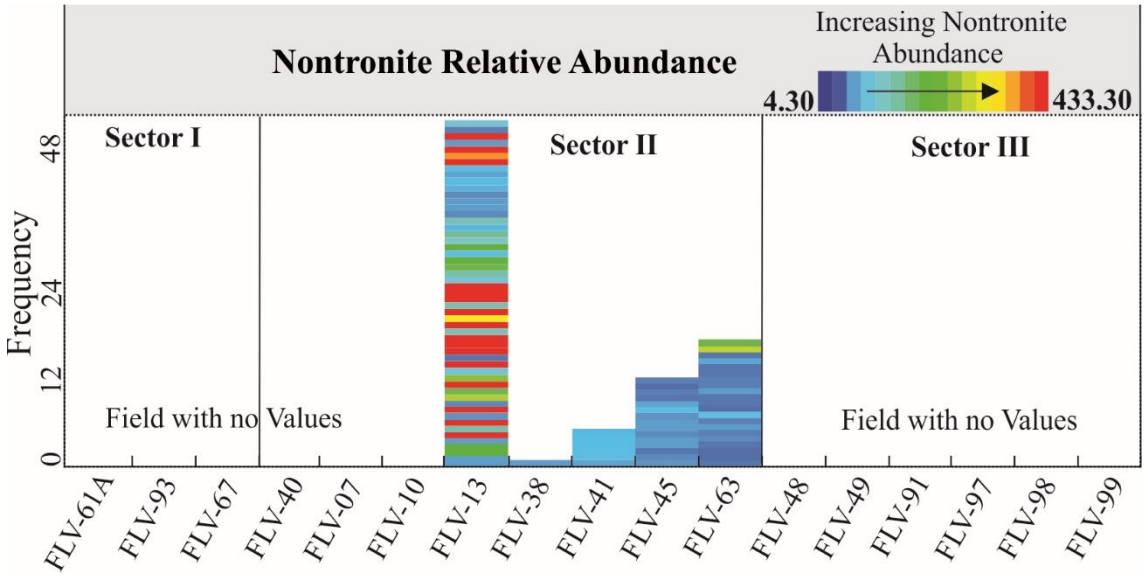

Figure 8) *Distribution of the purest smectite (nontronite) spectra in regolith profiles and its relative abundance along drill holes of the Lavra Velha deposit. Drill holes FLV_13, FLV_41, FLV_63, and FLV_45 displays values for nontronite relative abundance, while fields with no values represent drill holes in which nontronite was not identified.*

5.3.3 White Mica abundance, crystallinity, and composition

At Lavra Velha deposit, the Al-OH features of white mica in regolith can be observed in most of the drill holes, except in drill holes from sector I (e.g. FLV_61A, FLV_63 and FLV_67), where this clay mineral is absent or, if present, occur as a trace mineral, mainly in association with kaolinite. **Figure 9** shows three histograms where white mica abundance, composition and crystallinity are correlated to each drill used in this study.

White mica relative abundance showed higher frequencies in drill holes from the sectors II and III, on which the regolith was developed on the Ibitiara Granitoid. Concerning to the chemical composition, defined by the shifts in the wavelength of the feature at around 2200 nm, spectra of Al-poor mica (phengite) were mainly detected in drill holes from sector II, whereas Al-rich mica (muscovite) in sector III. The crystallinity index revealed that the well-crystalline white mica dominates regoliths within sector III mainly.

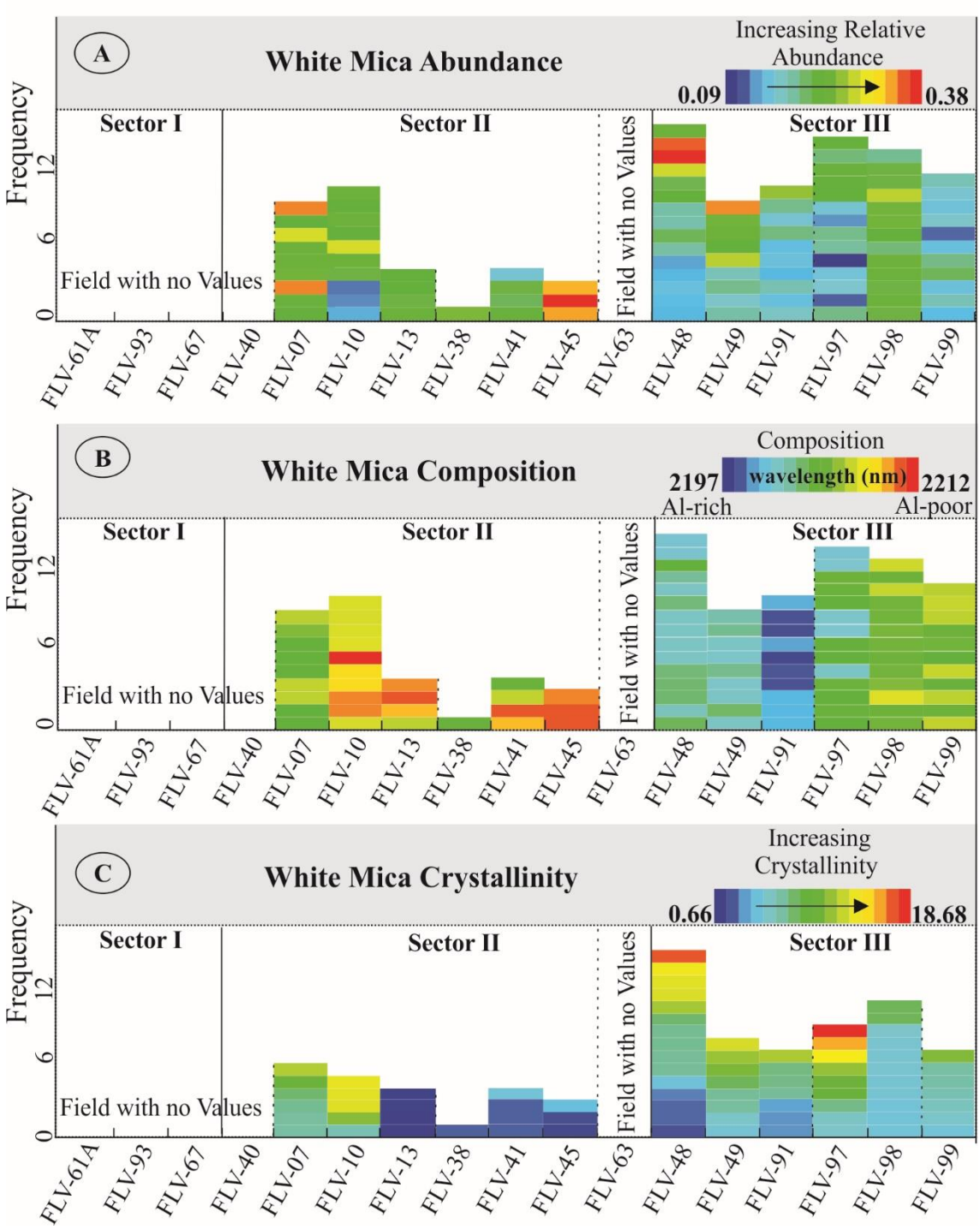

Figure 9) *Distribution of the white mica in regolith profiles of the Lavra Velha deposit. (A) White mica relative abundance is higher in sector II. (B) White mica composition tends to muscovite in drill holes of the sector II while in sector II the main white mica composition is phengite. (C) Well- crystalline white mica is found mainly in sector II. Field with no values represents drill holes in which white mica was not found or was spectrally impure.*

5.4 GEOCHEMISTRY

Three drill holes, which represent the variety of regoliths of the study area, were selected to investigate significant geochemical characteristics (**Table 1)**. They were chosen as follows:

1) a drill hole (FLV_61A) with thin regolith profile, promptly built upon the metaconglomerate from the Ouricuri do Ouro Formation, representing sector I **(Fig. 10)**;

2) a drill hole (FLV_45) with well-developed regolith profile, present immediately on the Ibitiara Granitoid with intrusions of mafic rocks along, representing sector II **(Fig.11)** and;

3) a drill hole (FLV_91) with poorly developed regolith formed on the Ibitiara Granitoid, representing sector III **(Fig.12)**;

FLV_61A presents in the soil surface horizon higher concentrations of Al, Fe, Ca, K, Na, Mg, Mn, Mo, Ag, As, Pb, Cu, Co, Ni, Cr, V, W, which decrease toward bedrock. In the saprolite, Al, Mo, and Fe increase slightly along with kaolinite and hematite. A very small concentration of Au (~0.005ppm) is associated with those elements of the surficial (soil) profile. Bismuth, Sb, Sn and U maintain the same concentration throughout the regolith profile.

The vertical distribution of chemical elements in the FLV_45 shows that Al, Fe and Mn are higher than other major elements. Surface cover (soil) is enriched in Mo, Ag, V, and shows a slight enrichment in Al, Fe, K, and Co. The Au content is concentrated vertically in the transition of mottled clay layer to the greenish saprolite with mafic rock fragments, and it has a positive geochemical association with As, Bi, Pb, Co, Cu, Mg, Mn, Ca, K, Co, Ni, Cr, V and W at around 11 meters of depth. The whole profile is marked by abundant pure kaolinite in the mottled clay layer that disappears in saprolite where it is with impurities. There is also an increase of Al- poor white mica (phengite) toward the saprolite, in which nontronite and goethite are dominant.

The regolith developed upon the Ibiatiara Granitoid (FLV_91) displays higher values of Mo, Ag, Cu in the saprock/bedrock, which progressively decreases upward from the Ibitiara Granitoid. The mottled clay layer/saprolite shows higher concentrations of Al, Fe, K, Na, Mg, Ag, As, Pb, Cu than the most of the surface soil cover; there is a slight enrichment of Mg, As, and Cu in this horizon. The regolith profile did not show any significant Au content.

The profile is mostly composed of Al-rich white (muscovite), which the abundance and crystallinity goes up toward the saprorock.

Drill hole	FLV_61A			FLV_45											FLV_91		
Depth(m)	0-0.8	1.5-2.2	2.9-3.9	1-2	3 - 4	5 -5.7	6.4-7.1	8 - 9	10 - 11	12-13	14-15	16-17	18-19	20-21	0-0.7	1.6-2.8	3.5-4.2
Al	0.82	0.35	0.12	1.43	1.01	0.87	0.72	0.83	1.80	1.74	1.83	1.74	1.72	2.02	6.79	7.00	6.01
Fe	4.51	1.87	2.28	5.10	5.95	8.55	1.38	1.37	4.64	3.68	5.06	2.66	7.27	8.02	4.95	5.2	5.37
Ca	0.09	0.01	0.01	0.01	0.01	0.01	0.04	0.05	0.16	0.15	0.13	0.15	0.10	0.14	0.01	0.01	0.01
K	0.06	0.03	0.01	0.11	0.08	0.04	0.08	0.10	0.09	0.07	0.05	0.07	0.04	0.06	4.45	5.3	6.14
Na	0.02	0.01	0.01	0.01	0.01	0.01	0.01	0.01	0.01	0.01	0.01	0.01	0.01	0.01	0.28	0.31	0.33
Mg	0.01	0.01	0.01	0.02	0.03	0.03	0.14	0.20	1.05	0.76	0.57	0.96	0.49	0.94	0.12	0.11	0.1
Mn	87	81	16	852	223	184	10200	22400	7800	1540	1010	7160	2280	5290	100	100	100
Au	0.005	0.002	0.002	0.02	0.01	0.02	0.01	0.01	0.05	0.00	0.01	0.01	0.01	0.01	0.002	0.002	0.002
Ag	34.4	1.8	0.2	2	3.5	0.40	0.9	1.8	0.8	0.2	0.2	0.2	0.2	0.9	3	24	69
As	23	6	4	30	86	194	41	60	152	92	159	51	360	347	33	33	23
Ba	50	130	10	260	140	60	2800	6620	2310	510	350	290	650	1540	728	865	863
Be	0.5	0.5	0.5	0.60	0.60	1.80	0.80	1.30	2.10	0.80	0.60	0.50	0.70	0.90	3.00	3.00	3.00
Bi	2	2	2	2	2	2	2	4	2	2	2	2	2	2	20	20	20
Cd	0.5	0.5	0.5	0.50	0.50	0.50	0.50	0.50	0.50	0.50	0.50	0.50	0.50	0.50	3.00	3.00	3.00
Co	1	1	1	45	9	21	70	117	106	55	24	26	39	45	8	8	8
Cr	40	17	12	98	128	475	8	12	135	99	216	52	285	77	21	11	7
Cu	68	23	2	30	54	56	44	66	32	36	35	30	18	224	12	41	67
Ga	10	10	10	10	10	10	10	10	10	10	10	10	10	10			
La	10	10	10	20	10	10	20	30	20	20	10	30	20	30	48	79	26
Li	10	10	10	10	10	10	10	10	10	10	10	10	10	10	3	3	3
Mo	3	1	2	7	10	1	1	1	1	1	1	1	1	1	4	40	75
Ni	9	5	1	14	18	87	25	30	97	71	86	46	113	106	12	12	15
P	190	140	30	180	170	620	130	260	330	250	360	80	610	640	377	556	206
Pb	5	5	2	2	2	3	4	7	4	2	3	2	2	3	8	13	8
S	0.03	0.02	0.01	0.01	0.01	0.01	0.01	0.01	0.01	0.01	0.01	0.01	0.01	0.01			
Sb	2	2	2	2	2	2	2	2	2	2	2	2	2	2	10	10	10
Sc	1	1	1	10	16	33	1	1	5	4	14	2	18	5	9	12	9
Se	10	10	10	10	10	10	10	10	10	10	10	10	10	10	20	20	20
Sn	10	10	10	10	10	10	10	10	10	10	10	10	10	10	20	20	20
Sr	9	8	1	9	4	3	36	81	30	22	16	17	13	19	103	130	116
Th	20	20	20	20	20	20	20	20	20	20	20	20	20	20	20	20	20
Ti	0.02	0.01	0.03	0.03	0.02	0.01	0.01	0.01	0.01	0.01	0.01	0.01	0.01	0.02	0.28	0.33	0.27
Tl	10	10	10	10	10	10	10	10	10	10	10	10	10	10	20	20	20
U	10	10	10	10	10	10	10	10	10	10	10	10	10	10	20	20	20
V	54	8	7	80	77	112	23	39	46	23	44	15	72	68	70	66	47
W	190	50	10	10	10	10	10	10	10	10	10	10	10	10	20	20	20
Y	10	10	10	10	10	10	10	10	10	10	10	10	10	10	3	6	6
Zn	9	13	2	14	16	48	17	24	105	71	67	84	79	93	3	3	3
Zr	10	8	8	5	5	5	5	5	5	5	5	5	5	5	54	71	43

Table 1) *Chemical composition of three regolith profiles of each sector of the Lavra Velha Prospect. FLV_61A is in sector I, FLV_ 45 is in sector II, while FLV_91 in sector III.. Al, Ca, Fe, K, Mg, Na, Ti and S are presented in % wt. Au is in grams per tonne, and the other elements are in ppm.*

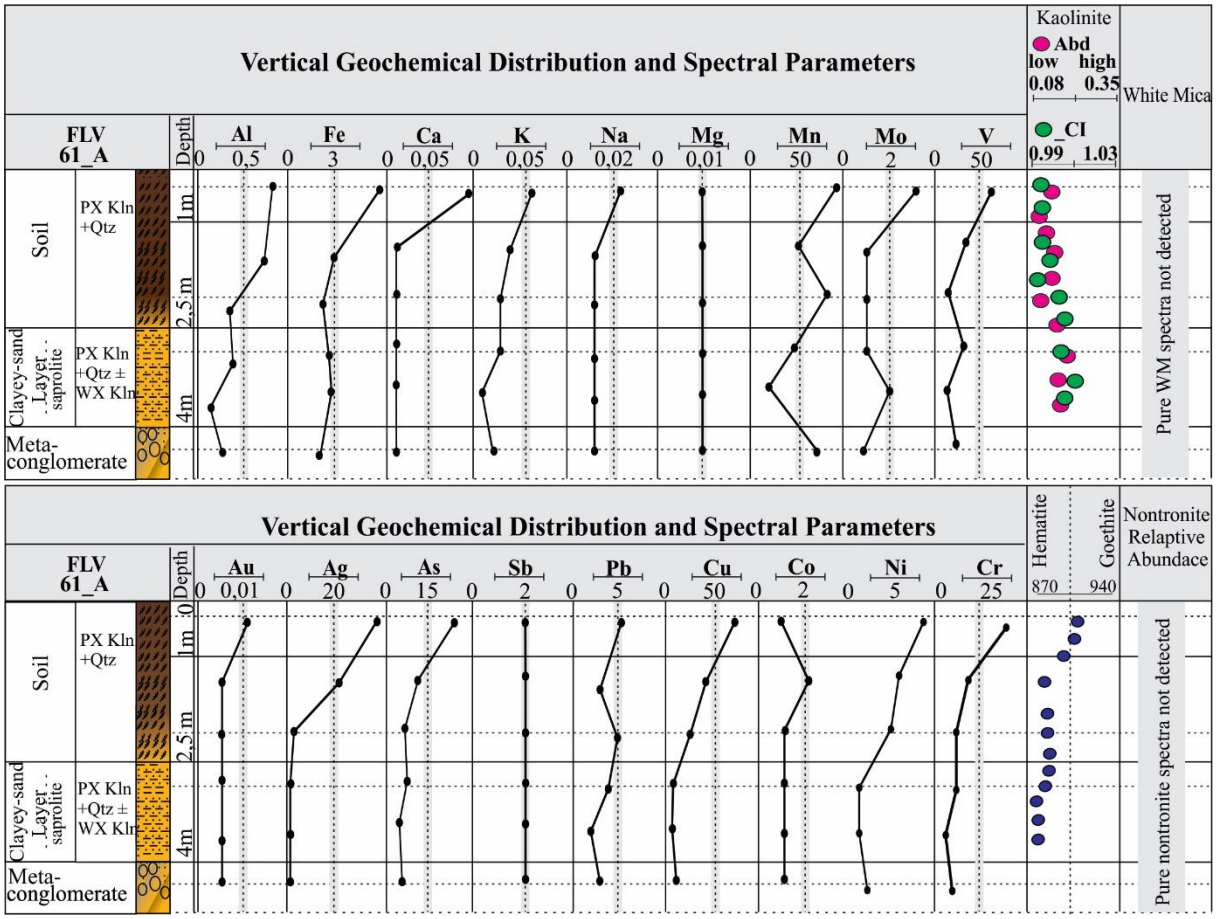

Figura 10) *FLV_61A showing vertical geochemical variations from ICP-MS analyses. Al, Fe, Ca, K, Na, and Mg are presented in % wt. Au is in grams per tonne, and the other elements are in ppm. A small gold concentration occurs in the soil surface followed by contents of Al, Fe, Ca, K, Na, Mg, Mo, Ag, As, Pb, Cu, Co, which decrease toward bedrock, but in the clayey-sand layer where the is a small enrichment of Al, Fe, Mo associated with a slight increasing relative abundance of kaolinite and hematite. Abbreviations: abundance (Abd); crystallinity index (CI), white mica (WM).*

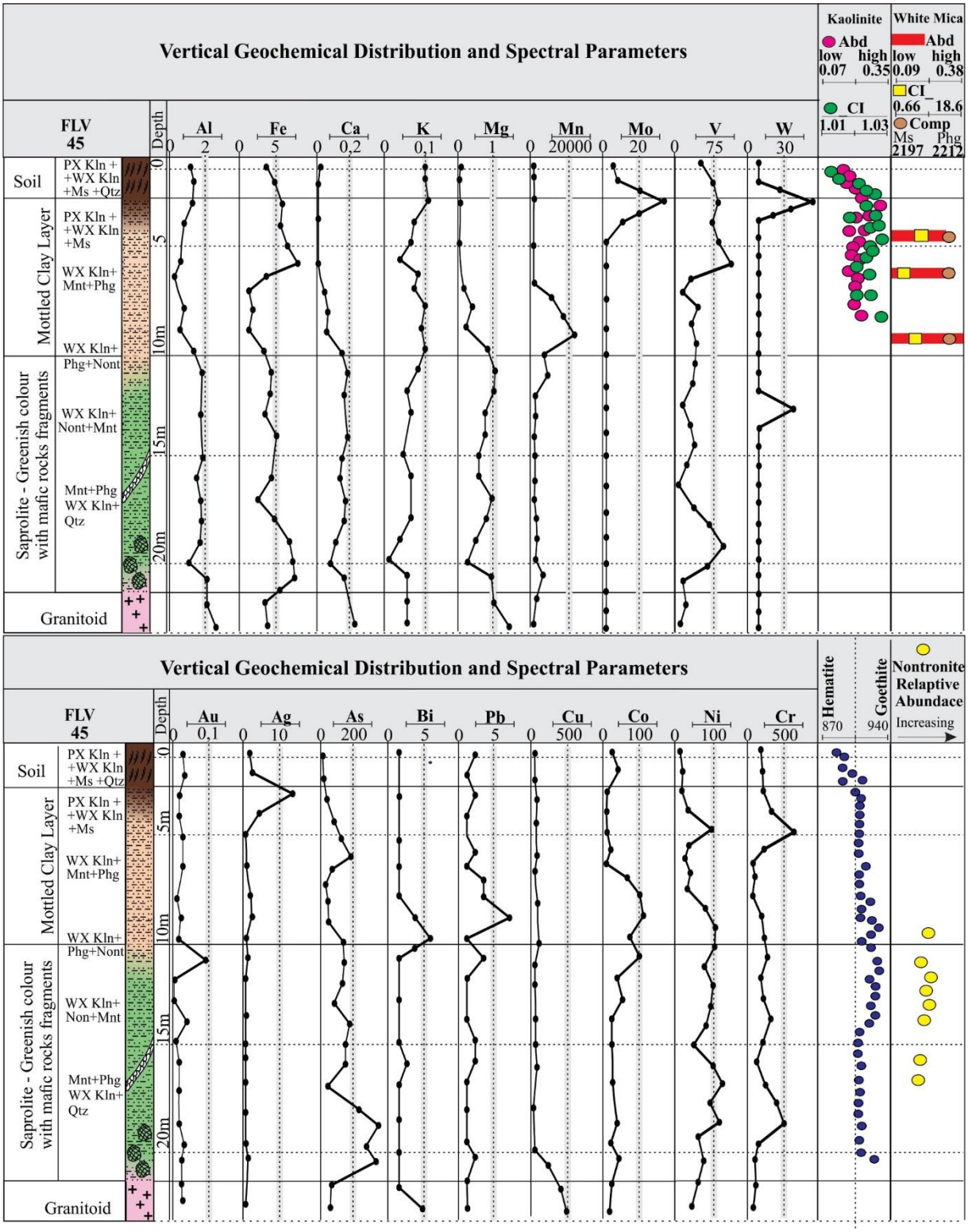

Figure 11) *FLV_45 displaying vertical geochemical variations from ICP-MS analyses. The Al, Fe, Ca, K, and Mg contents are presented in % wt. Au is in g/t, and the other elements are in ppm. Gold, Bi, As,Pb, Co, Cu, Mg, Mn, Ca and K are enriched in the transition from the mottled clay layer to the greenish saprolite with mafic rock fragments, along with increasing of phengite and changing from well-ordered kaolinite prevalence to nontronite.. The surface cover shows Mo and Ag contents, and a slight enrichment in Al, Fe, K, Co, and P. Abundance (Abd); crystallinity index (CI), composition (comp); muscovite (Ms); and phengite (Phg).*

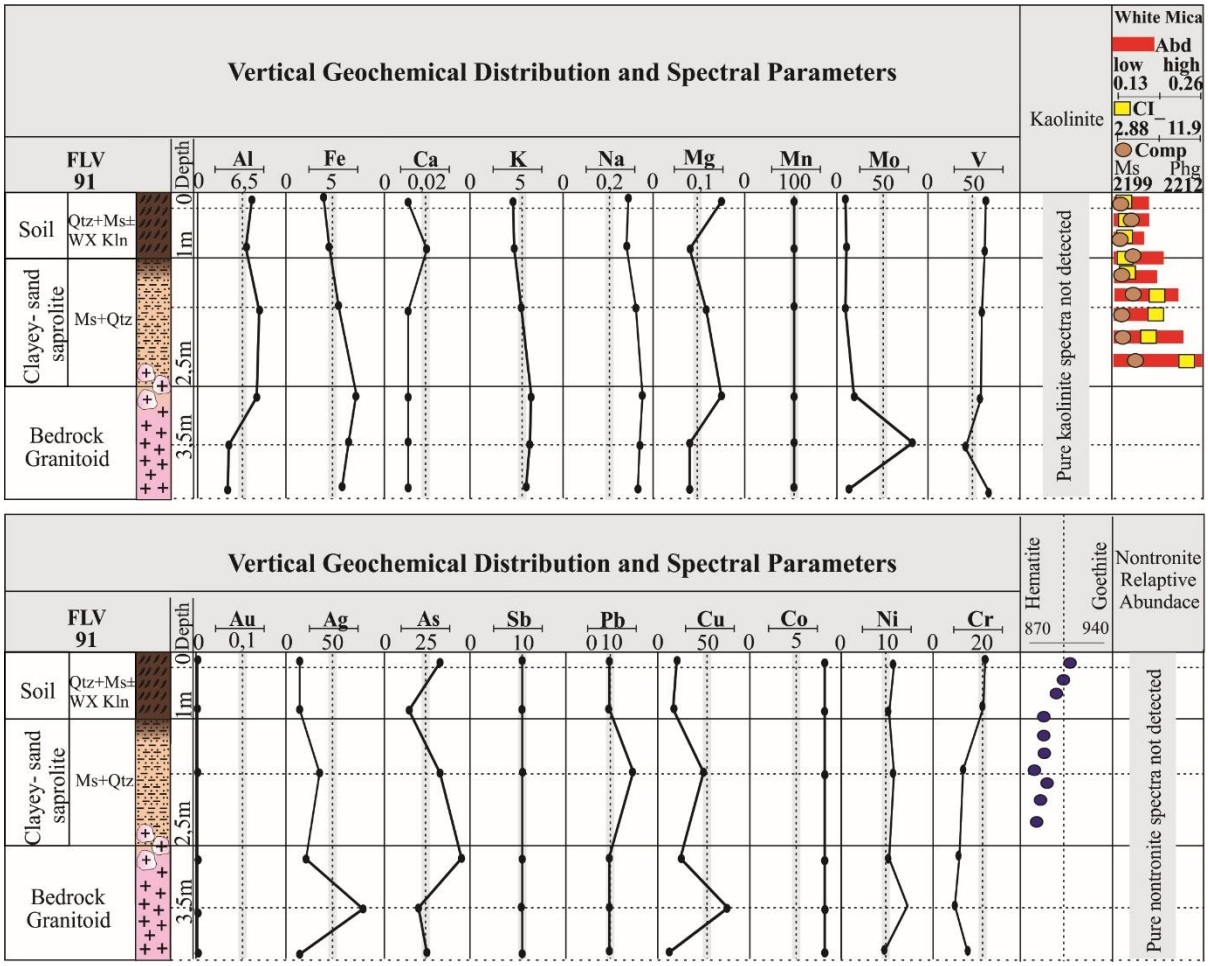

Figura 12) *FLV_91 showing vertical geochemical variations from ICP-MS analyses. The Al, Fe, Ca, K, Na, and Mg contents are presented in %wt. Au is in g/t, and the other elements are in ppm. An abundance of well-ordered muscovite is detected in the surface profiles, which becomes more expressive at depth, along with hematite. Mo, Ag and Cu contents occur in the saprock/bedrock (Ibitiara Granitoid), while higher contents of Al, Fe, K, Na, Mg, Ag, As, Pb, Cu in the mottled clay layer/saprolite. The surface soil cover shows a slightly enrichment of Mg, As, and Cu. Abbreviations: abundance (Abd); crystallinity index (CI); composition (comp); muscovite (Ms); and phengite (Phg).*

6 DISCUSSION

6.1 SIGNIFICANCE OF MINERALOGICAL ATTRIBUTES

Weathering changes rock characteristics and develops regolith profiles with different minerals, structures and geochemical signatures that are generally more stable at superficial environment conditions (MacDonald, 2007).

Al-OH features showed a noticeable variation in the structural order of kaolinite in the study area. Several works conducted in Australia have used the crystallinity of kaolinite to distinguish in situ regolith from transported, as the residual regolith is often characterized by abundant well-ordered kaolinite (Cudahy et al, 2005; Haest et al, 2012). From this perspective, it seems possible that low-ordered kaolinite of sector I (e.g. FLV_61A, FLV_63 and FLV_67) is related to transported materials, or perhaps to the heterogeneity due to clast-size and variations in the sample media, which would be inherited from the parental rock, the Ouricuri do Ouro metaconglomerate. Two main hypotheses could explain the origin and predominance of well-ordered kaolinite in the regolith profiles of the central area of the deposit. First, previous kaolinite could have been formed by hydrothermal alteration of the Ibitiara Granitoid during the emplacement of mafic rocks, and, therefore, persisted unaltered in the weathering profiles, and second, and most likely, kaolinite could have been formed by weathering of the components of the Ibitiara Granitoid mainly. The weathering of feldspars and white mica to kaolinite could easily take place through loss of sodium, calcium and potassium as described by Nesbit and Young (1984).

Smectite group minerals (montmorillonite or nontronite) are present in some parts of the Lavra Velha deposit. Nontronite is mainly restricted to the central portion area (e.g. FLV_13, FLV_41, FLV_63, and FLV_45). In these drill holes, this clay mineral was widely observed, mostly from subordinate features in spectra dominated by kaolinite (**Fig. 6**). The nontronite origin has often been described as weathering of mafic rocks (Ildefonse, 1980; Righi & Meunier, 1996; Naleto et al., 2019). Oxidative weathering of those rocks results in a loss of Ca and Mg coupled with Fe oxidation, which facilitates the transition from trioctahedral to dioctahedral minerals. In this respect, ferromagnesian minerals are often transformed into nontronite as reported by Ducloux et al. (1976). On account of this, the increasing abundance of nontronite in the Lavra Velha deposit may be mainly related to the weathering of the mafic rocks intruded in the Ibitiara Granitoid as observed, for instance, in FLV_13, FLV_63 and FLV_45.

A study linking white mica as a surficial footprint for mineral deposits below regolith profiles was conducted by Lampinen et al. (2017, 2019). In the regolith of the Lavra Velha deposit, white mica shows abundance, composition and crystallinity changings, mostly laterally. The spectral-mineralogical analysis revealed an increase of white mica abundance toward the central portion of the area as seen in the drill holes FLV_45, FLV_41, FLV_10 and FLV_07, thus showing that white mica abundance is directly related to the well-developed regolith profiles. The persistence of white mica upward through the regolith to the surface has been used as an indicator of fresh rock, as well as alteration mineral in hydrothermal systems by Cudahy (2016). The constancy of white mica up through regolith profiles of the Lavra Velha deposit could also be related to its relative resistance to weathering.

Despite being Al-poor white mica (phengite) widely known as a metamorphic mineral (e.g. Gouzu et al., 2005; Cibin et al., 2008), it is also a typical product of hydrothermal alteration (e.g. Roberts & Hudson, 1983), including of IOCG deposits (Tappert et al., 2013). Phengitic white mica, associated with mineralized zones, has also been pointed out as a footprint in regolith above the Abra Pb-Zn-Cu-Au deposit in western Australia (Lampinen et al., 2019). In the Lavra Velha deposit, the central area is noticeably dominated by Al-poor white mica as displayed in FLV_45, FLV_10, FLV_13 and FLV_41. Medina (2020) reported that at depth, white mica becomes more phengitic as higher concentrations of gold are found in the deposit. Similarly, our study shows that the regolith present in drill holes highly mineralized at depth (e.g. FLV_45, FLV_10, FLV_13) is dominated by phengite (**Fig. 9**). On the contrary, the muscovite, originated from the transformation of the Ibitiara Granitoid into poorly developed regolith, dominates in profiles marked by contents of gold lower than those (e.g. FL_91, among others).

The white mica crystallinity has been regularly recorded in phyllosilicates evolution due to increasing of temperature in hydrothermal deposits (Cudahy et al. 2008). It has also been used as an indicator of in situ regoliths (Lampinen et al. 2017; Lampinen et al. 2019). In the Lavra Velha deposit, well-crystalline white mica is mainly muscovite and was observed in samples of poorly developed regolith (e.g. FLV_99, FLV_98, FLV_97, FLV_48). This is likely to be related to the fact that these profiles were built on the Ibitiara Granitoid, and this mineral is solely remaining from the bedrock. On the other hand, the low-crystallinity white mica is mostly illite, which was observed in FLV_45, FLV_10, FLV_13. Despite the pedogenetic formation of this mineral requires further evidence before being settled, it could

conceivably be hypothesised that it derives from the weathering degradation of micaceous precursors, such as muscovite and phengite or even from feldspars of the Ibitiara Granitoid.

6.2 SIGNIFICANCE OF GEOCHEMICAL ATTRIBUTES

In the Lavra Velha deposit, the geochemical analysis showed that the chemical composition of regoliths depends mainly on the elements of the bedrocks. In areas in which the Ibitiara Granitoid is intruded by mafic rocks, there is a noticeable geochemical and mineral signature of both lithotypes. In the FLV_45, saprolite showed enrichment of alkali, alkali earth and transition metals, which suggests heterogeneity of the bedrock. The geochemical signature in the upper mottled clay layer is marked by the depletion of alkali earth metals (e.g. Ca and Mg) as well as a slightly decreasing of selected transition metals, such as Co, Ni, Cr. This might be the result of the abundant pure kaolinite present in this horizon, which is poor in those elements, or perhaps the absence or small amount of ferromagnesian minerals in it. The alkaline earth metals, and transition metals increase downward in association with higher values of nontronite and goethite, which are commonly formed by the alteration of minerals of mafic rocks (Ducloux et al., 1976).

The progression from the upper mottled clay profile to saprolite seems to be a previous wall alteration of the Ibitiara Granitoid during the emplacement of mafic intrusions, mainly in the transition between these profiles, which is marked by the concentration of Al, K, Na, Ca, As, Fe, Bi, Pb, Co, Cu, Mg, Mn, Co, Ni, Cr, V and W, in along with a strong positive correlation with Au. Toward saprolite, the mineral content comprises an association with an increase of white mica (phengite) of high structural order. These findings are consistent with that of Medina (2020) who also studied among others the drill hole FLV_45. The authors found out that the gold-bearing levels (in 49.50-52.80 and 70.60-74 meters of depth) are highly correlated with Cu-Bi-Fe-As-U-V-(Ag-Sb-Sn-W-Pb) besides Cr, Ni and Co. Besides the geochemical signature, higher gold levels were often associated with phengite and, sporadically, with nontronite. In this respect, comparison of these findings shows that the geochemical and mineral association that occur in regolith profiles may resemble those of deeper mineralized zones.

In areas where there are no noticeable mafic intrusions in the granitoid, regolith profiles display distinct geochemical and mineral signatures. In some drill holes, as an example the FLV_91, the bedrock and saprolite showed lower concentration of alkali earth

(e.g. Ca and Mg) and transition metals (e.g. Mn, Cu, Co, Cr, Ni), whilst alkali content (e.g. K and Na), and Al, Mo, V, Ag, Sb, Bi, and Pb are increased. Previous studies demonstrated the chemical signature associated with the Ibitiara Granitoid and its hydrothermal alteration (Guimarães et al., 2005; Campos, 2013; Medina, 2020). The elements that comprise the regoliths of the sector I (e.g. FLV_91) highlight the role of parent rock chemistry in their chemical composition. The alkalis content is associated with the high abundance of well-ordered muscovite detected in the profiles, which becomes more expressive at depth, along with hematite. This may be explained by the fact that the Ibitiara Granitoid was affected by a sericite and hematite alteration as reported by Campos (2013), which has been directly reflected in the mineralogical and regolith composition. Decreasing of alkali earth and transition metal contents may be attributed to the absence of mafic rocks as a material source for the development of these regolith profiles.

Regolith developed upon the sedimentary rocks also displayed a particular geochemical and mineral signature. Higher concentrations of alkali, alkali earth and transition metal are confined in the most surface soil levels. Overall, there is a decreasing of these elements occurring toward the saprolite and bedrock (e.g. FLV_61A). However, in the saprolite, Al, Mo, and Fe increase slightly along with kaolinite and hematite. The reason for this distribution may have something to do with not only the bedrock, that is naturally poor in alkali earth and transition metals, but also with the influence of surface soil organic matter that may retain transported metals. Prior studies have noted the importance of metal transfer mechanisms through transported cover (Anand et al, 2016), including plants, roots and organic matter to uptake metals related to ore deposit (Jones, 1998). Therefore, these factors may have contributed to the capture of metals in the topsoil profile despite the origin of the variety of these metals remains unclear.

6.3 IMPLICATIONS FOR MINERAL PROSPECTING AND EXPLORATION

There are several challenges for mineral prospecting and exploration in the Lavra Velha region. However, the processes and factors related to the development of the regolith in the deposit area as well as the main characteristics of the regolith mineral contents give rise to significant implications that may contribute to a more effective utilization of pedogeochemical datasets.

The current study pointed out that the regolith settings of the Lavra Velha deposit may be divided into three main sectors based on different aspects presented in this study: 1)

poorly developed regolith formed from the Ibitiara granitoid, comprising hills and ridges; 2) shallow weathered profiles developed from the metaconglomerate of the Ouricuri do Ouro Formation; and 3) intensively deep weathering profile formed from the Ibitiara Granitoid with several mafic intrusions in flat to gently undulating geoforms. This latter one encompasses regolith profiles, in which at depth there are rocks with higher grade of gold as described by Medina (2020) (e.g. FLV_45) and Yamana Gold intern reports (e.g. FLV_45, FLV_13, FLV_10).

The main footprint found in the regolith profiles is a mineral association that provides a guidance toward more effective exploration targets. These minerals identified from drill holes, in which rocks are highly mineralized at depth, are well-ordered kaolinite + phengite + nontronite (FLV_45, FLV_10, FLV_13) that also may indicate in situ regolith (Ribeiro, 1974; Lampinen et al 2017). This assemblage along with the geochemical data presented previously reflect clearly the occurrence of the Ibitiara Granitoid combined with ferromagnesian rocks. This result take after that of Medina. (2020) who also found that at depth white mica becomes more phengitic toward highly mineralized zones (Bonanza zones defined by the author), which may be often accompanied with nontronite, and marked by the following geochemical association: Au-Cu-Bi-Fe-As-U-V-(Ag-Sb-Sn-W-Pb), besides Cr, Ni and Co.

Although on the surface well-ordered kaolinite + phengite + nontronite are excellent indicators of mineralized zones at depth, there are other considerations that should be taken. Some regolith profiles may not show that mineral association despite being the mother rock mineralized (e.g. FLV_97, FLV_099). The reason for this may have something to do with the paleo-landscape evolution and the development of the regolith in the Lavra Velha area, at which some mineralized zones were not exposed to the surface and, consequently, transformed into regolith. Therefore, it is important to report that not always the regolith may indicate a high grade of gold at depth. However, the mineral footprint in regolith pointed out in this work along with the geochemical compounds outlined earlier are the best guides to lead better surface prospecting and exploration programs.

7 FINAL CONSIDERATIONS

The present study was designed to determine the mineralogical compounds of the regolith developed in the Lavra Velha deposit using spectral techniques as well as their significance for mineral prospecting and exploration.

Shallow regoliths developed above the metaconglomerate of the Ouricuri do Ouro formation are composed of mainly poorly ordered kaolinite while profiles formed from the Ibitiara Granitoid consists of abundant fine-crystalline muscovite. Even though having their SWIR mineral content characterized, these profiles did not show a great contribution for mineral prospecting as they could not indicate the presence of any mineralized rock downward. Notwithstanding this limitation, prior studies suggest that these profiles should not be totally overlooked, especially when they are developed from the Ibitiara granitoid since they may comprise mineralized rock with gold at depth (e.g., FLV_97; FLV_099).

Despite the considerations outlined above, the most significant finding to emerge from this study is that well-developed regolith may display typical profiles that reflect directly the mineralogical and geochemical compounds of deep mineralized zones. The mineral footprint in regolith of hydrothermally altered rocks with higher gold content at depth consists of well-ordered kaolinite + phengite + nontronite along with concentrations of Al, K, Na, Ca, As, Fe, Bi, Pb, Co, Cu, Mg, Mn, Co, Ni, Cr, V and W. This mineral and geochemical association have suggested not only in situ regolith, but also the transformation of mineralized zones strongly affected by wall alteration into regolith.

Therefore, this study endorses that the combined use of reflectance spectroscopy and geochemical data are valuable tools in mineral exploration. Applying these methods for determining the chemical and mineralogical compositions of weathered materials that often obscure outcrops and mineralized areas, it is an inexpensive, non-destructive, and fast alternative. Mineralogical characterization of the regolith may provide insights of the concealed rocky stratigraphy, which would be very helpful to design drilling programs.

8 REFERENCES

Agbenin, J. O.; Tiessen, H. 1995. Soil properties and their variations on two contiguous hillslopes in Northeast Brazil. Catena, v. 24, n. 2, p. 147-161.

Alckmin F. F., Neves B. B. B., Alves, J.A. C., 1993. Arcabouço Tectônico do Cráton do São Francisco: uma revisão.In: Misi, A.; Dominguez, J. M. L. (Ed.) O Cráton do São Francisco. Salvador: SBG. p. 45-62.

Almeida, F.F.M., Hasui, Y., De Brito Neves, B.B. and Fuck, R.A., 1981. Brazilian structural provinces: an introduction. Earth-Sci. Rev., 17: 1--29.

Anand, R.R., Paine, M., 2002. Regolith geology of the Yilgarn Craton, Western Australia: implications for exploration. Australian Journal of Earth Sciences 49, 3-162.

Anand, R.R., Butt, C.R.M., 2010. A guide for mineral exploration through the regolith in the Yilgarn Craton, Western Australia. Australian Journal of Earth Sciences 57, 1015-1114.

Anand, R. R. 2016. Regolith-landform processes and geochemical exploration for base metal deposits in regolith-dominated terrains of the Mt Isa region, northwest Queensland, Australia. Ore Geology Reviews, 73, 451-474.

Anand, R. R., Aspandiar, M. F., & Noble, R. R. 2016. A review of metal transfer mechanisms through transported cover with emphasis on the vadose zone within the Australian regolith. Ore Geology Reviews, 73, 394-416.

Bennema, J.; Camargo, M. N.; Wright, A. C. S.1962.Regional contrasts in South American soil formation in relation to soil classification and soil fertility. In: International Soil Conference, New Zealand, Transactions, p.2-15.

Burley, L. L., Barnes, S. J., Laukamp, C., Mole, D. R., Le Vaillant, M., & Fiorentini, M. L. 2017. Rapid mineralogical and geochemical characterisation of the Fisher East nickel sulphide prospects, Western Australia, using hyperspectral and pXRF data. Ore Geology Reviews, 90, 371-387.

Butt, C.R.M., Lintern, M.J., Anand, R.R. 2000. Evolution of regolith and landscapes in deeply weathered terrain- implications for geochemical exploration. Ore Geology Reviews 16, 167-183.

Cudahy, T. 2016. Mineral mapping for exploration: An Australian journey of evolving spectral sensing technologies and industry collaboration. Geosciences, 6(4), 52.

Cudahy, T.J., Jones, M., Thomas, M., Laukamp, C., Caccetta, M., Hewson, R., Rodger, A., Verrall, M., 2008. Next Generation Mineral Mapping: Queensland Airborne HyMap and Satellite ASTER Surveys. CSIRO Exploration & Mining Report P2007/364152.

Campos, L. D. O Depósito de Au-Cu Lavra Velha, Chapada Diamantina Ocidental: Um exemplo de depósito da classe IOCG associado aos terrenos paleoproterozoicos

do Bloco Gavião. 2013. (unpublished master's thesis), Instituto de Geociências, Universidade Federal de Brasília. Brasília, Brazil. (In Portuguese)

Carlin, A. C.; Zanardo, A.; Navarro, G. R. B. 2018. Caracterização petrográfica das rochas encaixantes da mineralização aurífera do Depósito Lavra Velha– região de Ibitiara, borda oeste da Chapada Diamantina, Bahia. Geociências, v. 37, n. 2, p. 253-265.

Clark, R. N., King, T. V., Klejwa, M., Swayze, G. A., & Vergo, N. 1990. High spectral resolution reflectance spectroscopy of minerals. Journal of Geophysical Research: Solid Earth, 95(B8), 12653-12680.

Cibin, G., Cinque, G., Marcelli, A., Mottana, A., Sassi, R., 2008. The octahedral sheet of metamoprhic 2M1-phengites: a combined EMPA and AXANES study. Am. Mineral.

93, 414–425.

Cruz, Simone C.P., and Alkmim, Fernando F., 2006., The Tectonic interaction between the Paramirim Aulacogen and the Araçuaí Belt, São Francisco craton region, Eastern Brazil. Anais da Academia Brasileira de Ciências, 78(1), 151-173.

De Souza, E.G. 2017. Depositional model and faiologic architecture of proterozoic alluvial fans - Ouricuri do Ouro Formation, Espinhaço Supergroup - Chapada Diamantina/BA (unpublished master's thesis). Universidade Federal do Rio Grande do Sul. Porto Alegre, Brazil.

Ducloux, J., Meunier, A., and Velde, B. 1976. Smectite, chlorite, and a regular interlayered chlorite-vermiculite in soils developed on a small serpentinite body, Massif Central, France. Clay Minerals, 11, 121–135

Frazier, C. S.; Graham, R. C. 2000. Pedogenic transformation of fractured granitic bedrock, southern California. Soil Science Society of America Journal, v. 64, n. 6, p. 2057-2069.

Gouzu, C., Itaya, T., Takeshita, H. 2005. Interlayer cation vacancies of phengites in calcshists from the Piemonte zone, wester Alps, Italy. J. Mineral. Petrol. Sci. 100, 142–149.

Guimarães J.T., Teixeira L.R., Silva M.G. Martins A.A.M., Filho E.L.A., Loureiro H.S.C., Arcanjo J.B., Dalton de Souza J., Neves J.P., Mascarenhas J.F., Melo R.C., Bento R.V. 2005. Datações U/Pb em rochas magmáticas intrusivas no Complexo

Paramirim e no Rifte Espinhaço: uma contribuição ao estudo da Evolução Geocronológica da Chapada Diamantina. In: SBG/BA-SE, Simpósio do Cráton do São Francisco, 3, Anais de Resumos Expandidos, p. 159-161. (In Portuguese)

Haest M., Cudahy T., Laukamp C., Gregory S. 2012. Quantitative mineralogy from visible to shortwave infrared spectroscopic data: II. 3D mineralogical characterization of the Rocklea Dome channel iron deposit, Western Australia. Economic Geology, 107:229–249.

Hunt, G.R., Ashley, R.P., 1979.Spectra of altered rocks in the visible and near-infrared.Econ. Geol. 74, 1613–1629.

Ildefonse, P. 1980. Mineral facies developed by weathering in a meta-gabbro, Loire-Atlantique, France. Geoderma, 24, 257–274.

Jones, D.L., 1998. Organic acids in the rhizosphere — a critical review. Plant Soil 205, 25–44.

Köppen, W. Das geographische System der Klimate. 1936. In: KÖPPEN, W.; GEIGER, R. Handbuch der Klimatologie. Berlin: Gebrüder Borntträger. 1- 44p.

Lampinen, H. M., Laukamp, C., Occhipinti, S. A., Metelka, V., & Spinks, S. C. 2017. Delineating Alteration Footprints from Field and ASTER SWIR Spectra, Geochemistry, and Gamma-Ray Spectrometry above Regolith-Covered Base Metal Deposits—An Example from Abra, Western Australia. Economic Geology, 112(8), 1977-2003.

Lampinen, H. M., Laukamp, C., Occhipinti, S. A., & Hardy, L. 2019. Mineral footprints of the Paleoproterozoic sediment-hosted Abra Pb-Zn-Cu-Au deposit Capricorn Orogen, Western Australia. Ore Geology Reviews, 104, 436-461.

LAUKAMP, C.; SALAMA, W.; GONZÁLEZ-ÁLVAREZ, I. 2016. Proximal and remote spectroscopic characterisation of regolith in the Albany–Fraser Orogen (Western Australia). Ore Geology Reviews, v. 73, p. 540-554.

MacDonald, E.H., 2007. Handbook of Gold Exploration and Evolução. Woodhead Publishing, New York, pp. 664.

Medina, C.M. Hydrothermal Alteration, Mineralization and Spectral Footprints at the Lavra Velha Gold Deposit, Bahía, Brazil. 2020. (Unpublished master´s thesis). Instituto

de Geociências, Universidade Estadual de Campinas, Campinas, São Paulo, Brazil.

Meunier, A. 2005. Clays in soils and weathered rocks. Clays, 231-293.

Naleto, J. L. C., Perrotta, M. M., da Costa, F. G., & Souza Filho, C. R. 2019. Point and imaging spectroscopy investigations on the Pedra Branca orogenic gold deposit, Troia Massif, Northeast Brazil: Implications for mineral exploration in amphibolite metamorphic-grade terrains. Ore Geology Reviews, 107, 283-309.

Nesbitt, H. W., & Young, G. M. 1984. Prediction of some weathering trends of plutonic and volcanic rocks based on thermodynamic and kinetic considerations. Geochimica et Cosmochimica Acta, 48 (7), 1523-1534.

Oliveira, J. J. 1968 . Contrib ution a l' etude morphologiq ue du piem onr de la Cha pada Diama nti na dans la region de Livramento do Bru mad o, et at de Bahia, Bresil. 'I'ese de doutorado Univ. de Paris (In French).

Ollier, C.; Pain, C. 1997. Regolith, Soils and Landforms. Geological Magazine. v. 134, n. 1, p. 121-142.

Passos, J.S., Ducart, D. F., Borges, A., Medina, C.M. (In Press). Rock-landform-soil relationship for geomorphopedological characterization in the region of Lavra Velha, Occidental Chapada Diamantina,Bahia. Revista Brasileira de Geomorfologia.

Prado, E. M. G., Silva, A. M., Ducart, D. F., Toledo, C. L. B., & De Assis, L. M. 2016. Reflectance spectroradiometry applied to a semi-quantitative analysis of the mineralogy of the N4ws deposit, Carajás Mineral Province, Pará, Brazil. Ore Geology Reviews, 78, 101-119.

Ribeiro, L. P. Caracterização dos solos de Ibitiara- BA. 1974. (Unpublished master´s thesis). Instituto de Geociências, Universidade Federal da Bahia, Salvador, Brazil.

Righi D. and Meunier A. 1995. Origin of clays by rock weathering. In Origin and Mineralogy of Clays (ed. B. Velde). Springer, pp. 43–161.

Roberts, D.E., Hudson, G.R.T., 1983. The Olympic Dam copper–uranium–gold deposit, Roxby Downs, South Australia. Econ. Geol. 78, 799–822.

Schobbenhaus C. 1996. As tafrogêneses superpostas Espinhaço e Santo Onofre, Estado da Bahia: revisão e novas propostas. Rev.Bras. de Geoci.26(4):265-276. (In Portuguese).

Senna, J. A., Souza Filho, C. R., & Angélica, R. S. 2008. Characterization of clays used in the ceramic manufacturing industry by reflectance spectroscopy: An experiment in the São Simão ball-clay deposit, Brazil. Applied clay science, 41(1-2), 85-98.

Tappert, M. C., Rivard, B., Giles, D., Tappert, R., & Mauger, A. 2013. The mineral chemistry, near infrared, and mid-infrared reflectance spectroscopy of phengite from the Olympic Dam IOCG deposit, South Australia. Ore Geology Reviews, 53, 26-38.

Teixeira L. R. 2005. Projeto Ibitiara - Rio de Contas: relatório temático de litogeoquímica. Salvador: CPRM. Programa Levantamentos Geológicos Básicos do Brasil - PLGB. Relatório interno.

Teixeira, J.B.G., Misi, A., Silva, M.G., and Brito, R.S.C., 2019. Reconstruction of Precambrian terranes of Northeastern Brazil along Cambrian strike-slip faults: A new model of geodynamic evolution and gold metallogeny in the State of Bahia: Brazilian Journal of Geology, v. 49.

Townsend, T.E., 1987.Discrimination of iron alteration minerals in visible andnear-infrared reflectance data. J. Geophys. Res. Solid Earth Planets 92,1441–1454

Van Der Meer, F. (2004). Analysis of spectral absorption features in hyperspectral imagery. International journal of applied earth observation and geoinformation, 5(1), 55-68.

REFERÊNCIAS BIBLIOGRÁFICAS

Agbenin, J. O.; Tiessen, H. 1995. Soil Properties And Their Variations On Two Contiguous Hillslopes In Northeast Brazil. Catena, V. 24, N. 2, P. 147-161.

Alckmin F. F., Neves B. B. B., Alves, J.A. C., 1993. Arcabouço Tectônico Do Cráton Do São Francisco: Uma Revisão.In: Misi, A.; Dominguez, J. M. L. (Ed.) O Cráton Do São Francisco. Salvador: SBG. P. 45-62.

Almeida, F.F.M., Hasui, Y., De Brito Neves, B.B. And Fuck, R.A., 1981. Brazilian Structural Provinces: An Introduction. Earth-Sci. Rev., 17: 1--29.

Anand, R.R., Paine, M., 2002. Regolith Geology Of The Yilgarn Craton, Western Australia: Implications For Exploration. Australian Journal Of Earth Sciences 49, 3-162.

Anand, R.R., Butt, C.R.M., 2010. A Guide For Mineral Exploration Through The Regolith In The Yilgarn Craton, Western Australia. Australian Journal Of Earth Sciences 57, 1015-1114.

Anand, R. R. 2016. Regolith-Landform Processes And Geochemical Exploration For Base Metal Deposits In Regolith-Dominated Terrains Of The Mt Isa Region, Northwest Queensland, Australia. Ore Geology Reviews, 73, 451-474.

Anand, R. R., Aspandiar, M. F., & Noble, R. R. 2016. A Review Of Metal Transfer Mechanisms Through Transported Cover With Emphasis On The Vadose Zone Within The Australian Regolith. Ore Geology Reviews, 73, 394-416.

Battilani, G. A.; Gomes, N. S.; Guerra, W. J. Evolução Diagenética Dos Arenitos Da Formação Morro Do Chapéu, Grupo Chapada Diamantina, Na Região De Morro Do Chapéu, Bahia. Revista Geonomos. V. 4, N. 2, P. 81-89, 1996. Doi: 10.18285/Geonomos.V4i2.203.

Benites, V. M.; Schaefer, C. E. G.; Simas, F. N.; & Santos, H. G. Soils Associated With Rock Outcrops In The Brazilian Mountain Ranges Mantiqueira And Espinhaço. Brazilian Journal Of Botany, V. 30, N. 4, P. 569-577, 2007.

Bennema, J.; Camargo, M. N.; Wright, A. C. S.1962.Regional Contrasts In South American Soil Formation In Relation To Soil Classification And Soil Fertility. In: International Soil Conference, New Zealand, Transactions, P.2-15.

Burley, L. L., Barnes, S. J., Laukamp, C., Mole, D. R., Le Vaillant, M., & Fiorentini, M. L. 2017. Rapid Mineralogical And Geochemical Characterisation Of The Fisher East Nickel Sulphide Prospects, Western Australia, Using Hyperspectral And Pxrf Data. Ore Geology Reviews, 90, 371-387.

Butt, C.R.M., Lintern, M.J., Anand, R.R. 2000. Evolution Of Regolith And Landscapes In Deeply Weathered Terrain- Implications For Geochemical Exploration. Ore Geology Reviews 16, 167-183.

Castro, S. S.; Salomão, F. X. T. Compartimentação Morfopedológica E Sua Aplicação: Considerações Metodológicas. Geousp, São Paulo, N. 7, P. 27-37, 2000.

Campos, L. D. O Depósito De Au-Cu Lavra Velha, Chapada Diamantina Ocidental: Um Exemplo De Depósito Da Classe Iocg Associado Aos Terrenos Paleoproterozoicos Do Bloco Gavião. Dissertação (Mestrado), Instituto De Geociências, Universidade Federal De Brasília. 2013. 104p.

Carlin, A. C.; Zanardo, A.; Navarro, G. R. B. Caracterização Petrográfica Das Rochas Encaixantes Da Mineralização Aurífera Do Depósito Lavra Velha– Região De Ibitiara, Borda Oeste Da Chapada Diamantina, Bahia. Geociências, V. 37, N. 2, P. 253-265, 2018.

Clark, R. N., King, T. V., Klejwa, M., Swayze, G. A., & Vergo, N. 1990. High Spectral Resolution Reflectance Spectroscopy Of Minerals. Journal Of Geophysical Research: Solid Earth, 95(B8), 12653-12680.

Cawood, A. J.; Bond, C. E. Broadhaven Revisited: A New Look At Models Of Fault–Fold Interaction. Geological Society Of London, Special Publications, V. 487. 2019.

Cibin, G., Cinque, G., Marcelli, A., Mottana, A., Sassi, R., 2008. The Octahedral Sheet Of Metamoprhic 2m1-Phengites: A Combined Empa And Axanes Study. Am. Mineral.

93, 414–425.

Cruz, Simone C.P., And Alkmim, Fernando F., 2006., The Tectonic Interaction Between The Paramirim Aulacogen And The Araçuaí Belt, São Francisco Craton Region, Eastern Brazil. Anais Da Academia Brasileira De Ciências, 78(1), 151-173.

Cruz, S.C.P. & Alkimim F.F. The Tectonic Interaction Between The Paramirim Aulacogen And The Araçuai Belt, São Francisco Craton Region, Eastern Brazil. Anais Da Academia Brasileira De Ciências, V. 78, N. 1, P.151-173, 2006

Curi, N.; Franzmeier, D. P. Toposequence Of Oxisols From The Central Plateau Of Brazil 1. Soil Science Society Of America Journal, V. 48, N. 2, P. 341-346, 1984.

Cudahy, T. 2016. Mineral Mapping For Exploration: An Australian Journey Of Evolving Spectral Sensing Technologies And Industry Collaboration. Geosciences, 6(4), 52.

Cudahy, T.J., Jones, M., Thomas, M., Laukamp, C., Caccetta, M., Hewson, R., Rodger, A., Verrall, M., 2008. Next Generation Mineral Mapping: Queensland Airborne

Hymap And Satellite Aster Surveys. Csiro Exploration & Mining Report P2007/364152.

De Barros, A.C.; Azevedo, C. T. B.; Lira, D. R.; Silva M. D.; Souza C. L.C. The Semi-Arid Domain Of The Northeast Of Brazil. In Salgado, A.; Santos, L.; Paisani, J. (Org) The Physical Geography Of Brazil. Geography Of The Physical Environment. 2019. 119-150p.

De Souza, E.G. 2017. Depositional Model And Faiologic Architecture Of Proterozoic Alluvial Fans - Ouricuri Do Ouro Formation, Espinhaço Supergroup - Chapada Diamantina/Ba (Unpublished Master's Thesis). Universidade Federal Do Rio Grande Do Sul. Porto Alegre, Brazil.

De Vries, H. C.; Benthem, M. Analysis Of Fracture Network Geometries And Orientations Within A Fold-And-Thrust Structure In The Northern Apennines, Italy. Semantic Scholar. 2013. 21p.

Dos Santos, J. M.; Salgado, A. A. R. Gênese Da Superfície Erosiva Em Ambiente Semi-Árido-Milagres/Ba: Considerações Preliminares. Revista De Geografia (Recife), V. 27, N. 1, P. 236-247, 2010.

Ducloux, J., Meunier, A., And Velde, B. 1976. Smectite, Chlorite, And A Regular Interlayered Chlorite-Vermiculite In Soils Developed On A Small Serpentinite Body, Massif Central, France. Clay Minerals, 11, 121–135

Frazier, C. S.; Graham, R. C. 2000. Pedogenic Transformation Of Fractured Granitic Bedrock, Southern California. Soil Science Society Of America Journal, V. 64, N. 6, P. 2057-2069.

Fontes, M. P. F.; Weed, S. B. Iron Oxides In Selected Brazilian Oxisols: I. Mineralogy. Soil Science Society Of America Journal, V. 55, N. 4, P. 1143-1149, 1991. Doi: 10.2136/Sssaj1991.03615995005500040040x

Gouzu, C., Itaya, T., Takeshita, H. 2005. Interlayer Cation Vacancies Of Phengites In Calcshists From The Piemonte Zone, Wester Alps, Italy. J. Mineral. Petrol. Sci. 100, 142–149.

Guimarães, J.T.; Martins, A.A.M.; Andrade Filho, E.L.; Loureiro, H.S.C.; Arcanjo, J.B.A.; Neves J.P.; Abram, M.B.; Silva, M.G.; Bento, R.V. Projeto Ibitiara-Rio De Contas: Estado Da Bahia, Programa Recursos Minerais Do Brasil, Escala 1:200.000. Publicação Cprm. Convênio Cbpm/Cprm. Salvador, 2005. 193p.

Guimarães J.T., Teixeira L.R., Silva M.G. Martins A.A.M., Filho E.L.A., Loureiro H.S.C., Arcanjo J.B., Dalton De Souza J., Neves J.P., Mascarenhas J.F., Melo R.C., Bento R.V. 2005. Datações U/Pb Em Rochas Magmáticas Intrusivas No Complexo Paramirim E No Rifte Espinhaço: Uma Contribuição Ao Estudo Da Evolução Geocronológica Da Chapada Diamantina. In: Sbg/Ba-Se, Simpósio Do Cráton Do São Francisco, 3, Anais De Resumos Expandidos, P. 159-161. (In Portuguese)

Haest M., Cudahy T., Laukamp C., Gregory S. 2012. Quantitative Mineralogy From Visible To Shortwave Infrared Spectroscopic Data: Ii. 3d Mineralogical Characterization Of The Rocklea Dome Channel Iron Deposit, Western Australia. Economic Geology, 107:229–249.

Hunt, G.R., Ashley, R.P., 1979.Spectra Of Altered Rocks In The Visible And Near-Infrared.Econ. Geol. 74, 1613–1629.

Ildefonse, P. 1980. Mineral Facies Developed By Weathering In A Meta-Gabbro, Loire-Atlantique, France. Geoderma, 24, 257–274.

Inema (2014). Instituto De Meio Ambiente E Recursos Hídricos. Solos Da Bahia.

Http://Www.Inema.Ba.Gov.Br/Wp-Content/Files/Mtematico_Solos.Pdf

[Accessed: January 20, 2019]

Hill, S. M. The Differential Weathering Of Granitic Rocks In Victoria, Australia. Agso Journal Of Australian Geology And Geophysics, V. 16, P. 271-276, 1995.

Jones, D.L., 1998. Organic Acids In The Rhizosphere — A Critical Review. Plant Soil 205, 25–44.

Kokaly, R.F., Clark, R.N., Swayze, G.A., Livo, K.E., Hoefen, T.M., Pearson, N.C., Wise, R.A., Benzel, W.M., Lowers, H.A., Driscoll, R.L., And Klein, A.J., 2017, Usgs Spectral Library Version 7: U.S. Geological Survey Data Series 1035, 61 P.

Köppen, W. Das Geographische System Der Klimate. 1936. In: Köppen, W.; Geiger, R. Handbuch Der Klimatologie. Berlin: Gebrüder Bornträger. 1- 44p.

Lampinen, H. M., Laukamp, C., Occhipinti, S. A., & Hardy, L. 2019. Mineral Footprints Of The Paleoproterozoic Sediment-Hosted Abra Pb-Zn-Cu-Au Deposit Capricorn Orogen, Western Australia. Ore Geology Reviews, 104, 436-461.

Laukamp, C.; Salama, W.; González-Álvarez, I. Proximal And Remote Spectroscopic Characterisation Of Regolith In The Albany–Fraser Orogen (Western Australia). Ore Geology Reviews, V. 73, P. 540-554, 2016.

Lacerda, M. P. C.; Queméneur, J. J. G., Andrade, H.; Alves, H. M. R.; Vieira, T. G. C. Study Of The Relationship Pedo-Geomorphological In The Soil Distribution With Argillic Horizons In The Landscape Of Lavras (Mg), Brazi. Revista Brasileira De Ciência Do Solo, V. 32, N. 1, P. 274-284, 2008. DOI: Http://Dx.Doi.Org/10.1590/S0100-06832008000100026.

Lepsch, I. F.; Buol, S. W.; Daniels, R. B. Soil-Landscape Relationships In The Occidental Plateau Of São Paulo State, Brazil: Ii. Soil Morphology, Genesis, And Classification 1. Soil Science Society Of America Journal, V. 41, N. 1, P. 109-115, 1977. Doi:10.2136/Sssaj1977.03615995004100010031x

Macdonald, E.H., 2007. Handbook Of Gold Exploration And Evolução. Woodhead Publishing, New York, Pp. 664.

Medina, C.M. Hydrothermal Alteration, Mineralization And Spectral Footprints At The Lavra Velha Gold Deposit, Bahía, Brazil. 2020. (Unpublished Master´S Thesis). Instituto De Geociências, Universidade Estadual De Campinas, Campinas, São Paulo, Brazil.

Meunier, A. 2005. Clays In Soils And Weathered Rocks. Clays, 231-293.

Naleto, J. L. C., Perrotta, M. M., Da Costa, F. G., & Souza Filho, C. R. 2019. Point And Imaging Spectroscopy Investigations On The Pedra Branca Orogenic Gold Deposit, Troia Massif, Northeast Brazil: Implications For Mineral Exploration In Amphibolite Metamorphic-Grade Terrains. Ore Geology Reviews, 107, 283-309.

Nascimento, S. T., Castro, P. D. T. A., Azevedo, Ú. R. D. Geodiversidade Dos Compartimentos Geomorfológicos Do Anticlinal De Mariana, Minas Gerais. Geociências, V. 37, N. 3, P. 497-504, 2018.

Nesbitt, H. W., & Young, G. M. 1984. Prediction Of Some Weathering Trends Of Plutonic And Volcanic Rocks Based On Thermodynamic And Kinetic Considerations. Geochimica Et Cosmochimica Acta, 48 (7), 1523-1534.

Ollier, C.; Pain, C. Regolith, Soils And Landforms. Geological Magazine. V. 134, N. 1, P. 121-142, 1997. Doi:10.1017/S0016756897386130

Passos, J.S., Ducart, D. F., Borges, A., Medina, C.M. (In Press). Rock-Landform-Soil Relationship For Geomorphopedological Characterization In The Region Of Lavra Velha, Occidental Chapada Diamantina,Bahia. Revista Brasileira De Geomorfologia.

Prado, E. M. G., Silva, A. M., Ducart, D. F., Toledo, C. L. B., & De Assis, L. M. 2016. Reflectance Spectroradiometry Applied To A Semi-Quantitative Analysis Of The Mineralogy Of The N4ws Deposit, Carajás Mineral Province, Pará, Brazil. Ore Geology Reviews, 78, 101-119.

Pedrosa-Soares, A.C.; Noce, C. M.; Wiedmann, C.; Pinto, C.P. The Araçuaí-West-Congo Orogen In Brazil: An Overview Of A Confined Orogen Formed During Gondwana Assembly. Precambrian Research, N. 110, P. 307-323, 2001.

Pontual S., Merry N.J., Gamson P. 2008a. Gmex - Spectral Analysis Guides For Mineral Exploration: Spectral Interpretation Field Manual. Ausspec International Ltd, 1, 188 P.

Pontual S., Merry N.J., Gamson P. 2008b. Gmex - Spectral Analysis Guides For Mineral Exploration: Practical Applications Handbook. Ausspec International Ltd, 2, 86 P.

Ribeiro, L. P. Caracterização Dos Solos De Ibitiara- Ba. Dissertação (Mestrado Em Geociências). Instituto De Geociências, Universidade Federal Da Bahia, Salvador. 1974. 113p.

Righi D. And Meunier A. 1995. Origin Of Clays By Rock Weathering. In Origin And Mineralogy Of Clays (Ed. B. Velde). Springer, Pp. 43–161.

Roberts, D.E., Hudson, G.R.T., 1983. The Olympic Dam Copper–Uranium–Gold Deposit, Roxby Downs, South Australia. Econ. Geol. 78, 799–822.

Schobbenhaus C. 1996. As Tafrogêneses Superpostas Espinhaço E Santo Onofre, Estado Da Bahia: Revisão E Novas Propostas. Rev.Bras. De Geoci.26(4):265-276. (In Portuguese).

Senna, J. A., Souza Filho, C. R., & Angélica, R. S. 2008. Characterization Of Clays Used In The Ceramic Manufacturing Industry By Reflectance Spectroscopy: An Experiment In The São Simão Ball-Clay Deposit, Brazil. Applied Clay Science, 41(1-2), 85-98.

Sei. Superintendent Of Economic And Social Studies Of Bahia. Mapa Topográfico.

Http://Www.Sei.Ba.Gov.Br/Site/Geoambientais/Mapas/Pdf/Municipal/Mapa_Descritivo_2913002.Pdf . [January 20, 2019]

Severo, G. D.; Melo, R. Geologia E Geoturismo Na Chapada Diamantina. Gestión Turística, N.14, P. 69-81, 2018.

Suertegaray, M.A. Terra: Feições Ilustradas. Editora Da Ufrgs, 2003. 264p.

Tappert, M. C., Rivard, B., Giles, D., Tappert, R., & Mauger, A. 2013. The Mineral Chemistry, Near Infrared, And Mid-Infrared Reflectance Spectroscopy Of Phengite From The Olympic Dam Iocg Deposit, South Australia. Ore Geology Reviews, 53, 26-38.

Teixeira L. R. 2005. Projeto Ibitiara - Rio De Contas: Relatório Temático De Litogeoquímica. Salvador: Cprm. Programa Levantamentos Geológicos Básicos Do Brasil - Plgb. Relatório Interno.

Teixeira, J.B.G., Misi, A., Silva, M.G., And Brito, R.S.C., 2019. Reconstruction Of Precambrian Terranes Of Northeastern Brazil Along Cambrian Strike-Slip Faults: A New Model Of Geodynamic Evolution And Gold Metallogeny In The State Of Bahia: Brazilian Journal Of Geology, V. 49.

Thomas, A. L., Dambrine, E., King, D., Party, J. P., & Probst, A. A Spatial Study Of The Relationships Between Streamwater Acidity And Geology, Soils And Relief (Vosges, Northeastern France). Journal Of Hydrology, V. 217, N. 1-2, P. 35-45, 1999.

Townsend, T.E., 1987.Discrimination Of Iron Alteration Minerals In Visible Andnear-Infrared Reflectance Data. J. Geophys. Res. Solid Earth Planets 92,1441–1454

Torrado, P. V.; Lepsh, I.F.; Castro, S. S. Conceitos E Aplicações Das Relações Pedologia-Geomorfologia Em Regiões Tropicais Úmidas. Tópicos Ciências Do Solo, V. 4, P.145-192, 2005.

Torrado, P. V.; Macias, F., Calvo, R., Carvalho, S. G. D., & Silva, A. C. Gênese De Solos Derivados De Rochas Ultramáficas Serpentinizadas No Sudoeste De Minas Gerais. Revista Brasileira De Ciência Do Solo, V. 30, N. 3, P. 523-541, 2006. Doi: Http://Dx.Doi.Org/10.1590/S0100-06832006000300013

Tricart, J.; Kilian, J. La Eco-Geografia Y La Ordenación Del Medio Natural. Barcelona: Anagrama, 1979. 288 P.

Troeh, F. R. Landform Parameters Correlated To Soil Drainage 1. Soil Science Society Of America Journal, V. 28, N. 6, P. 808-812, 1964.

Van Der Meer, F. (2004). Analysis Of Spectral Absorption Features In Hyperspectral Imagery. International Journal Of Applied Earth Observation And Geoinformation, 5(1), 55-68.

Villela, F. N. J.; Ross, J. L. S.; Manfredini, S. Análise Geomorfopedológica Na Borda Leste Da Bacia Sedimentar Do Paraná, Sudeste Do Brasil. Revista Brasileira De Geomorfologia, V. 16, N. 4, P. 669-682, 2015.

Villela, F. N. J.; Ross, J. L. S.; Manfredini, S. Relief-Rock-Soil Relationship In The Transition Of Atlantic Plateau To Peripheral Depression, Sao Paulo, Brazil. Journal Of Maps, V. 9, N. 3, P. 343-352, 2013.

ANEXOS

ANEXO: Relevo Sombreado (Região de Lavra Velha)

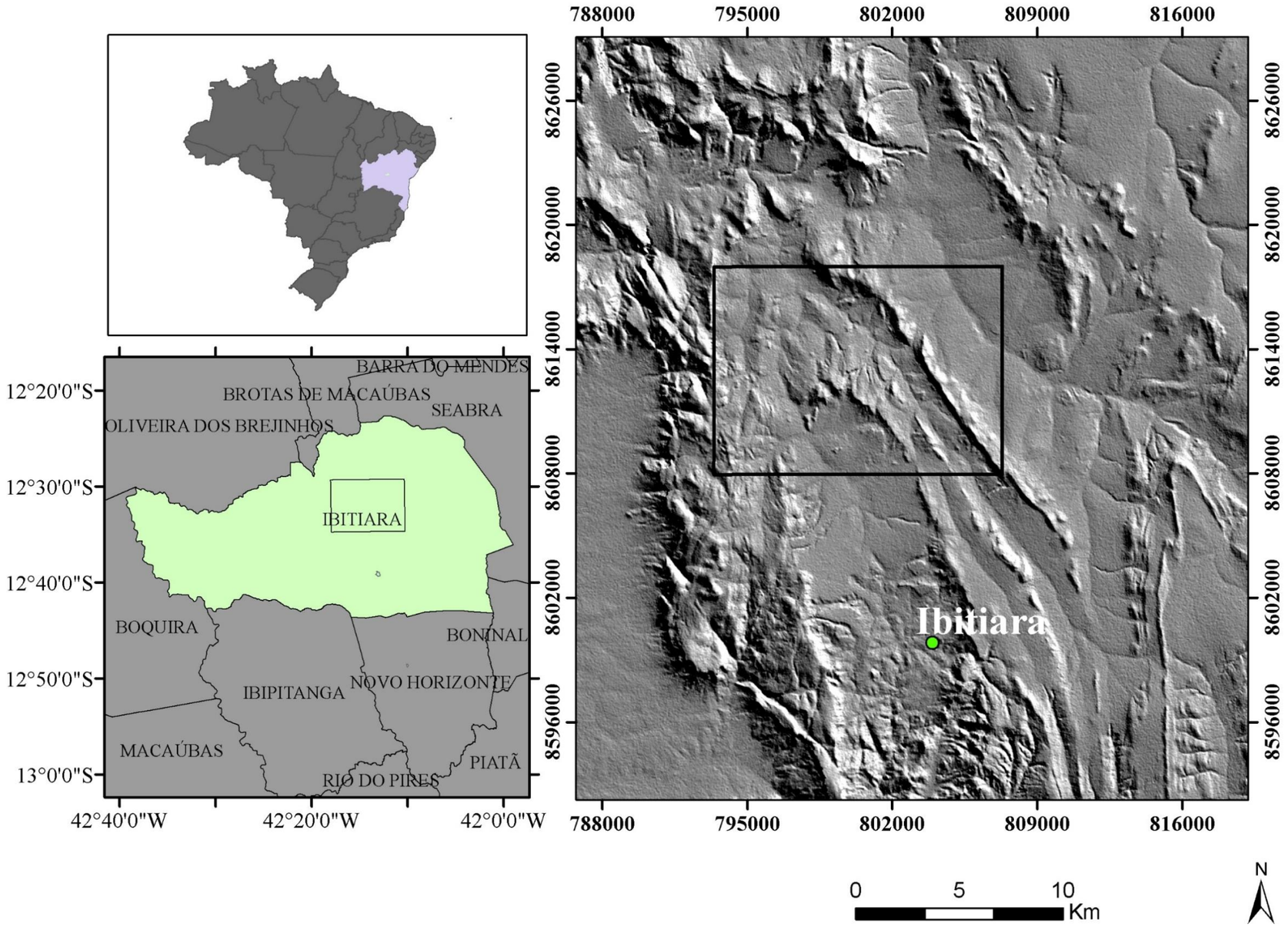

Anexo: Mapa de Declividade (Região de Lavra Velha):

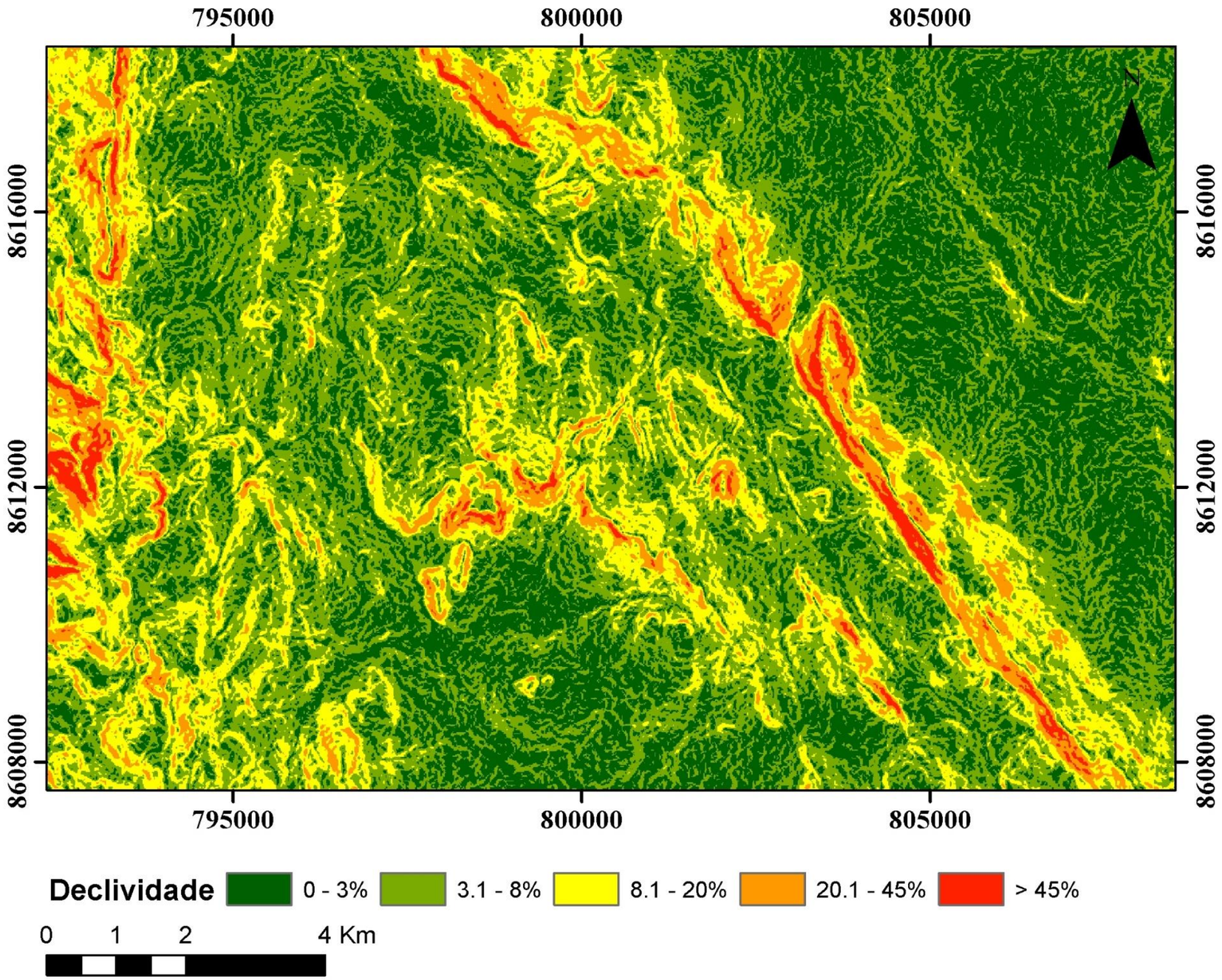

ANEXO, DADOS DE GEOQUÍMICA:

DHID	FLV_93	FLV_93	FLV_93	FLV_93	FLV_93	FLV_93	FLV_93	FLV_67	FLV_67	FLV_67	FLV_67	FLV_67
FROM	0.00	1.00	2.00	3.00	3.60	4.45	5.00	0.00	1.00	2.00	2.70	3.43
TO	1.00	2.00	3.00	3.60	4.45	5.00	6.00	1.00	2.00	2.70	3.43	4.10
Au	0.00	0.00	0.00	0.00	0.00	0.00	0.00	0.01	0.00	0.00	0.00	0.00
Ag_ppm_	1.20	6.90	13.20	10.60	0.50	5.20	0.80	1.00	0.20	0.30	0.20	0.20
Cu_ppm_	2.10	2.73	1.78	1.71	1.14	1.82	1.48	0.74	0.14	0.11	0.16	0.16
Fe_pc_	23.00	39.00	25.00	31.00	9.00	37.00	7.00	32.00	3.00	4.00	3.00	3.00
Al_pc_	80.00	110.00	70.00	70.00	110.00	460.00	510.00	20.00	10.00	10.00	20.00	40.00
As_ppm_	0.50	0.50	0.50	0.50	0.50	0.50	0.50	0.50	0.50	0.50	0.50	0.50
Ba_ppm_	2.00	2.00	4.00	2.00	2.00	2.00	2.00	2.00	2.00	2.00	2.00	2.00
Be_ppm_	0.06	0.03	0.02	0.04	0.01	0.01	0.01	0.04	0.01	0.01	0.01	0.01
Bi_ppm_	0.50	0.50	0.50	0.50	0.50	0.50	0.50	0.50	0.50	0.50	0.50	0.50
Ca_pc_	1.00	1.00	1.00	1.00	1.00	1.00	1.00	1.00	1.00	1.00	1.00	1.00
Cd_ppm_	39.00	57.00	44.00	41.00	19.00	34.00	28.00	55.00	10.00	6.00	7.00	6.00
Co_ppm_	11.00	21.00	29.00	24.00	4.00	17.00	7.00	6.00	1.00	1.00	2.00	1.00
Cr_ppm_	5.23	7.49	4.92	5.10	3.79	5.90	3.33	9.46	1.45	0.94	1.08	1.12
Ga_ppm_	10.00	10.00	10.00	10.00	10.00	10.00	10.00	10.00	10.00	10.00	10.00	10.00
K_pc_	0.35	0.52	0.26	0.21	0.23	0.26	0.17	0.04	0.01	0.03	0.01	0.04
La_ppm_	10.00	20.00	10.00	10.00	20.00	40.00	40.00	10.00	10.00	10.00	10.00	10.00
Li_ppm_								10.00	10.00	10.00	10.00	10.00
Mg_pc_	0.06	0.05	0.03	0.04	0.04	0.04	0.03	0.01	0.01	0.01	0.01	0.01
Mn_ppm_	73.00	63.00	65.00	56.00	54.00	69.00	92.00	94.00	54.00	52.00	53.00	57.00
Mo_ppm_	1.00	1.00	1.00	1.00	1.00	1.00	4.00	1.00	1.00	1.00	1.00	1.00
Na_pc_	0.03	0.04	0.02	0.05	0.02	0.05	0.02	0.02	0.01	0.01	0.01	0.01
Ni_ppm_	6.00	3.00	1.00	3.00	1.00	5.00	5.00	1.00	1.00	2.00	2.00	1.00
P_ppm_	240.00	370.00	230.00	220.00	190.00	540.00	440.00	350.00	30.00	20.00	50.00	690.00
Pb_ppm_	7.00	10.00	8.00	8.00	14.00	24.00	16.00	7.00	2.00	2.00	2.00	2.00
S_pc_	0.01	0.01	0.01	0.01	0.01	0.02	0.01	0.01	0.01	0.01	0.01	0.01
Sb_ppm_	5.00	5.00	5.00	5.00	5.00	5.00	5.00	2.00	2.00	2.00	2.00	2.00
Sc_ppm_	5.00	7.00	4.00	4.00	2.00	5.00	2.00	2.00	1.00	1.00	1.00	1.00
Se_ppm_								10.00	10.00	10.00	10.00	10.00
Sn_ppm_								10.00	10.00	10.00	10.00	10.00
Sr_ppm_	15.00	20.00	13.00	14.00	31.00	117.00	95.00	5.00	2.00	2.00	5.00	14.00
Th_ppm_	20.00	20.00	20.00	20.00	20.00	20.00	20.00	20.00	20.00	20.00	20.00	20.00
Ti_pc_	0.09	0.10	0.07	0.06	0.03	0.07	0.05	0.02	0.01	0.01	0.01	0.01
Tl_ppm_	10.00	10.00	10.00	10.00	10.00	10.00	10.00	10.00	10.00	10.00	10.00	10.00
U_ppm_	10.00	10.00	10.00	10.00	10.00	10.00	10.00	10.00	10.00	10.00	10.00	10.00
V_ppm_	72.00	107.00	75.00	77.00	22.00	76.00	15.00	119.00	5.00	3.00	2.00	2.00
W_ppm_	10.00	40.00	80.00	60.00	10.00	40.00	10.00	10.00	10.00	10.00	10.00	10.00
Y_ppm_								10.00	10.00	10.00	10.00	20.00
Zn_ppm_	12.00	12.00	14.00	14.00	4.00	11.00	9.00	3.00	2.00	2.00	2.00	2.00
Zr_ppm_								8.00	5.00	5.00	5.00	6.00

DHID	FLV_07	FLV_07	FLV_07	FLV_07	FLV_07	FLV_07	FLV_07	FLV_07	FLV_07	FLV_07	FLV_10	FLV_10	FLV_10	FLV_10	FLV_10	FLV_10	FLV_10	FLV_10
FROM	0.00	1.00	2.00	2.70	3.38	4.30	5.00	6.00	7.00	8.00	0.00	1.00	1.85	3.00	4.00	5.00	5.75	7.00
TO	1.00	2.00	2.70	3.38	4.30	5.00	6.00	7.00	8.00	9.00	1.00	1.85	3.00	4.00	5.00	5.75	7.00	8.00
Au	0.08	0.30	0.22	0.18	0.14	0.11	0.04	0.08	0.21	0.09	0.01	0.01	0.01	0.01	0.01	0.01	0.00	0.01
Ag_ppm_	0.20	0.50	0.40	0.20	0.20	0.20	0.20	0.20	0.20	0.20	0.60	0.60	2.10	0.90	3.00	0.70	0.40	0.70
Cu_ppm_	1.22	1.16	1.40	1.16	0.82	0.71	0.68	0.77	0.80	0.76	0.67	0.72	0.51	0.35	0.39	0.39	0.28	0.50
Fe_pc_	64.00	93.00	63.00	45.00	36.00	31.00	16.00	20.00	23.00	14.00	7.00	8.00	4.00	3.00	2.00	5.00	9.00	16.00
Al_pc_	1218.00	1064.00	908.00	193.00	44.00	496.00	65.00	33.00	33.00	33.00	340.00	1130.00	907.00	254.00	179.00	192.00	161.00	496.00
As_ppm_	0.00	0.00	0.00	0.00	0.00	0.00	0.00	0.00	0.00	0.00	0.00	0.00	0.00	0.00	0.00	0.00	0.00	0.00
Ba_ppm_	2.00	7.00	3.00	2.00	5.00	2.00	2.00	2.00	2.00	2.00	2.00	2.00	2.00	3.00	2.00	2.00	2.00	2.00
Be_ppm_	0.01	0.01	0.01	0.01	0.01	0.01	0.01	0.01	0.01	0.01	0.01	0.01	0.01	0.01	0.01	0.01	0.01	0.01
Bi_ppm_	0.30	0.30	0.30	0.30	0.30	0.30	0.30	0.30	0.30	0.30	0.30	0.30	0.30	0.30	0.30	0.30	0.30	0.30
Ca_pc_	91.00	73.00	63.00	19.00	12.00	39.00	9.00	7.00	8.00	8.00	1.00	1.00	1.00	1.00	1.00	1.00	1.00	1.00
Cd_ppm_	30.00	34.00	60.00	47.00	22.00	25.00	35.00	42.00	33.00	26.00	15.00	20.00	15.00	12.00	13.00	14.00	17.00	58.00
Co_ppm_	97.00	162.00	115.00	105.00	104.00	80.00	25.00	27.00	25.00	21.00	12.00	12.00	9.00	7.00	10.00	8.00	10.00	33.00
Cr_ppm_	5.69	5.96	5.90	5.46	4.08	3.37	3.18	3.59	3.57	3.26	2.56	3.49	2.60	2.27	2.03	2.27	3.00	6.58
Ga_ppm_	7.00	7.00	8.00	8.00	5.00	3.00	3.00	3.00	3.00	3.00	3.00	3.00	3.00	3.00	3.00	3.00	3.00	3.00
K_pc_	0.15	0.23	0.17	0.09	0.16	0.21	0.20	0.13	0.17	0.20	0.20	0.20	0.17	0.10	0.11	0.10	0.08	0.12
La_ppm_	5.00	6.00	4.00	4.00	4.00	6.00	4.00	5.00	3.00	5.00	8.00	14.00	12.00	4.00	2.00	4.00	3.00	3.00
Li_ppm_	0.00	0.00	0.00	0.00	0.00	0.00	0.00	0.00	0.00	0.00	0.00	0.00	0.00	0.00	0.00	0.00	0.00	0.00
Mg_pc_	0.02	0.03	0.03	0.02	0.01	0.01	0.01	0.01	0.01	0.01	0.02	0.02	0.02	0.01	0.01	0.01	0.01	0.02
Mn_ppm_	10000.00	8210.00	7912.00	1746.00	160.00	6457.00	381.00	154.00	105.00	69.00	34.00	40.00	23.00	29.00	19.00	36.00	55.00	33.00
Mo_ppm_	1.00	1.00	2.00	1.00	1.00	2.00	1.00	1.00	1.00	1.00	1.00	1.00	5.00	2.00	8.00	2.00	2.00	2.00
Na_pc_	0.01	0.01	0.01	0.01	0.01	0.01	0.01	0.01	0.01	0.01	0.01	0.01	0.03	0.02	0.02	0.02	0.01	0.02
Ni_ppm_	21.00	16.00	12.00	12.00	15.00	13.00	12.00	11.00	13.00	12.00	5.00	4.00	2.00	2.00	3.00	2.00	3.00	4.00
P_ppm_	660.00	810.00	500.00	450.00	580.00	640.00	520.00	500.00	570.00	530.00	210.00	570.00	370.00	90.00	40.00	70.00	140.00	440.00
Pb_ppm_	3.00	7.00	2.00	2.00	2.00	4.00	2.00	2.00	2.00	2.00	2.00	2.00	2.00	2.00	2.00	2.00	2.00	2.00
S_pc_	0.03	0.03	0.03	0.03	0.03	0.03	0.03	0.03	0.03	0.03	0.03	0.03	0.03	0.03	0.03	0.03	0.03	0.03
Sb_ppm_	2.00	2.00	2.00	2.00	2.00	2.00	2.00	2.00	2.00	2.00	2.00	2.00	2.00	2.00	2.00	2.00	2.00	2.00
Sc_ppm_	16.00	25.00	23.00	17.00	9.00	9.00	5.00	13.00	15.00	8.00	3.00	3.00	3.00	3.00	3.00	3.00	3.00	7.00
Se_ppm_	0.00	0.00	0.00	0.00	0.00	0.00	0.00	0.00	0.00	0.00	0.00	0.00	0.00	0.00	0.00	0.00	0.00	0.00
Sn_ppm_	0.00	0.00	0.00	0.00	0.00	0.00	0.00	0.00	0.00	0.00	0.00	0.00	0.00	0.00	0.00	0.00	0.00	0.00
Sr_ppm_	36.00	15.00	17.00	5.00	4.00	20.00	4.00	4.00	4.00	5.00	9.00	22.00	19.00	6.00	2.00	3.00	3.00	11.00
Th_ppm_	4.00	2.00	3.00	3.00	4.00	6.00	2.00	3.00	3.00	2.00	4.00	3.00	3.00	4.00	5.00	3.00	4.00	3.00
Ti_pc_	0.01	0.01	0.01	0.01	0.00	0.00	0.00	0.01	0.00	0.00	0.03	0.04	0.06	0.05	0.05	0.05	0.04	0.08
Tl_ppm_	0.00	0.00	0.00	0.00	0.00	0.00	0.00	0.00	0.00	0.00	0.00	0.00	0.00	0.00	0.00	0.00	0.00	0.00
U_ppm_	4.00	4.00	4.00	4.00	4.00	4.00	4.00	4.00	4.00	4.00	4.00	4.00	4.00	4.00	4.00	4.00	4.00	4.00
V_ppm_	68.00	55.00	62.00	51.00	22.00	18.00	17.00	29.00	21.00	17.00	24.00	31.00	23.00	24.00	29.00	28.00	41.00	61.00
W_ppm_	1.00	1.00	1.00	1.00	1.00	1.00	1.00	1.00	1.00	1.00	15.00	5.00	4.00	1.00	6.00	1.00	1.00	3.00
Y_ppm_	0.00	0.00	0.00	0.00	0.00	0.00	0.00	0.00	0.00	0.00	0.00	0.00	0.00	0.00	0.00	0.00	0.00	0.00
Zn_ppm_	51.00	48.00	41.00	39.00	39.00	35.00	24.00	26.00	29.00	28.00	5.00	4.00	3.00	2.00	2.00	2.00	3.00	7.00
Zr_ppm_	0.00	0.00	0.00	0.00	0.00	0.00	0.00	0.00	0.00	0.00	0.00	0.00	0.00	0.00	0.00	0.00	0.00	0.00

DHID	FLV_13	FLV_13	FLV_13	FLV_13	FLV_13	FLV_13	FLV_13	FLV_13	FLV_13	FLV_13	FLV_13	FLV_13	FLV_13	FLV_13	FLV_13	FLV_13	FLV_13	FLV_13	FLV_13	FLV_13	FLV_13	FLV_13
FROM	0.00	1.00	2.00	3.00	4.00	5.00	6.00	7.00	8.00	9.00	10.00	11.00	12.00	13.00	14.00	15.00	15.80	16.55	17.25	18.00	18.90	20.00
TO	1.00	2.00	3.00	4.00	5.00	6.00	7.00	8.00	9.00	10.00	11.00	12.00	13.00	14.00	15.00	15.80	16.55	17.25	18.00	18.90	20.00	21.00
Au	0.01	0.01	0.01	0.01	0.00	0.00	0.01	0.00	0.01	0.01	0.01	0.01	0.01	0.00	0.01	0.01	0.00	0.00	0.01	0.01	0.03	0.00
Ag_ppm_	0.20	0.20	0.30	0.40	0.40	0.80	0.10	0.10	0.10	0.10	0.20	0.20	0.10	0.50	0.40	0.30	0.20	0.10	0.50	0.70	0.30	0.20
Cu_ppm_	1.75	1.51	1.97	2.04	2.99	2.81	3.50	3.40	2.71	3.40	3.39	3.52	2.74	2.50	2.10	1.77	1.96	2.46	2.36	2.17	1.73	1.63
Fe_pc_	54.00	59.00	42.00	27.00	13.00	33.00	19.00	28.00	28.00	22.00	24.00	14.00	41.00	55.00	59.00	80.00	98.00	71.00	50.00	43.00	60.00	87.00
Al_pc_	900.00	330.00	370.00	370.00	680.00	410.00	760.00	950.00	730.00	960.00	680.00	720.00	830.00	300.00	190.00	160.00	210.00	470.00	1350.00	2100.00	530.00	420.00
As_ppm_	1.00	1.00	1.00	1.40	2.40	2.50	2.60	3.40	2.40	2.40	1.90	1.60	1.90	1.30	1.40	2.00	2.50	1.50	2.00	2.50	1.50	1.70
Ba_ppm_	1.00	1.00	1.00	1.00	1.00	2.00	1.00	1.00	1.00	2.00	1.00	1.00	1.00	1.00	1.00	1.00	1.00	1.00	1.00	1.00	1.00	1.00
Be_ppm_	0.01	0.01	0.01	0.01	0.04	0.05	0.07	0.08	0.07	0.09	0.09	0.11	0.10	0.08	0.07	0.05	0.06	0.09	0.10	0.09	0.06	0.05
Bi_ppm_	0.25	0.25	0.25	0.25	0.25	0.25	0.25	0.25	0.25	0.25	0.25	0.25	0.25	0.25	0.25	0.25	0.25	0.25	0.50	0.70	0.25	0.25
Ca_pc_	64.00	37.00	32.00	46.00	544.00	140.00	303.00	368.00	182.00	412.00	161.00	253.00	158.00	33.00	16.00	23.00	32.00	98.00	214.00	344.00	87.00	67.00
Cd_ppm_	213.00	198.00	227.00	352.00	663.00	521.00	643.00	652.00	276.00	610.00	582.00	602.00	372.00	470.00	435.00	428.00	399.00	523.00	423.00	341.00	266.00	349.00
Co_ppm_	112.00	166.00	91.00	109.00	92.00	95.00	77.00	127.00	137.00	64.00	55.00	39.00	232.00	150.00	57.00	50.00	86.00	110.00	87.00	149.00	103.00	85.00
Cr_ppm_	9.81	10.50	10.15	10.90	10.75	8.50	10.15	10.35	7.55	9.56	8.95	9.34	10.00	9.89	8.97	10.90	12.25	9.58	10.60	9.66	6.99	7.60
Ga_ppm_	10.00	10.00	10.00	10.00	10.00	10.00	10.00	10.00	10.00	10.00	10.00	10.00	10.00	10.00	10.00	10.00	10.00	10.00	10.00	10.00	10.00	10.00
K_pc_	0.15	0.11	0.10	0.07	0.08	0.06	0.13	0.09	0.08	0.09	0.14	0.10	0.18	0.08	0.03	0.03	0.05	0.05	0.08	0.11	0.03	0.01
La_ppm_	10.00	10.00	10.00	20.00	50.00	60.00	90.00	60.00	40.00	50.00	40.00	40.00	30.00	20.00	10.00	20.00	20.00	30.00	30.00	30.00	20.00	20.00
Li_ppm_	20.00	10.00	10.00	10.00	30.00	20.00	20.00	20.00	20.00	20.00	20.00	20.00	20.00	10.00	10.00	10.00	10.00	20.00	20.00	30.00	20.00	20.00
Mg_pc_	0.03	0.03	0.05	0.16	1.11	1.43	3.05	2.34	1.50	2.28	2.76	2.88	1.72	1.04	0.67	0.52	0.73	1.24	1.42	1.31	0.65	0.45
Mn_ppm_	3850.00	1060.00	1180.00	1250.00	3130.00	1340.00	2740.00	3620.00	2680.00	3740.00	2230.00	3050.00	3730.00	314.00	174.00	270.00	371.00	1760.00	11100.00	17900.00	2450.00	1920.00
Mo_ppm_	1.00	1.00	0.50	0.50	0.50	1.00	0.50	0.50	0.50	0.50	0.50	0.50	0.50	0.50	0.50	0.50	0.50	0.50	0.50	0.50	0.50	0.50
Na_pc_	0.02	0.01	0.02	0.03	0.04	0.04	0.05	0.04	0.03	0.03	0.02	0.02	0.02	0.01	0.01	0.01	0.01	0.01	0.02	0.03	0.01	0.01
Ni_ppm_	33.00	32.00	40.00	60.00	366.00	229.00	441.00	364.00	224.00	322.00	291.00	351.00	177.00	104.00	83.00	93.00	115.00	144.00	196.00	185.00	104.00	103.00
P_ppm_	440.00	430.00	240.00	190.00	50.00	110.00	60.00	70.00	100.00	100.00	100.00	100.00	180.00	200.00	320.00	560.00	610.00	300.00	370.00	430.00	420.00	540.00
Pb_ppm_	4.00	7.00	5.00	8.00	2.00	3.00	1.00	2.00	4.00	1.00	3.00	2.00	2.00	1.00	2.00	4.00	1.00	3.00	3.00	4.00	2.00	2.00
S_pc_	0.01	0.01	0.01	0.01	0.01	0.01	0.01	0.01	0.01	0.01	0.01	0.01	0.01	0.01	0.01	0.01	0.01	0.01	0.01	0.01	0.01	0.01
Sb_ppm_	1.00	1.00	1.00	1.00	1.00	1.00	1.00	1.00	1.00	1.00	1.00	1.00	1.00	1.00	1.00	1.00	1.00	1.00	1.00	1.00	1.00	1.00
Sc_ppm_	39.00	36.00	50.00	60.00	70.00	55.00	70.00	68.00	50.00	63.00	58.00	56.00	41.00	57.00	45.00	41.00	33.00	52.00	43.00	32.00	29.00	34.00
Se_ppm_	5.00	5.00	5.00	5.00	5.00	5.00	5.00	5.00	5.00	5.00	5.00	5.00	5.00	5.00	5.00	5.00	5.00	5.00	5.00	5.00	5.00	5.00
Sn_ppm_	5.00	5.00	5.00	5.00	5.00	5.00	5.00	5.00	5.00	5.00	5.00	5.00	5.00	5.00	5.00	5.00	5.00	5.00	5.00	5.00	5.00	5.00
Sr_ppm_	10.00	4.00	5.00	5.00	11.00	11.00	15.00	19.00	18.00	18.00	17.00	33.00	32.00	10.00	8.00	6.00	8.00	25.00	145.00	211.00	23.00	13.00
Th_ppm_	10.00	10.00	10.00	10.00	10.00	10.00	10.00	10.00	20.00	10.00	10.00	10.00	10.00	10.00	10.00	10.00	10.00	10.00	10.00	10.00	10.00	10.00
Ti_pc_	0.03	0.04	0.04	0.06	0.07	0.03	0.05	0.04	0.02	0.04	0.04	0.03	0.03	0.03	0.02	0.03	0.02	0.02	0.03	0.02	0.01	0.02
Tl_ppm_	5.00	5.00	5.00	5.00	5.00	5.00	5.00	5.00	5.00	5.00	5.00	5.00	5.00	5.00	5.00	5.00	5.00	5.00	5.00	5.00	5.00	5.00
U_ppm_	10.00	10.00	5.00	5.00	5.00	5.00	5.00	5.00	5.00	5.00	5.00	5.00	5.00	5.00	5.00	5.00	5.00	5.00	5.00	5.00	5.00	5.00
V_ppm_	300.00	284.00	246.00	232.00	170.00	155.00	142.00	147.00	123.00	134.00	123.00	111.00	164.00	132.00	135.00	178.00	177.00	156.00	177.00	178.00	117.00	133.00
W_ppm_	5.00	10.00	5.00	5.00	5.00	5.00	5.00	5.00	5.00	5.00	5.00	5.00	5.00	5.00	5.00	5.00	5.00	5.00	5.00	5.00	5.00	5.00
Y_ppm_	20.00	10.00	10.00	20.00	40.00	50.00	60.00	50.00	40.00	40.00	30.00	30.00	30.00	20.00	20.00	30.00	30.00	30.00	40.00	30.00	20.00	10.00
Zn_ppm_	34.00	37.00	38.00	57.00	294.00	255.00	502.00	416.00	252.00	350.00	368.00	438.00	304.00	155.00	123.00	143.00	203.00	256.00	326.00	375.00	155.00	111.00
Zr_ppm_	2.50	2.50	6.00	5.00	2.50	2.50	2.50	2.50	2.50	2.50	2.50	2.50	2.50	2.50	2.50	2.50	2.50	2.50	2.50	2.50	2.50	2.50

DHID	FLV_38	FLV_38	FLV_38	FLV_38	FLV_38	FLV_38	FLV_38	FLV_38	FLV_40	FLV_40	FLV_40	FLV_40	FLV_40	FLV_40	FLV_40	FLV_40	FLV_40	FLV_40	FLV_40	FLV_41	FLV_41	FLV_41	FLV_41	FLV_41	FLV_41	FLV_41	FLV_41	FLV_41	FLV_41
FROM	0.00	1.00	2.00	3.00	4.14	5.00	6.00	7.00	0.00	0.85	2.00	3.00	4.16	5.00	6.00	7.00	8.00	9.00	10.00	0.00	1.00	2.05	3.00	4.00	4.90	6.00	6.85	8.00	9.00	10.00
TO	1.00	2.00	3.00	4.14	5.00	6.00	7.00	8.00	0.85	2.00	3.00	4.16	5.00	6.00	7.00	8.00	9.00	10.00	11.00	1.00	2.05	3.00	4.00	4.90	6.00	6.85	8.00	9.00	10.00	10.88
Au	0.01	0.00	0.01	0.02	0.01	0.00	0.01	0.00	0.00	0.01	0.00	0.00	0.00	0.00	0.00	0.00	0.00	0.00	0.00	0.00	0.00	0.00	0.00	0.00	0.00	0.01	0.00	0.00	0.00	0.01
Ag_ppm_	0.50	0.50	7.50	4.80	0.90	1.10	0.20	0.20	0.80	0.20	0.20	0.20	0.20	0.20	0.20	0.20	0.20	0.20	0.20	0.20	0.20	0.30	6.10	0.50	0.30	0.30	0.30	0.20	0.20	0.40
Cu_ppm_	1.20	1.34	1.12	0.89	0.83	1.01	2.07	2.23	1.31	1.67	1.42	1.23	1.84	2.72	2.49	2.18	2.90	3.10	3.04	1.16	1.21	1.45	1.15	2.34	4.25	4.02	3.97	4.12	3.98	3.45
Fe_pc_	9.00	10.00	7.00	9.00	9.00	7.00	8.00	4.00	26.00	18.00	13.00	12.00	20.00	16.00	11.00	15.00	9.00	7.00	3.00	7.00	9.00	5.00	5.00	3.00	4.00	7.00	5.00	4.00	27.00	83.00
Al_pc_	680.00	910.00	330.00	110.00	70.00	150.00	180.00	600.00	100.00	50.00	60.00	50.00	180.00	190.00	330.00	630.00	520.00	440.00	450.00	80.00	70.00	100.00	100.00	190.00	330.00	290.00	400.00	370.00	390.00	550.00
As_ppm_	1.00	1.30	0.80	0.80	0.90	1.10	1.80	1.50	0.50	0.50	0.60	0.50	0.90	1.90	2.30	2.90	2.90	2.70	1.80	0.50	0.50	0.50	0.50	0.70	0.70	1.00	1.00	0.80	1.00	0.70
Ba_ppm_	2.00	2.00	2.00	2.00	2.00	2.00	2.00	2.00	2.00	3.00	2.00	2.00	2.00	2.00	2.00	2.00	2.00	2.00	2.00	2.00	2.00	2.00	2.00	2.00	2.00	8.00	2.00	2.00	2.00	2.00
Be_ppm_	0.03	0.01	0.01	0.01	0.01	0.01	0.01	0.01	0.01	0.01	0.01	0.01	0.02	0.03	0.05	0.11	0.23	0.33	0.41	0.05	0.07	0.04	0.03	0.16	0.47	0.59	0.46	0.45	0.57	0.54
Bi_ppm_	0.50	0.50	0.50	0.50	0.50	0.50	0.50	0.50	0.50	0.50	0.50	0.50	0.50	0.50	0.50	0.50	0.50	0.50	0.50	0.50	0.50	0.50	0.50	0.50	0.50	0.50	0.50	0.50	0.50	0.50
Ca_pc_	41.00	57.00	21.00	6.00	4.00	9.00	25.00	44.00	11.00	20.00	8.00	10.00	31.00	49.00	108.00	357.00	325.00	98.00	62.00	15.00	14.00	6.00	4.00	22.00	54.00	47.00	55.00	54.00	47.00	46.00
Cd_ppm_	59.00	64.00	47.00	47.00	61.00	76.00	107.00	87.00	85.00	137.00	126.00	139.00	113.00	136.00	116.00	124.00	108.00	104.00	93.00	67.00	73.00	89.00	91.00	100.00	111.00	102.00	106.00	114.00	106.00	118.00
Co_ppm_	29.00	34.00	49.00	58.00	39.00	56.00	85.00	62.00	29.00	40.00	42.00	39.00	111.00	130.00	127.00	155.00	119.00	70.00	43.00	15.00	19.00	46.00	45.00	34.00	72.00	469.00	146.00	76.00	52.00	77.00
Cr_ppm_	5.45	5.96	4.86	4.75	5.07	5.83	7.86	6.40	10.85	10.40	10.35	10.50	10.70	9.57	9.41	9.73	7.48	6.23	4.76	5.41	5.31	4.03	3.74	3.72	6.65	6.78	6.47	6.25	6.43	8.24
Ga_ppm_	10.00	10.00	10.00	10.00	10.00	10.00	20.00	20.00	10.00	10.00	10.00	10.00	10.00	20.00	20.00	10.00	10.00	10.00	10.00	10.00	10.00	10.00	10.00	10.00	20.00	20.00	20.00	10.00	20.00	20.00
K_pc_	0.14	0.15	0.14	0.13	0.14	0.17	0.70	0.83	0.09	0.05	0.05	0.05	0.06	0.12	0.13	0.17	0.29	0.51	0.25	0.09	0.09	0.11	0.09	0.08	0.04	0.02	0.02	0.01	0.02	0.29
La_ppm_	20.00	20.00	60.00	30.00	10.00	10.00	20.00	20.00	10.00	10.00	10.00	10.00	20.00	40.00	50.00	50.00	100.00	120.00	150.00	20.00	20.00	20.00	20.00	20.00	10.00	10.00	10.00	10.00	10.00	10.00
Li_ppm_	10.00	10.00	10.00	10.00	10.00	10.00	10.00	10.00	10.00	10.00	10.00	10.00	10.00	20.00	10.00	20.00	30.00	30.00	30.00	10.00	10.00	10.00	10.00	10.00	10.00	10.00	10.00	10.00	10.00	10.00
Mg_pc_	0.08	0.10	0.04	0.02	0.02	0.14	0.87	1.13	0.02	0.01	0.02	0.02	0.05	0.18	0.20	0.42	1.37	2.17	2.46	0.04	0.04	0.03	0.03	0.57	2.38	2.64	3.25	3.50	3.05	2.11
Mn_ppm_	3640.00	5390.00	1600.00	383.00	171.00	862.00	983.00	3160.00	129.00	213.00	153.00	189.00	815.00	866.00	1530.00	4070.00	2490.00	1630.00	1085.00	374.00	340.00	128.00	70.00	293.00	1140.00	1160.00	1440.00	1310.00	1240.00	1500.00
Mo_ppm_	1.00	1.00	21.00	13.00	1.00	1.00	1.00	1.00	1.00	1.00	1.00	1.00	1.00	1.00	1.00	1.00	1.00	1.00	1.00	1.00	1.00	1.00	1.00	1.00	1.00	1.00	1.00	1.00	1.00	1.00
Na_pc_	0.01	0.01	0.01	0.01	0.01	0.01	0.02	0.02	0.01	0.01	0.01	0.01	0.03	0.03	0.02	0.02	0.01	0.01	0.01	0.01	0.01	0.01	0.01	0.02	0.04	0.05	0.04	0.03	0.02	0.02
Ni_ppm_	12.00	15.00	12.00	9.00	10.00	11.00	26.00	29.00	18.00	54.00	39.00	36.00	37.00	61.00	68.00	147.00	265.00	240.00	258.00	10.00	11.00	18.00	16.00	38.00	94.00	84.00	97.00	99.00	87.00	69.00
P_ppm_	290.00	330.00	350.00	410.00	450.00	320.00	360.00	280.00	450.00	420.00	300.00	210.00	210.00	270.00	260.00	280.00	220.00	200.00	240.00	150.00	150.00	100.00	60.00	50.00	180.00	220.00	320.00	270.00	400.00	370.00
Pb_ppm_	3.00	5.00	3.00	2.00	2.00	2.00	3.00	3.00	3.00	4.00	2.00	2.00	5.00	7.00	7.00	8.00	5.00	3.00	4.00	2.00	2.00	3.00	3.00	3.00	6.00	9.00	6.00	5.00	6.00	5.00
S_pc_	0.01	0.01	0.01	0.01	0.01	0.01	0.01	0.01	0.01	0.01	0.01	0.01	0.01	0.01	0.01	0.01	0.01	0.01	0.01	0.01	0.01	0.01	0.01	0.01	0.01	0.01	0.01	0.01	0.01	0.01
Sb_ppm_	2.00	2.00	2.00	2.00	2.00	2.00	3.00	2.00	2.00	2.00	2.00	2.00	2.00	2.00	2.00	2.00	2.00	2.00	2.00	2.00	2.00	2.00	2.00	2.00	2.00	2.00	2.00	2.00	2.00	2.00
Sc_ppm_	11.00	13.00	10.00	10.00	12.00	15.00	20.00	15.00	13.00	27.00	37.00	35.00	42.00	47.00	44.00	40.00	29.00	23.00	17.00	10.00	10.00	12.00	11.00	17.00	19.00	16.00	17.00	16.00	19.00	16.00
Se_ppm_	10.00	10.00	10.00	10.00	10.00	10.00	10.00	10.00	10.00	10.00	10.00	10.00	10.00	10.00	10.00	10.00	10.00	10.00	10.00	10.00	10.00	10.00	10.00	10.00	10.00	10.00	10.00	10.00	10.00	10.00
Sn_ppm_	10.00	10.00	10.00	10.00	10.00	10.00	10.00	10.00	10.00	10.00	10.00	10.00	10.00	10.00	10.00	10.00	10.00	10.00	10.00	10.00	10.00	10.00	10.00	10.00	10.00	10.00	10.00	10.00	10.00	10.00
Sr_ppm_	21.00	25.00	15.00	9.00	5.00	7.00	18.00	40.00	5.00	2.00	2.00	2.00	6.00	8.00	11.00	26.00	17.00	25.00	20.00	6.00	7.00	6.00	5.00	11.00	24.00	30.00	22.00	22.00	26.00	27.00
Th_ppm_	20.00	20.00	20.00	20.00	20.00	20.00	20.00	20.00	20.00	20.00	20.00	20.00	20.00	20.00	20.00	20.00	20.00	20.00	20.00	20.00	20.00	20.00	20.00	20.00	20.00	20.00	20.00	20.00	20.00	20.00
Ti_pc_	0.03	0.03	0.02	0.01	0.01	0.01	0.01	0.01	0.04	0.04	0.04	0.05	0.03	0.04	0.04	0.03	0.02	0.02	0.01	0.06	0.06	0.03	0.02	0.02	0.10	0.03	0.08	0.12	0.04	0.01
Tl_ppm_	10.00	10.00	10.00	10.00	10.00	10.00	10.00	10.00	10.00	10.00	10.00	10.00	10.00	10.00	10.00	10.00	10.00	10.00	10.00	10.00	10.00	10.00	10.00	10.00	10.00	10.00	10.00	10.00	10.00	10.00
U_ppm_	10.00	10.00	10.00	10.00	10.00	10.00	10.00	10.00	10.00	10.00	10.00	10.00	10.00	10.00	10.00	10.00	10.00	10.00	10.00	10.00	10.00	10.00	10.00	10.00	10.00	10.00	10.00	10.00	10.00	10.00
V_ppm_	71.00	83.00	55.00	50.00	52.00	65.00	115.00	96.00	185.00	232.00	256.00	254.00	268.00	257.00	227.00	249.00	184.00	150.00	93.00	91.00	90.00	89.00	100.00	121.00	144.00	146.00	153.00	125.00	140.00	172.00
W_ppm_	10.00	10.00	30.00	20.00	10.00	10.00	10.00	10.00	10.00	10.00	10.00	10.00	10.00	10.00	10.00	10.00	10.00	10.00	10.00	10.00	10.00	20.00	30.00	10.00	10.00	10.00	10.00	10.00	10.00	10.00
Y_ppm_	20.00	30.00	20.00	20.00	10.00	10.00	20.00	20.00	10.00	20.00	10.00	10.00	40.00	80.00	80.00	90.00	200.00	260.00	320.00	10.00	10.00	10.00	10.00	20.00	20.00	20.00	20.00	20.00	20.00	10.00
Zn_ppm_	34.00	37.00	23.00	20.00	25.00	47.00	148.00	173.00	20.00	53.00	43.00	37.00	46.00	68.00	84.00	132.00	223.00	235.00	245.00	13.00	14.00	10.00	10.00	37.00	87.00	93.00	108.00	103.00	100.00	134.00
Zr_ppm_	5.00	5.00	5.00	6.00	6.00	5.00	6.00	5.00	9.00	9.00	9.00	8.00	6.00	5.00	5.00	5.00	5.00	5.00	5.00	5.00	5.00	5.00	5.00	5.00	5.00	5.00	5.00	5.00	5.00	5.00

DHID	FLV_63	FLV_63	FLV_63	FLV_63	FLV_63	FLV_63	FLV_63	FLV_63	FLV_63	FLV_63	FLV_63	FLV_63	FLV_63	FLV_63	FLV_63	FLV_63	FLV_63	FLV_63	FLV_63	FLV_63	FLV_63	FLV_63	FLV_63	FLV_63	FLV_63	FLV_63	FLV_63	FLV_63	FLV_63	FLV_63	FLV_63	FLV_63	FLV_63	FLV_63	FLV_63
FROM	0.00	1.00	2.00	3.00	4.00	5.00	6.00	7.00	8.00	9.00	10.00	11.00	12.00	12.80	12.80	13.55	14.30	15.00	16.00	17.00	18.00	19.00	20.00	21.00	22.00	23.00	24.00	24.70	25.80	27.00	28.00	29.00	30.14	31.23	32.20
TO	1.00	2.00	3.00	4.00	5.00	6.00	7.00	8.00	9.00	10.00	11.00	12.00	12.80	13.55	14.30	15.00	16.00	17.00	18.00	19.00	20.00	21.00	22.00	23.00	24.00	24.70	25.80	27.00	28.00	29.00	30.14	31.23	32.20	33.00	
Au	0.00	0.01	0.00	0.00	0.00	0.00	0.00	0.00	0.00	0.00	0.00	0.00	0.00	0.00	0.00	0.00	0.01	0.00	0.00	0.00	0.00	0.00	0.00	0.00	0.00	0.00	0.00	0.00	0.00	0.00	0.00	0.04	0.00	0.01	
Ag_ppm_	0.20	13.00	88.90	39.10	4.20	0.20	7.50	0.20	0.20	0.20	0.20	0.20	0.20	0.20	0.20	0.20	0.20	0.20	0.20	0.20	0.20	0.20	0.20	0.20	0.20	0.20	0.20	0.20	0.20	0.20	0.20	0.20	0.20	0.20	
Cu_ppm_	1.82	1.43	1.45	2.13	1.28	1.08	0.84	1.03	1.17	1.06	1.21	1.03	1.16	1.16	1.18	1.17	1.44	1.17	1.26	1.08	1.46	1.29	1.59	1.31	1.73	1.59	1.94	1.56	1.75	1.99	2.22	2.44	2.87	2.89	
Fe_pc_	24.00	21.00	23.00	41.00	13.00	23.00	12.00	21.00	37.00	31.00	24.00	21.00	14.00	10.00	11.00	12.00	21.00	31.00	11.00	36.00	38.00	13.00	13.00	15.00	14.00	15.00	13.00	16.00	27.00	27.00	24.00	26.00	24.00	36.00	
Al_pc_	80.00	70.00	90.00	40.00	30.00	30.00	30.00	30.00	20.00	20.00	10.00	10.00	10.00	10.00	10.00	10.00	20.00	20.00	20.00	20.00	20.00	20.00	20.00	20.00	300.00	710.00	2460.00	620.00	940.00	2110.00	890.00	1240.00	940.00	920.00	
As_ppm_	0.80	0.90	0.50	1.70	0.60	0.60	0.50	0.50	0.50	0.50	0.50	0.50	0.50	0.50	0.50	0.50	0.50	0.50	0.50	0.50	0.60	0.70	0.70	0.70	0.70	0.70	1.40	0.80	1.10	2.00	1.50	1.90	2.40	4.30	
Ba_ppm_	2.00	2.00	2.00	2.00	2.00	2.00	2.00	2.00	2.00	2.00	2.00	2.00	2.00	2.00	2.00	2.00	2.00	2.00	2.00	2.00	2.00	2.00	2.00	2.00	2.00	3.00	2.00	2.00	2.00	2.00	3.00	2.00	2.00	2.00	
Be_ppm_	0.44	0.21	0.03	0.02	0.01	0.01	0.01	0.01	0.01	0.01	0.01	0.01	0.01	0.01	0.01	0.01	0.01	0.01	0.01	0.01	0.01	0.01	0.01	0.01	0.04	0.16	0.21	0.21	0.27	0.30	0.39	0.44	0.42	0.47	
Bi_ppm_	0.50	0.50	0.50	0.50	0.50	0.50	0.50	0.50	0.50	0.50	0.50	0.50	0.50	0.50	0.50	0.50	0.50	0.50	0.50	0.50	0.50	0.50	0.50	0.50	0.50	0.50	0.50	0.50	0.50	0.50	0.50	0.50	0.50	0.50	
Ca_pc_	15.00	13.00	8.00	25.00	14.00	10.00	3.00	7.00	20.00	5.00	4.00	3.00	3.00	4.00	4.00	3.00	3.00	4.00	2.00	3.00	3.00	4.00	4.00	7.00	13.00	36.00	153.00	54.00	89.00	566.00	574.00	759.00	645.00	203.00	
Cd_ppm_	136.00	112.00	67.00	150.00	136.00	136.00	76.00	102.00	100.00	73.00	58.00	52.00	57.00	66.00	97.00	104.00	106.00	139.00	69.00	137.00	242.00	232.00	157.00	149.00	143.00	113.00	74.00	106.00	100.00	106.00	86.00	87.00	96.00	104.00	
Co_ppm_	43.00	67.00	155.00	174.00	54.00	49.00	46.00	43.00	80.00	49.00	46.00	37.00	36.00	38.00	39.00	44.00	49.00	46.00	30.00	35.00	78.00	91.00	72.00	84.00	87.00	84.00	183.00	147.00	149.00	176.00	138.00	116.00	114.00	95.00	
Cr_ppm_	10.50	9.55	8.72	21.00	11.70	11.40	7.02	7.80	11.45	9.50	9.38	8.80	8.43	9.00	10.35	11.35	12.00	12.20	8.70	11.00	13.30	13.00	11.90	12.00	10.60	8.01	5.65	5.56	5.71	5.65	5.17	5.25	5.63	6.35	
Ga_ppm_	10.00	10.00	10.00	20.00	10.00	10.00	10.00	10.00	10.00	10.00	10.00	10.00	10.00	10.00	10.00	10.00	10.00	10.00	10.00	10.00	10.00	10.00	10.00	10.00	10.00	10.00	10.00	10.00	10.00	10.00	10.00	10.00	10.00	10.00	
K_pc_	0.09	0.08	0.12	0.05	0.02	0.04	0.05	0.04	0.03	0.03	0.03	0.03	0.03	0.04	0.03	0.04	0.05	0.04	0.06	0.05	0.05	0.04	0.06	0.04	0.06	0.05	0.23	0.08	0.05	0.06	0.05	0.06	0.04	0.06	
La_ppm_	10.00	10.00	10.00	10.00	10.00	10.00	10.00	10.00	10.00	10.00	10.00	10.00	10.00	10.00	10.00	10.00	10.00	10.00	10.00	10.00	10.00	10.00	10.00	10.00	10.00	10.00	130.00	150.00	190.00	240.00	200.00	130.00	120.00	90.00	
Li_ppm_	10.00	10.00	10.00	10.00	10.00	10.00	10.00	10.00	10.00	10.00	10.00	10.00	10.00	10.00	10.00	10.00	10.00	10.00	10.00	10.00	10.00	10.00	10.00	10.00	10.00	10.00	10.00	10.00	20.00	40.00	40.00	40.00	30.00	10.00	
Mg_pc_	0.03	0.02	0.02	0.01	0.01	0.01	0.01	0.01	0.01	0.01	0.01	0.01	0.01	0.01	0.01	0.01	0.01	0.01	0.01	0.01	0.02	0.02	0.02	0.02	0.03	0.10	0.35	1.01	1.10	1.23	1.20	1.31	1.44	1.88	2.22
Mn_ppm_	175.00	141.00	147.00	262.00	132.00	199.00	66.00	111.00	515.00	257.00	209.00	189.00	175.00	182.00	187.00	224.00	323.00	406.00	236.00	280.00	215.00	213.00	236.00	268.00	1150.00	2830.00	14500.00	2440.00	3070.00	7540.00	3240.00	4900.00	3140.00	2710.00	
Mo_ppm_	1.00	1.00	1.00	1.00	1.00	1.00	1.00	1.00	1.00	1.00	1.00	1.00	1.00	1.00	1.00	1.00	1.00	1.00	1.00	1.00	1.00	1.00	1.00	1.00	1.00	1.00	1.00	1.00	1.00	1.00	1.00	1.00	1.00	1.00	
Na_pc_	0.02	0.02	0.01	0.01	0.02	0.01	0.01	0.02	0.02	0.02	0.02	0.01	0.01	0.02	0.03	0.02	0.03	0.02	0.02	0.02	0.02	0.01	0.02	0.01	0.01	0.02	0.01	0.01	0.01	0.01	0.01	0.01	0.01	0.01	
Ni_ppm_	25.00	27.00	27.00	42.00	34.00	25.00	13.00	17.00	37.00	29.00	24.00	13.00	12.00	14.00	18.00	21.00	27.00	34.00	22.00	31.00	67.00	84.00	77.00	74.00	46.00	65.00	173.00	157.00	157.00	266.00	316.00	420.00	423.00	505.00	
P_ppm_	770.00	830.00	640.00	1820.00	410.00	400.00	350.00	300.00	370.00	380.00	500.00	490.00	490.00	540.00	450.00	560.00	510.00	440.00	370.00	260.00	270.00	220.00	160.00	190.00	230.00	260.00	360.00	340.00	360.00	440.00	380.00	330.00	300.00	560.00	
Pb_ppm_	2.00	2.00	2.00	4.00	2.00	2.00	2.00	2.00	2.00	2.00	2.00	2.00	2.00	2.00	2.00	2.00	2.00	2.00	2.00	2.00	2.00	3.00	3.00	2.00	10.00	15.00	23.00	6.00	8.00	6.00	5.00	8.00	5.00	3.00	
S_pc_	0.03	0.03	0.02	0.04	0.02	0.01	0.01	0.01	0.02	0.01	0.02	0.02	0.02	0.02	0.02	0.02	0.02	0.02	0.01	0.01	0.02	0.01	0.01	0.01	0.01	0.01	0.01	0.01	0.01	0.01	0.01	0.01	0.01	0.01	
Sb_ppm_	2.00	2.00	2.00	4.00	2.00	2.00	2.00	2.00	2.00	2.00	2.00	2.00	2.00	2.00	3.00	2.00	2.00	2.00	2.00	2.00	2.00	2.00	3.00	2.00	2.00	2.00	2.00	2.00	2.00	2.00	2.00	2.00	2.00	2.00	
Sc_ppm_	20.00	19.00	11.00	32.00	26.00	24.00	16.00	19.00	28.00	30.00	36.00	35.00	41.00	42.00	37.00	42.00	35.00	28.00	26.00	25.00	37.00	39.00	36.00	48.00	83.00	61.00	46.00	26.00	27.00	25.00	20.00	20.00	23.00	21.00	
Se_ppm_	10.00	10.00	10.00	10.00	10.00	10.00	10.00	10.00	10.00	10.00	10.00	10.00	10.00	10.00	10.00	10.00	10.00	10.00	10.00	10.00	10.00	10.00	10.00	10.00	10.00	10.00	10.00	10.00	10.00	10.00	10.00	10.00	10.00	10.00	
Sn_ppm_	10.00	10.00	10.00	10.00	10.00	10.00	10.00	10.00	10.00	10.00	10.00	10.00	10.00	10.00	10.00	10.00	10.00	10.00	10.00	10.00	10.00	10.00	10.00	10.00	10.00	10.00	10.00	10.00	10.00	10.00	10.00	10.00	10.00	10.00	
Sr_ppm_	24.00	13.00	7.00	5.00	1.00	2.00	1.00	1.00	1.00	1.00	1.00	1.00	1.00	1.00	1.00	1.00	1.00	1.00	1.00	1.00	1.00	1.00	2.00	1.00	2.00	10.00	19.00	14.00	17.00	16.00	26.00	36.00	25.00	36.00	
Th_ppm_	20.00	20.00	20.00	20.00	20.00	20.00	20.00	20.00	20.00	20.00	20.00	20.00	20.00	20.00	20.00	20.00	20.00	20.00	20.00	20.00	20.00	20.00	20.00	20.00	20.00	20.00	20.00	20.00	20.00	20.00	20.00	20.00	20.00	20.00	
Ti_pc_	0.04	0.03	0.03	0.04	0.04	0.03	0.02	0.03	0.04	0.04	0.04	0.04	0.03	0.04	0.04	0.05	0.05	0.05	0.03	0.04	0.05	0.05	0.05	0.06	0.04	0.02	0.02	0.03	0.02	0.02	0.01	0.01	0.01	0.02	
Tl_ppm_	10.00	10.00	10.00	10.00	10.00	10.00	10.00	10.00	10.00	10.00	10.00	10.00	10.00	10.00	10.00	10.00	10.00	10.00	10.00	10.00	10.00	10.00	10.00	10.00	10.00	10.00	10.00	10.00	10.00	10.00	10.00	10.00	10.00	10.00	
U_ppm_	10.00	10.00	10.00	10.00	10.00	10.00	10.00	10.00	10.00	10.00	10.00	10.00	10.00	10.00	10.00	10.00	10.00	10.00	10.00	10.00	10.00	10.00	10.00	10.00	10.00	10.00	10.00	10.00	10.00	10.00	10.00	10.00	10.00	10.00	
V_ppm_	316.00	253.00	127.00	281.00	180.00	133.00	72.00	124.00	278.00	227.00	221.00	193.00	184.00	194.00	176.00	200.00	211.00	218.00	129.00	174.00	244.00	215.00	212.00	190.00	155.00	137.00	146.00	149.00	140.00	159.00	90.00	133.00	99.00	109.00	
W_ppm_	10.00	30.00	220.00	60.00	10.00	10.00	10.00	10.00	10.00	10.00	10.00	10.00	10.00	10.00	10.00	10.00	10.00	10.00	10.00	10.00	10.00	10.00	10.00	10.00	10.00	10.00	10.00	10.00	10.00	10.00	10.00	10.00	10.00	10.00	
Y_ppm_	10.00	10.00	10.00	10.00	10.00	10.00	10.00	10.00	10.00	10.00	10.00	10.00	10.00	10.00	10.00	10.00	10.00	10.00	10.00	10.00	10.00	10.00	10.00	10.00	20.00	90.00	180.00	280.00	340.00	320.00	260.00	210.00	200.00	290.00	
Zn_ppm_	32.00	31.00	19.00	62.00	45.00	33.00	18.00	19.00	31.00	23.00	18.00	10.00	8.00	9.00	12.00	12.00	15.00	18.00	11.00	16.00	39.00	48.00	40.00	35.00	33.00	55.00	279.00	253.00	254.00	321.00	291.00	220.00	291.00	302.00	
Zr_ppm_	15.00	11.00	7.00	11.00	10.00	11.00	11.00	11.00	11.00	8.00	6.00	6.00	5.00	5.00	5.00	6.00	7.00	8.00	5.00	9.00	8.00	7.00	6.00	6.00	5.00	5.00	5.00	5.00	5.00	5.00	5.00	5.00	5.00	5.00	

DHID	FLV_40	FLV_40	FLV_40	FLV_40	FLV_40	FLV_40	FLV_40	FLV_40	FLV_40	FLV_40	FLV_40	FLV_63	FLV_63	FLV_63	FLV_63
FROM	0.00	0.85	2.00	3.00	4.16	5.00	6.00	7.00	8.00	9.00	10.00	0.00	1.00	2.00	3.00
TO	0.85	2.00	3.00	4.16	5.00	6.00	7.00	8.00	9.00	10.00	11.00	1.00	2.00	3.00	4.00
Au	0.00	0.01	0.00	0.00	0.00	0.00	0.00	0.00	0.00	0.00	0.00	0.00	0.01	0.00	0.00
Ag_ppm_	0.80	0.20	0.20	0.20	0.20	0.20	0.20	0.20	0.20	0.20	0.20	0.20	13.00	88.90	39.10
Cu_ppm_	1.31	1.67	1.42	1.23	1.84	2.72	2.49	2.18	2.90	3.10	3.04	1.82	1.43	1.45	2.13
Fe_pc_	26.00	18.00	13.00	12.00	20.00	16.00	11.00	15.00	9.00	7.00	3.00	24.00	21.00	23.00	41.00
Al_pc_	100.00	50.00	60.00	50.00	180.00	190.00	330.00	630.00	520.00	440.00	450.00	80.00	70.00	90.00	40.00
As_ppm_	0.50	0.50	0.60	0.50	0.90	1.90	2.30	2.90	2.90	2.70	1.80	0.80	0.90	0.50	1.70
Ba_ppm_	2.00	3.00	2.00	2.00	2.00	2.00	2.00	2.00	2.00	2.00	2.00	2.00	2.00	2.00	2.00
Be_ppm_	0.01	0.01	0.01	0.01	0.02	0.03	0.05	0.11	0.23	0.33	0.41	0.44	0.21	0.03	0.02
Bi_ppm_	0.50	0.50	0.50	0.50	0.50	0.50	0.50	0.50	0.50	0.50	0.50	0.50	0.50	0.50	0.50
Ca_pc_	11.00	20.00	8.00	10.00	31.00	49.00	108.00	357.00	325.00	98.00	62.00	15.00	13.00	8.00	25.00
Cd_ppm_	85.00	137.00	126.00	139.00	113.00	136.00	116.00	124.00	108.00	104.00	93.00	136.00	112.00	67.00	150.00
Co_ppm_	29.00	40.00	42.00	39.00	111.00	130.00	127.00	155.00	119.00	70.00	43.00	43.00	67.00	155.00	174.00
Cr_ppm_	10.85	10.40	10.35	10.50	10.70	9.57	9.41	9.73	7.48	6.23	4.76	10.50	9.55	8.72	21.00
Ga_ppm_	10.00	10.00	10.00	10.00	10.00	20.00	20.00	10.00	10.00	10.00	10.00	10.00	10.00	10.00	20.00
K_pc_	0.09	0.05	0.05	0.05	0.06	0.12	0.13	0.17	0.29	0.51	0.25	0.09	0.08	0.12	0.05
La_ppm_	10.00	10.00	10.00	10.00	20.00	40.00	50.00	50.00	100.00	120.00	150.00	10.00	10.00	10.00	10.00
Li_ppm_	10.00	10.00	10.00	10.00	10.00	20.00	10.00	20.00	30.00	30.00	30.00	10.00	10.00	10.00	10.00
Mg_pc_	0.02	0.01	0.02	0.02	0.05	0.18	0.20	0.42	1.37	2.17	2.46	0.03	0.02	0.02	0.01
Mn_ppm_	129.00	213.00	153.00	189.00	815.00	866.00	1530.00	4070.00	2490.00	1630.00	1085.00	175.00	141.00	147.00	262.00
Mo_ppm_	1.00	1.00	1.00	1.00	1.00	1.00	1.00	1.00	1.00	1.00	1.00	1.00	1.00	1.00	1.00
Na_pc_	0.01	0.01	0.01	0.01	0.03	0.03	0.02	0.02	0.01	0.01	0.01	0.02	0.02	0.01	0.01
Ni_ppm_	18.00	54.00	39.00	36.00	37.00	61.00	68.00	147.00	265.00	240.00	258.00	25.00	27.00	27.00	42.00
P_ppm_	450.00	420.00	300.00	210.00	210.00	270.00	260.00	280.00	220.00	200.00	240.00	770.00	830.00	640.00	1820.00
Pb_ppm_	3.00	4.00	2.00	2.00	5.00	7.00	7.00	8.00	5.00	3.00	4.00	2.00	2.00	2.00	4.00
S_pc_	0.01	0.01	0.01	0.01	0.01	0.01	0.01	0.01	0.01	0.01	0.01	0.03	0.03	0.02	0.04
Sb_ppm_	2.00	2.00	2.00	2.00	2.00	2.00	2.00	2.00	2.00	2.00	2.00	2.00	2.00	2.00	4.00
Sc_ppm_	13.00	27.00	37.00	35.00	42.00	47.00	44.00	40.00	29.00	23.00	17.00	20.00	19.00	11.00	32.00
Se_ppm_	10.00	10.00	10.00	10.00	10.00	10.00	10.00	10.00	10.00	10.00	10.00	10.00	10.00	10.00	10.00
Sn_ppm_	10.00	10.00	10.00	10.00	10.00	10.00	10.00	10.00	10.00	10.00	10.00	10.00	10.00	10.00	10.00
Sr_ppm_	5.00	2.00	2.00	2.00	6.00	8.00	11.00	26.00	17.00	25.00	20.00	24.00	13.00	7.00	5.00
Th_ppm_	20.00	20.00	20.00	20.00	20.00	20.00	20.00	20.00	20.00	20.00	20.00	20.00	20.00	20.00	20.00
Ti_pc_	0.04	0.04	0.04	0.05	0.03	0.04	0.04	0.03	0.02	0.02	0.01	0.04	0.03	0.03	0.04
Tl_ppm_	10.00	10.00	10.00	10.00	10.00	10.00	10.00	10.00	10.00	10.00	10.00	10.00	10.00	10.00	10.00
U_ppm_	10.00	10.00	10.00	10.00	10.00	10.00	10.00	10.00	10.00	10.00	10.00	10.00	10.00	10.00	10.00
V_ppm_	185.00	232.00	256.00	254.00	268.00	257.00	227.00	249.00	184.00	150.00	93.00	316.00	253.00	127.00	281.00
W_ppm_	10.00	10.00	10.00	10.00	10.00	10.00	10.00	10.00	10.00	10.00	10.00	10.00	30.00	220.00	60.00
Y_ppm_	10.00	20.00	10.00	10.00	40.00	80.00	80.00	90.00	200.00	260.00	320.00	10.00	10.00	10.00	10.00
Zn_ppm_	20.00	53.00	43.00	37.00	46.00	68.00	84.00	132.00	223.00	235.00	245.00	32.00	31.00	19.00	62.00
Zr_ppm_	9.00	9.00	9.00	8.00	6.00	5.00	5.00	5.00	5.00	5.00	5.00	15.00	11.00	7.00	11.00

DHID	FLV_63	FLV_63	FLV_63	FLV_63	FLV_63	FLV_63	FLV_63	FLV_63	FLV_63	FLV_63	FLV_63	FLV_63	FLV_63	FLV_63	FLV_63	FLV_63
FROM	4.00	5.00	6.00	7.00	8.00	9.00	10.00	11.00	12.00	12.80	13.55	14.30	15.00	16.00	17.00	18.00
TO	5.00	6.00	7.00	8.00	9.00	10.00	11.00	12.00	12.80	13.55	14.30	15.00	16.00	17.00	18.00	19.00
Au	0.00	0.00	0.00	0.00	0.00	0.00	0.00	0.00	0.00	0.00	0.00	0.00	0.01	0.00	0.00	0.00
Ag_ppm_	4.20	0.20	7.50	0.20	0.20	0.20	0.20	0.20	0.20	0.20	0.20	0.20	0.20	0.20	0.20	0.20
Cu_ppm_	1.28	1.08	0.84	1.03	1.17	1.06	1.21	1.03	1.16	1.16	1.18	1.17	1.44	1.17	1.26	1.08
Fe_pc_	13.00	23.00	12.00	21.00	37.00	31.00	24.00	21.00	14.00	10.00	11.00	12.00	21.00	31.00	11.00	36.00
Al_pc_	30.00	30.00	30.00	30.00	20.00	20.00	10.00	10.00	10.00	10.00	10.00	10.00	20.00	20.00	20.00	20.00
As_ppm_	0.60	0.60	0.50	0.50	0.50	0.50	0.50	0.50	0.50	0.50	0.50	0.50	0.50	0.50	0.50	0.50
Ba_ppm_	2.00	2.00	2.00	2.00	2.00	2.00	2.00	2.00	2.00	2.00	2.00	2.00	2.00	2.00	2.00	2.00
Be_ppm_	0.01	0.01	0.01	0.01	0.01	0.01	0.01	0.01	0.01	0.01	0.01	0.01	0.01	0.01	0.01	0.01
Bi_ppm_	0.50	0.50	0.50	0.50	0.50	0.50	0.50	0.50	0.50	0.50	0.50	0.50	0.50	0.50	0.50	0.50
Ca_pc_	14.00	10.00	3.00	7.00	20.00	5.00	4.00	3.00	3.00	4.00	4.00	3.00	3.00	4.00	2.00	3.00
Cd_ppm_	136.00	136.00	76.00	102.00	100.00	73.00	58.00	52.00	57.00	66.00	97.00	104.00	106.00	139.00	69.00	137.00
Co_ppm_	54.00	49.00	46.00	43.00	80.00	49.00	46.00	37.00	36.00	38.00	39.00	44.00	49.00	46.00	30.00	35.00
Cr_ppm_	11.70	11.40	7.02	7.80	11.45	9.50	9.38	8.80	8.43	9.00	10.35	11.35	12.00	12.20	8.70	11.00
Ga_ppm_	10.00	10.00	10.00	10.00	10.00	10.00	10.00	10.00	10.00	10.00	10.00	10.00	10.00	10.00	10.00	10.00
K_pc_	0.02	0.04	0.05	0.04	0.03	0.03	0.03	0.03	0.03	0.04	0.03	0.04	0.05	0.04	0.06	0.05
La_ppm_	10.00	10.00	10.00	10.00	10.00	10.00	10.00	10.00	10.00	10.00	10.00	10.00	10.00	10.00	10.00	10.00
Li_ppm_	10.00	10.00	10.00	10.00	10.00	10.00	10.00	10.00	10.00	10.00	10.00	10.00	10.00	10.00	10.00	10.00
Mg_pc_	0.01	0.01	0.01	0.01	0.01	0.01	0.01	0.01	0.01	0.01	0.01	0.01	0.01	0.01	0.01	0.02
Mn_ppm_	132.00	199.00	66.00	111.00	515.00	257.00	209.00	189.00	175.00	182.00	187.00	224.00	323.00	406.00	236.00	280.00
Mo_ppm_	1.00	1.00	1.00	1.00	1.00	1.00	1.00	1.00	1.00	1.00	1.00	1.00	1.00	1.00	1.00	1.00
Na_pc_	0.02	0.01	0.01	0.02	0.02	0.02	0.02	0.01	0.01	0.02	0.03	0.02	0.03	0.02	0.02	0.02
Ni_ppm_	34.00	25.00	13.00	17.00	37.00	29.00	24.00	13.00	12.00	14.00	18.00	21.00	27.00	34.00	22.00	31.00
P_ppm_	410.00	400.00	350.00	300.00	370.00	380.00	500.00	490.00	490.00	540.00	450.00	560.00	510.00	440.00	370.00	260.00
Pb_ppm_	2.00	2.00	2.00	2.00	2.00	2.00	2.00	2.00	2.00	2.00	2.00	2.00	2.00	2.00	2.00	2.00
S_pc_	0.02	0.01	0.01	0.01	0.02	0.01	0.02	0.02	0.02	0.02	0.02	0.02	0.02	0.02	0.01	0.01
Sb_ppm_	2.00	2.00	2.00	2.00	2.00	2.00	2.00	2.00	2.00	2.00	3.00	2.00	2.00	2.00	2.00	2.00
Sc_ppm_	26.00	24.00	16.00	19.00	28.00	30.00	36.00	35.00	41.00	42.00	37.00	42.00	35.00	28.00	26.00	25.00
Se_ppm_	10.00	10.00	10.00	10.00	10.00	10.00	10.00	10.00	10.00	10.00	10.00	10.00	10.00	10.00	10.00	10.00
Sn_ppm_	10.00	10.00	10.00	10.00	10.00	10.00	10.00	10.00	10.00	10.00	10.00	10.00	10.00	10.00	10.00	10.00
Sr_ppm_	1.00	2.00	1.00	1.00	1.00	1.00	1.00	1.00	1.00	1.00	1.00	1.00	1.00	1.00	1.00	1.00
Th_ppm_	20.00	20.00	20.00	20.00	20.00	20.00	20.00	20.00	20.00	20.00	20.00	20.00	20.00	20.00	20.00	20.00
Ti_pc_	0.04	0.03	0.02	0.03	0.04	0.04	0.04	0.04	0.03	0.04	0.04	0.05	0.05	0.05	0.03	0.04
Tl_ppm_	10.00	10.00	10.00	10.00	10.00	10.00	10.00	10.00	10.00	10.00	10.00	10.00	10.00	10.00	10.00	10.00
U_ppm_	10.00	10.00	10.00	10.00	10.00	10.00	10.00	10.00	10.00	10.00	10.00	10.00	10.00	10.00	10.00	10.00
V_ppm_	180.00	133.00	72.00	124.00	278.00	227.00	221.00	193.00	184.00	194.00	176.00	200.00	211.00	218.00	129.00	174.00
W_ppm_	10.00	10.00	10.00	10.00	10.00	10.00	10.00	10.00	10.00	10.00	10.00	10.00	10.00	10.00	10.00	10.00
Y_ppm_	10.00	10.00	10.00	10.00	10.00	10.00	10.00	10.00	10.00	10.00	10.00	10.00	10.00	10.00	10.00	10.00
Zn_ppm_	45.00	33.00	18.00	19.00	31.00	23.00	18.00	10.00	8.00	9.00	12.00	12.00	15.00	18.00	11.00	16.00
Zr_ppm_	10.00	11.00	11.00	11.00	11.00	8.00	6.00	6.00	5.00	5.00	5.00	6.00	7.00	8.00	5.00	9.00

DHID	FLV_63	FLV_63	FLV_63	FLV_63	FLV_63	FLV_63	FLV_63	FLV_63	FLV_63	FLV_63	FLV_63	FLV_63	FLV_63	FLV_63
FROM	19.00	20.00	21.00	22.00	23.00	24.00	24.70	25.80	27.00	28.00	29.00	30.14	31.23	32.20
TO	20.00	21.00	22.00	23.00	24.00	24.70	25.80	27.00	28.00	29.00	30.14	31.23	32.20	33.00
Au	0.00	0.00	0.00	0.00	0.00	0.00	0.00	0.00	0.00	0.00	0.00	0.04	0.00	0.01
Ag_ppm_	0.20	0.20	0.20	0.20	0.20	0.20	0.20	0.20	0.20	0.20	0.20	0.20	0.20	0.20
Cu_ppm_	1.46	1.29	1.59	1.31	1.73	1.59	1.94	1.56	1.75	1.99	2.22	2.44	2.87	2.89
Fe_pc_	38.00	13.00	13.00	15.00	14.00	15.00	13.00	16.00	27.00	27.00	24.00	26.00	24.00	36.00
Al_pc_	20.00	20.00	20.00	20.00	300.00	710.00	2460.00	620.00	940.00	2110.00	890.00	1240.00	940.00	920.00
As_ppm_	0.60	0.70	0.70	0.70	0.70	0.70	1.40	0.80	1.10	2.00	1.50	1.90	2.40	4.30
Ba_ppm_	2.00	2.00	2.00	2.00	2.00	3.00	2.00	2.00	2.00	2.00	3.00	2.00	2.00	2.00
Be_ppm_	0.01	0.01	0.01	0.01	0.04	0.16	0.21	0.21	0.27	0.30	0.39	0.44	0.42	0.47
Bi_ppm_	0.50	0.50	0.50	0.50	0.50	0.50	0.50	0.50	0.50	0.50	0.50	0.50	0.50	0.50
Ca_pc_	3.00	4.00	4.00	7.00	13.00	36.00	153.00	54.00	89.00	566.00	574.00	759.00	645.00	203.00
Cd_ppm_	242.00	232.00	157.00	149.00	143.00	113.00	74.00	106.00	100.00	106.00	86.00	87.00	96.00	104.00
Co_ppm_	78.00	91.00	72.00	84.00	87.00	84.00	183.00	147.00	149.00	176.00	138.00	116.00	114.00	95.00
Cr_ppm_	13.30	13.00	11.90	12.00	10.60	8.01	5.65	5.56	5.71	5.65	5.17	5.25	5.63	6.35
Ga_ppm_	10.00	10.00	10.00	10.00	10.00	10.00	10.00	10.00	10.00	10.00	10.00	10.00	10.00	10.00
K_pc_	0.05	0.04	0.06	0.04	0.06	0.05	0.23	0.08	0.05	0.06	0.05	0.06	0.04	0.06
La_ppm_	10.00	10.00	10.00	10.00	10.00	10.00	130.00	150.00	190.00	240.00	200.00	130.00	120.00	90.00
Li_ppm_	10.00	10.00	10.00	10.00	10.00	10.00	10.00	10.00	20.00	40.00	40.00	40.00	30.00	10.00
Mg_pc_	0.02	0.02	0.02	0.03	0.10	0.35	1.01	1.10	1.23	1.20	1.31	1.44	1.88	2.22
Mn_ppm_	215.00	213.00	236.00	268.00	1150.00	2830.00	14500.00	2440.00	3070.00	7540.00	3240.00	4900.00	3140.00	2710.00
Mo_ppm_	1.00	1.00	1.00	1.00	1.00	1.00	1.00	1.00	1.00	1.00	1.00	1.00	1.00	1.00
Na_pc_	0.02	0.01	0.02	0.01	0.01	0.02	0.01	0.01	0.01	0.01	0.01	0.01	0.01	0.01
Ni_ppm_	67.00	84.00	77.00	74.00	46.00	65.00	173.00	157.00	157.00	266.00	316.00	420.00	423.00	505.00
P_ppm_	270.00	220.00	160.00	190.00	230.00	260.00	360.00	340.00	360.00	440.00	380.00	330.00	300.00	560.00
Pb_ppm_	2.00	3.00	3.00	2.00	10.00	15.00	23.00	6.00	8.00	6.00	5.00	8.00	5.00	3.00
S_pc_	0.02	0.01	0.01	0.01	0.01	0.01	0.01	0.01	0.01	0.01	0.01	0.01	0.01	0.01
Sb_ppm_	2.00	2.00	3.00	2.00	2.00	2.00	2.00	2.00	2.00	2.00	2.00	2.00	2.00	2.00
Sc_ppm_	37.00	39.00	36.00	48.00	83.00	61.00	46.00	26.00	27.00	25.00	20.00	20.00	23.00	21.00
Se_ppm_	10.00	10.00	10.00	10.00	10.00	10.00	10.00	10.00	10.00	10.00	10.00	10.00	10.00	10.00
Sn_ppm_	10.00	10.00	10.00	10.00	10.00	10.00	10.00	10.00	10.00	10.00	10.00	10.00	10.00	10.00
Sr_ppm_	1.00	1.00	2.00	1.00	2.00	10.00	19.00	14.00	17.00	16.00	26.00	36.00	25.00	36.00
Th_ppm_	20.00	20.00	20.00	20.00	20.00	20.00	20.00	20.00	20.00	20.00	20.00	20.00	20.00	20.00
Ti_pc_	0.05	0.05	0.05	0.06	0.04	0.02	0.02	0.03	0.02	0.02	0.01	0.01	0.01	0.02
Tl_ppm_	10.00	10.00	10.00	10.00	10.00	10.00	10.00	10.00	10.00	10.00	10.00	10.00	10.00	10.00
U_ppm_	10.00	10.00	10.00	10.00	10.00	10.00	10.00	10.00	10.00	10.00	10.00	10.00	10.00	10.00
V_ppm_	244.00	215.00	212.00	190.00	155.00	137.00	146.00	149.00	140.00	159.00	90.00	133.00	99.00	109.00
W_ppm_	10.00	10.00	10.00	10.00	10.00	10.00	10.00	10.00	10.00	10.00	10.00	10.00	10.00	10.00
Y_ppm_	10.00	10.00	10.00	10.00	20.00	90.00	180.00	280.00	340.00	320.00	260.00	210.00	200.00	290.00
Zn_ppm_	39.00	48.00	40.00	35.00	33.00	55.00	279.00	253.00	254.00	321.00	291.00	220.00	291.00	302.00
Zr_ppm_	8.00	7.00	6.00	6.00	5.00	5.00	5.00	5.00	5.00	5.00	5.00	5.00	5.00	5.00

DHID	FLV_97	FLV_97	FLV_97	FLV_97	FLV_98	FLV_98	FLV_98	FLV_98	FLV_98	FLV_98	FLV_98	FLV_98	FLV_98	FLV_98	FLV_98	FLV_98	FLV_98	FLV_98	FLV_99	FLV_99	FLV_99	FLV_99
FROM	0.00	1.00	1.80	2.54	0.00	0.50	1.00	1.70	2.41	3.00	4.00	5.00	6.00	7.00	7.80	9.00	10.00	11.00	0.00	1.00	1.60	2.50
TO	1.00	1.80	2.54	3.19	0.50	1.00	1.70	2.41	3.00	4.00	5.00	6.00	7.00	7.80	9.00	10.00	11.00	12.00	1.00	1.60	2.50	3.54
Au	0.00	0.00	0.00	0.00	0.01	0.01	0.00	0.01	0.01	0.00	0.00	0.00	0.00	0.00	0.00	0.00	0.00	0.00	0.01	0.00	0.00	0.00
Ag_ppm_	0.50	0.50	0.50	0.50	1.80	0.70	0.60	0.50	3.10	1.10	0.50	0.50	0.50	0.50	0.50	0.50	0.50	0.50	0.50	0.50	0.50	0.50
Cu_ppm_	9.14	8.87	8.54	7.70	11.00	10.90	9.48	10.20	9.96	7.84	9.07	9.56	8.80	9.31	9.24	11.40	9.91	10.35	8.21	8.54	7.66	7.86
Fe_pc_	9.00	12.00	8.00	5.00	25.00	24.00	7.00	8.00	19.00	5.00	13.00	9.00	12.00	19.00	19.00	17.00	19.00	19.00	9.00	5.00	9.00	5.00
Al_pc_	1600.00	1510.00	1670.00	1660.00	770.00	780.00	950.00	880.00	680.00	830.00	760.00	810.00	680.00	780.00	690.00	620.00	700.00	690.00	840.00	860.00	700.00	850.00
As_ppm_	1.90	1.80	1.80	1.80	2.10	2.20	2.20	2.20	2.00	2.00	2.20	2.30	2.20	2.50	2.30	1.90	2.10	2.20	1.70	1.70	1.60	1.70
Ba_ppm_	2.00	2.00	2.00	2.00	4.00	5.00	2.00	2.00	2.00	2.00	2.00	2.00	3.00	2.00	2.00	2.00	2.00	2.00	2.00	2.00	2.00	2.00
Be_ppm_	0.07	0.04	0.01	0.01	0.14	0.06	0.02	0.02	0.06	0.02	0.02	0.02	0.03	0.03	0.03	0.03	0.02	0.02	0.06	0.04	0.04	0.01
Bi_ppm_	0.50	0.50	0.50	0.50	0.50	0.50	0.50	0.50	0.50	0.50	0.50	0.50	0.50	0.50	0.50	0.50	0.50	0.50	0.50	0.50	0.50	0.50
Ca_pc_	5.00	4.00	2.00	4.00	7.00	7.00	3.00	2.00	4.00	1.00	2.00	1.00	1.00	1.00	1.00	2.00	1.00	1.00	4.00	3.00	3.00	2.00
Cd_ppm_	82.00	77.00	87.00	79.00	69.00	71.00	27.00	51.00	70.00	16.00	41.00	63.00	93.00	59.00	63.00	69.00	60.00	99.00	76.00	36.00	35.00	18.00
Co_ppm_	2.00	2.00	4.00	1.00	12.00	11.00	19.00	20.00	19.00	16.00	16.00	25.00	39.00	22.00	25.00	32.00	23.00	28.00	16.00	9.00	7.00	6.00
Cr_ppm_	5.63	5.46	5.95	4.99	6.76	6.80	3.60	4.91	6.29	2.77	4.41	5.51	7.17	5.73	5.64	5.58	5.05	6.34	4.97	3.24	3.70	3.17
Ga_ppm_	20.00	20.00	20.00	20.00	20.00	20.00	20.00	20.00	20.00	20.00	20.00	20.00	20.00	20.00	20.00	20.00	20.00	20.00	20.00	20.00	20.00	20.00
K_pc_	4.21	4.34	4.05	3.74	4.40	4.32	3.48	3.34	3.31	3.15	3.13	3.36	2.81	3.52	3.19	2.85	3.05	3.20	3.52	4.21	3.70	3.97
La_ppm_	20.00	20.00	20.00	20.00	20.00	20.00	20.00	30.00	40.00	20.00	10.00	20.00	30.00	10.00	20.00	60.00	40.00	40.00	50.00	40.00	40.00	60.00
Li_ppm_																						
Mg_pc_	0.27	0.25	0.23	0.22	0.29	0.27	0.30	0.26	0.23	0.26	0.27	0.27	0.24	0.30	0.25	0.22	0.24	0.25	0.29	0.33	0.28	0.28
Mn_ppm_	47.00	54.00	41.00	45.00	84.00	84.00	71.00	82.00	104.00	56.00	91.00	79.00	59.00	72.00	98.00	68.00	132.00	127.00	142.00	94.00	157.00	99.00
Mo_ppm_	1.00	1.00	1.00	1.00	2.00	2.00	1.00	1.00	2.00	1.00	1.00	1.00	1.00	1.00	1.00	1.00	1.00	1.00	1.00	1.00	1.00	1.00
Na_pc_	0.20	0.20	0.19	0.17	0.21	0.21	0.12	0.11	0.15	0.11	0.11	0.12	0.10	0.13	0.12	0.11	0.11	0.13	0.13	0.15	0.13	0.14
Ni_ppm_	12.00	13.00	11.00	11.00	11.00	13.00	4.00	4.00	9.00	1.00	3.00	4.00	7.00	4.00	5.00	9.00	5.00	7.00	15.00	9.00	9.00	9.00
P_ppm_	250.00	320.00	330.00	350.00	420.00	380.00	360.00	370.00	460.00	250.00	380.00	640.00	960.00	720.00	720.00	830.00	620.00	680.00	310.00	240.00	230.00	390.00
Pb_ppm_	2.00	2.00	4.00	2.00	8.00	8.00	2.00	2.00	2.00	3.00	2.00	2.00	2.00	2.00	2.00	4.00	5.00	2.00	2.00	2.00	2.00	2.00
S_pc_	0.01	0.01	0.01	0.01	0.01	0.01	0.01	0.01	0.01	0.01	0.01	0.01	0.01	0.01	0.01	0.01	0.01	0.01	0.02	0.01	0.01	0.01
Sb_ppm_	7.00	5.00	5.00	5.00	5.00	5.00	5.00	5.00	5.00	5.00	5.00	5.00	5.00	5.00	5.00	5.00	5.00	5.00	5.00	5.00	5.00	5.00
Sc_ppm_	23.00	23.00	21.00	20.00	23.00	24.00	12.00	21.00	24.00	10.00	18.00	26.00	35.00	26.00	25.00	26.00	23.00	31.00	20.00	13.00	10.00	8.00
Se_ppm_																						
Sn_ppm_																						
Sr_ppm_	69.00	72.00	65.00	59.00	82.00	84.00	73.00	83.00	90.00	63.00	44.00	80.00	99.00	65.00	80.00	191.00	138.00	117.00	66.00	61.00	52.00	77.00
Th_ppm_	20.00	20.00	20.00	20.00	20.00	20.00	20.00	20.00	20.00	20.00	20.00	20.00	20.00	20.00	20.00	20.00	20.00	20.00	20.00	20.00	20.00	20.00
Ti_pc_	0.33	0.32	0.30	0.28	0.29	0.28	0.17	0.21	0.24	0.11	0.21	0.20	0.21	0.17	0.18	0.17	0.19	0.24	0.27	0.25	0.19	0.18
Tl_ppm_	10.00	10.00	10.00	10.00	10.00	10.00	10.00	10.00	10.00	10.00	10.00	10.00	10.00	10.00	10.00	10.00	10.00	10.00	10.00	10.00	10.00	10.00
U_ppm_	10.00	10.00	10.00	10.00	10.00	10.00	10.00	10.00	10.00	10.00	10.00	10.00	10.00	10.00	10.00	10.00	10.00	10.00	10.00	10.00	10.00	10.00
V_ppm_	94.00	80.00	97.00	116.00	90.00	91.00	66.00	112.00	107.00	48.00	95.00	138.00	164.00	157.00	139.00	152.00	127.00	171.00	116.00	84.00	67.00	45.00
W_ppm_	10.00	10.00	10.00	10.00	20.00	10.00	10.00	10.00	20.00	10.00	10.00	10.00	10.00	10.00	10.00	10.00	10.00	10.00	10.00	10.00	10.00	10.00
Y_ppm_																						
Zn_ppm_	16.00	9.00	8.00	4.00	12.00	12.00	11.00	12.00	12.00	7.00	11.00	16.00	25.00	19.00	18.00	22.00	16.00	21.00	17.00	14.00	20.00	13.00

FUROS DE SONDAGEM:

FLV_67 0 - 1 metro: preto, arenoso com matéria orgânica. Presença de pequenos fragmentos de rochas, com grãos de quartzo e K-F. A partir de 2 metros de profundidade, a rocha é um conglomerado (Ouricuri do Ouro).	**FLV_093** 0-1 metro: preto, arenoso e contém matéria orgânica. Ocorre a presença de fragmentos de rocha, arenito ferrificado, matriz hematítica e nível areno-argiloso. Em 2 metros de rocha é um conglomerado.	**FLV_63** 1 a 4 metros: solo é marrom, areno argiloso, com fragmentos orgânicos e fragmentos de quartzo. De 4 a 8 metros, é argiloso, com níveis de caulim, e, localmente, FeO. De 8m a 20m, composição predominantemente argilosa com coloração rosa-acinzentada. Ocorre, localmente, nesse intervalo, vênulas ou lâminas de material preto com traço de mesma cor (MnO). A partir de 20 metros, é rosa esbranquiçado; feldspático -caulinítico. A partir de 26 metros, o solo se torna branco-esverdeado, argiloso. Em 31 metros (saprólito com fragmentos de xisto esverdeado). partir de 35 metros, o que se nota é a presença de rocha máfica xistosa.	**FLV_41** 0 a 2 metros: marrom, areno-argiloso; com M.O. De 2 a 3,4m, o solo é marrom, levemente mosqueado, argilo arenoso. De 3,4 a 4,9, o solo saprolítico com fragmentos de rocha de composição granítica, com qtz e fedspatos alterados que dão aspecto cinza-esbranquiçado no nível, e origem à matriz argilosa. De 4,9 a 8m, o solo é vermelho esverdeado com fragmentos de rocha alterada. Destaca-se a presença de óxido de Mn, cujo hábito, localmente, é dendrítico (pirolusita?). Localmente, ocorre a presença de argila branca que junto a algum óxido exibem aspecto mosqueado. Os fragmentos de rocha são isotrópicos. 8-10 metros, a coloração esverdeada é mais viva, realçada, Mn ainda se faz presente, bem como algumas manchas de FeO. O material é silto-argiloso. Em 11,5 metros ocorre veio de qtz. Até 14 metros, ocorre saprólito de cor vermelhado com cristais de plg, K-f alterados (granito).	**FLV_099** 0 -0,3 m: marrom, areno argiloso, com fragmentos orgânicos. Segue para um nível arenoso-argiloso, com manchas avermelhadas até 1,9 m. A partir de 1,9, saprólito com fragmentos de rocha alterada, rica em mica branca. Em 2,5 a rocha aflora: rocha com feldspatos argilizados, alterada (rocha granítica).	**FLV_40** 0- 3 metros: solo marrom, arenoso com M.O. De 4 a 6 metros é argiloso, vermelho - esbranquiçado, com blogs de caulim, esbranquiçado. De 6 - 8,5, tons laranjas (oriundos de FeO?) e fragmentos de rocha saprolitizada e manchadas por MnO. A partir de 9 metros o solo é saprolítico esverdeado, origem de rocha máfica que aflora a partir de 12m.	**FLV_38** 0-2 metros: solo vermelho- amarronzado, arenoso. A partir de 2 m, tons mosqueados em material areno-argiloso. Entre 4-6 metros, uma mistura de cores vermelho, laranja e amarelo nos graos areno-argilosos, com porções esbranquiçadas, localizadas e argílicas estão presentes (aparentam ser feldspatos altamente alterados). A partir de 8 metros, granitoide alterado Aflora.
FLV_48 1 a 2 metros: solo é marrom, arenoso e contém M.O. De 2 a 3,5 metros, é saprolítico: rosa-esbranquiçado, com fragmentos de rocha granítica com K-F e Qtz, bastante alterada. Em aproximadamente 3,6m ocorrem vênulas de manganês? turmalina? E exposição do granitoide.	**FLV_49** 0-30 cm: solo silte-argiloso, marrom. De 30cm a 2m: silto-argiloso, rosado, saprolítico. Os fragmentos de rocha presentes são de granito micáceo alterado (sericita?), ocorrem nestes fragmentos uma matriz hematítica e venulas com turmalina e magnetita. A partir de 2 m, granitoie aflorante.	**FLV_10** 0 a 2 metros: solo areno-argiloso, amarelado, com porções mosqueadas (manchas avermelhadas, FeO e presença de M.O). 2 a 4m, saprólito de rocha foliada, acizentada, com clorita, muscovita e quartzo, e feldspato caulinizados. De 4 a 5,2m, o saprolito de rocha acizentada, argilosa, friável, manchas alaranjadas ocorrem, FeO? Entre 5, 2 m a 7m, há um veio de quartzo, manchado por óxido de ferro, em 6, 3 m, presença de material argiloso rosa-esbranquiçado. Em 7 metros, o material se torna amarelo-avermelhado a laranja-avermelhado, argiloso, e grada para um saprólito de rocha foliada, cinza esverdeada e manchado por oxido de ferro. Em 7,35 m, argila esbranquiçada, e em 7,70m, material saprolítico, avermelhado e ferrificado com argila na matriz. vênulas de magnetita. Em 8m, a zona é oxidada com magnetita euédrica, presença de especularita ou martita? A partir de 8,50, aflora uma rocha granítica alterada.	**FLV_07** 0-2 metros: solo marrom-esbranquiçado, argilo-arenoso, com fragmentos de rocha alterada bastante caulinizada. Manchas amareladas e avermelhadas estão presentes, e, por vezes, vênulas, aparentemente óxido de Mn. Em 3,5 metros, há predomínio de material argiloso, rosado. Em 4,5 a 4,6 m, veio de quartzo manchado por oxido de ferro e óxido de Mn (manchas pretas, com traço preto). Os fragmentos em 5 metros são xistosos, amarelados, ricos em Qtz. Os feldspatos estão bastante alterados para uma argila branca (caulim? ou outra mica branca?), ocorrem, ainda, vênulas com oxido de Fe e Mn. Até 8 metros, os fragmentos estão dispostos em meio ao pó friável argiloso e amarelado da rocha. O solo saprolítico vai até 8 m até 13 metros e, então, um metatonalito/ granítico porfiritico alterado, saprolitico, ocorre. Os K-F alterados alcançam até 2cm. E o granito/tonalito com vários níveis de alteração segue no perfil.	**FLV_098** 0 a 1,7 metros: solo marrom pálido com manchas avermelhas (FeO), arenoso e com M.O. A partir de 1,70 é argilo- arenoso, com fragmentos de rocha alterada, saprolítico,. Entre 2,5 e 3 metros é bastante esbranquiçado, com martita disseminada e fragmentos de rocha alterada com mica de alteração. Nestes fragmentos, o Qtz está presente junto com a mica levemente esverdeada. Até 12 metros, os fragmentos de rocha alterada estão com o material argiloso-arenoso, com porços esbranquiçadas e mosqueadas, evidente em 10, 5 m. A partir de 12 metros, o granitoide aflora.	**FLV_097** 0 a 2 metros: saprolítico: rosa-esbranquiçado, com fragmentos de rocha granítica com muscovita, K-F e Qtz, e segue para exposição do granitoide.	**FLV_13** 0 -4 metros: solo marrom avermelhado com tons bastante avermelhados que predominam entre 3 e 4 m. Entre 1 e 2 metros, ocorrência de fragmentos de Qtz no material argilo arenoso com fragmentos de rocha oxidada, brechada. Entre 4 e 10 metros, o solo é saprolítico com tons esverdeados que vão se destacando à medida que a profundidade é aumentada. Neste nível, são claras as vênulas e ocorrência de óxidos de manganês, bem como a presença de martita disseminada. Tons esbranquiçados típicos de argila também estão presentes. Entre 10, 5 e 21 metros, O solo permanece saprolítico com os tons esverdeados mais ressaltantes, com solo de coloração vermelho esverdeado a verde avermelhado. As vênulas de Mn ocorrem. Porções mosqueadas com presença de caulim são comuns. Em 15,8 (fragmento de rocha fílica a xistosa, constituída por mica fina e Qtz). Em 17, 5 a rocha está bem alterada esverdeada e com Qtz. Nesse nível, em 19, 5 a rocha aparenta ser um granito com quartzo e matriz argilosa, produto de alteração. Em 21, 50, a rocha tem textura grossa e contém Qtz e feldspatos alterados.